PREDICTION OF INTERFACIAL TRANSFER KINETICS

by

MICHAEL JOHN RATHBONE

A thesis submitted for the degree of

DOCTOR OF PHILOSOPHY

in the

Department of Pharmacy

of the

University of Aston in Birmingham

December 1985.

Prediction of interfacial transfer kinetics

by Michael John Rathbone

submitted for the degree of Doctor of Philosophy, 1985.

Interfacial transfer kinetics were determined for a number of homologous series comprising non-ionised model solutes across a variety of aqueous : organic interfaces in the two-phase transfer cell. Experimentally determined transport rate constants were compared to those estimated from a theoretical equation. The importance of aqueous and organic diffusional resistances to solute transfer was examined. A method was described to calculate a theoretical solute and solvent dependent ratio that enabled the estimation of the dominant diffusional resistance to which a given solute was subject during interfacial transfer in a particular solvent system. Variation of solute and solvent systems allowed the predictive theories to be tested under conditions where aqueous, organic and mixed diffusional control predominated. Successful prediction of the non-ionised transfer kinetics of homologues in a series was possible from a knowledge of the partition coefficient and transfer kinetics of the parent compound, the partition coefficient of the homologue and some easily determined system-dependent variables.

Octanol : aqueous interfacial transfer kinetics of a variety of model solutes were investigated as a function of aqueous phase pH and ionic strength in the two-phase transfer cell. Transfer rate constants varied unpredictably with pH and fell significantly with increasing aqueous phase ionic strength. Results could not be explained by ionic strength induced variations in partition coefficient, pK_a or kinematic viscosity of the phases. When the same solutes were studied in the rotating diffusion cell transfer rate constants fell with increasing pH in agreement with theoretical predictions. In the rotating diffusion cell, which has a mechanically stabilised interface, aqueous diffusivities were unaffected by pH or ionic strength. Interfacial resistance to transfer was negligable for each solute under study. Interfacial instability, which was affected by the presence of ions in the aqueous phase, appeared to be the reason for the unpredictable results in the two-phase transfer cell.

Keywords: Interfacial transfer kinetics; two-phase transfer cell; rotating diffusion cell; diffusional resistance; partition coefficient.

MEMORANDUM

This dissertation, which is being submitted for the degree of Doctor of Philosophy in the University of Aston in Birmingham, is an account of the work carried out under the supervision of Dr. P.R. Byron in the Department of Pharmacy the University of Aston in Birmingham from October 1981 to October 1984. Except where acknowledged by references in the text, the work described herein is claimed to be original and has not been submitted for any other award.

Michael John Rathbone

MICHAEL JOHN RATHBONE

December 1985.

ACKNOWLEDGEMENTS

I would like to acknowledge the help and guidance given to me throughout the duration of this work by Dr. P.R. Byron.

Thanks are also due to Dr. W.J. Irwin for his useful criticisms and assistance in the completion of this thesis.

I am grateful to the Science and Engineering Research Council for the award of a Research Grant.

My thanks to Mrs. Heather Jones for typing this thesis.

Finally, I wish to express my thanks to my parents for their encouragement during the preparation of this thesis.

TO MY PARENTS

LIST OF CONTENTS

LIST OF FIGURES

LIST OF TABLES

LIST OF APPENDICES

CHAPTER ONE

INTRODUCTION

1.1 INTRODUCTION

This thesis is concerned with a critical analysis of factors controlling solute transport kinetics in the two-phase transfer cell. Many authors have employed two- and three-phase transfer cells to investigate the transport kinetics of model drugs across a variety of aqueous : organic interfaces in an attempt to establish the chemical and physicochemical relationships that govern solute transport (1 - 14). These studies provided little insight into the fundamental processes that control the transfer of solutes across aqueous : organic interfaces. This thesis has investigated the information that could be provided by mass transfer studies performed in two-phase systems. Theories that predict transport kinetics in the two-phase transfer cell are tested. The factors that control interfacial transfer kinetics are elucidated and the limitations of mass transfer studies in two-phase systems are recognised.

For a drug to exert its pharmacologic effect it must transport from its site of administration to its site of action through a series of lipophilic and lipophobic regions. The magnitude of the transport rate constants, at each partitioning step, determine the rate at which a therapeutic concentration is attained and affect the duration and intensity of the resultant biological response. Transport and distribution of most drugs are considered to result from passive diffusion of the non-ionised species (15 - 18) which is thought to depend primarily on the lipophilicity of the compound (19 - 22).

Experimental techniques for studying factors that influence rates of drug transfer have been largely confined to investigating the effect of molecular modification on drug absorption into the systemic circulation (15 - 18). The ultimate goal of these experiments would be, given an initial active compound (and assuming that an equimolar concentration for its structurally related analogues has the same

intrinsic activity at the site of action) to design molecular modifications of that compound *a priori* with optimised absorption so as to achieve a desired therapeutic activity versus time profile (23). This goal contrasts markedly with the present costly and time consuming process of empirically screening large numbers of analogues.

Several authors have performed investigations using *in vitro* two- and three-phase transfer cell models (Fig. 1.1) to simulate drug absorption from the gastrointestinal tract (1 - 14). These studies were performed on the basis that principles governing the transport of solutes in more complex systems may be elucidated by the simple ones. Indeed, if solute transport kinetics cannot be defined, or concentration versus time profiles predicted *a priori* in simple two-phase systems, the goal of drug design by molecular modification may never supersede empirical screening.

In the *in vitro* three-phase models the solute under investigation is in solution in one of two aqueous phases, each buffered to suitable pH values e.g. pH 2 or pH 5 to simulate gastrointestinal pH and pH 7.4 to simulate plasma. The aqueous phases are physically separated from each other and are overlaid by an organic phase (simulating a lipoidal barrier) which is in contact with both phases.

Doluisio and Swintosky (1) devised an *in vitro* model comprising an inverted rocking Y-tube (Fig. 1.1b), with an aqueous phase in each of the two arms overlaid by a connecting layer of an immiscible organic phase. A rocking apparatus agitated the liquids without mixing, causing the liquid : liquid interfaces to continually expand and contract. The degree of tilt and rocking speed were carefully monitored and the rocking apparatus designed to accommodate a large number of inverted Y-tubes. This apparatus offered simplicity in design and rapidity of data collection. However, a continually

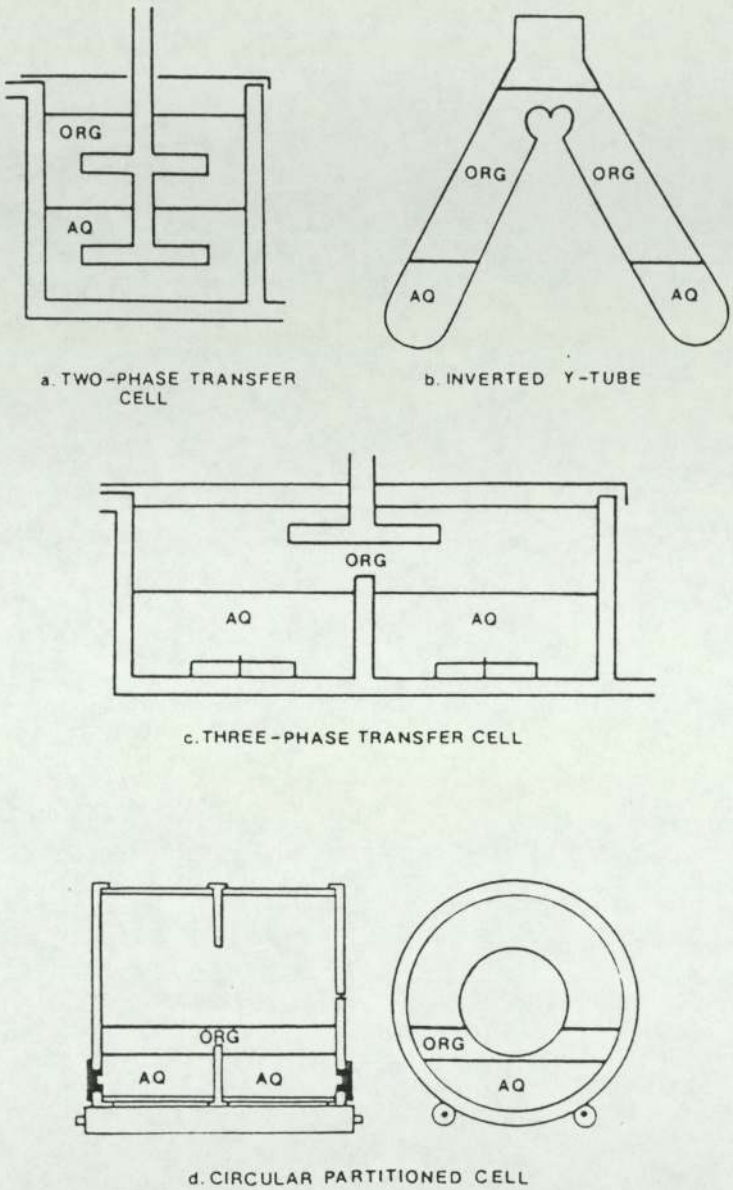

Figure 1.1 Two- and three-phase transfer cell designs used as *in vitro* drug absorption models. The terms AQ and ORG refer to the aqueous and organic phases, respectively.

expanding and contracting area of liquid : liquid contact and the need to terminate mixing to withdraw samples for analysis were a disadvantage when employing this technique to study processes that controlled interphase mass transfer.

Perrin (2) suggested a rectangular cell with a partition separating two aqueous phases, each overlaid by an organic phase (Fig. 1.1c). The organic phase was stirred using an overhead paddle stirrer, while aqueous phases were stirred, using magnetic stirrers, from beneath the apparatus. In contrast to the inverted Y-tube (1), the Perrin apparatus (2) offered fixed interfacial areas throughout the transport process and gave greater control over stirring conditions. In addition, stirring need not be terminated to withdraw samples for analysis when using the Perrin apparatus.

Robertson and Bode (3) proposed the use of a circular partitioned cell which slowly rotated on rollers (Fig. 1.1d). Two half cells were separated by a central partition in which a circular hole was bored. The central partition separated the two aqueous phases while an organic phase, overlaid on each aqueous phase, interconnected through the circular hole. Rotation of the cell via the rollers was rapid enough to allow mixing within each of the individual phases, but slow enough to prevent mixing of the different phases. The rollers were designed to accommodate a number of cells allowing rapid data collection. However, the design offered no advantages over either the inverted Y-tube or Perrin apparatus.

The simplest design proposed as an <u>in vitro</u> model for drug absorption is the two-phase transfer cell (Fig. 1.1a), which comprises an aqueous and organic phase contained within a jacketed glass beaker and stirred using a double bladed stirrer. Many authors have preferentially employed the two-phase transfer cell

because of the simple design, operation, ease with which temperature, stirring conditions, aqueous and organic phase composition and volume and sampling procedure may be controlled (5 - 14, 23 - 32). In addition, organic phases denser than water may be investigated using a two-phase transfer cell.

Doluisio and Swintosky used an inverted Y-tube model (Fig. 1.1b) containing an aqueous : cyclohexane system, in which the aqueous phase pH was varied, to study the interfacial transport kinetics of a variety of weak acids and bases (salicylic acid, barbital, antipyrine, aminopyrine and tetracycline) (1). Equilibrium partition coefficient studies were in agreement with predicted values for each solute under investigation. Kinetic studies performed using barbital and aminopyrine were in agreement with predicted values, antipyrine showed some variability, while for salicylic acid no agreement between theory and experiment was observed. For the case of salicylic acid, Doluisio and Swintosky proposed that the large change in the concentration of ionised species with pH influenced the transfer rate of the non-ionised species between the immiscible phases. In general however, the results obtained were consistent with the assumption that interfacial transport rate constants were dependent upon the migration of the non-ionised solute (1). This assumption was supported by Zecchi et al (12) who studied the effect of aqueous phase pH on salicylic acid transport across an aqueous : benzene interface in the two-phase transfer cell (Fig. 1.1a).

The effect of lipid polarity was independently investigated by Khalil and Martin (4) and Augustine and Swarbrick (14). Khalil and Martin (4) used an inverted Y-tube to study the interfacial transfer kinetics of carboxyl salicylic acid between an aqueous phase and a variety of organic phases exhibiting a range of solubility parameter values (used to model the extent of lipophilicity of the organic

phase). They showed (4) that the rate of transfer of solute from the aqueous donor phase to the organic phase increased, while transfer of the solute from the organic phase to the receptor aqueous phase decreased, as the value of the solubility parameter of the solvent approached that of the solute under investigation. A Perrin-type apparatus (2) (Fig. 1.1c) was employed by Augustine and Swarbrick (14) to investigate the effect of lipid polarity on transport kinetics of a model solute (salicylic acid). Their results supported the observations made by Khalil *et al* (4) upon the transport of solute from the aqueous donor phase to the organic phase. However, transfer of solute from the organic phase to the aqueous receptor phase was shown to increase or decrease with lipid polarity, dependent upon the stirring arrangement used in the study (14).

The effect of molecular modification on solute transport was investigated by Robertson and Bode (3), using an *in vitro* model of the type depicted in Fig. 1.1d, and Schumacher *et al* (10, 11), using a two-phase transfer cell (Fig. 1.1a). Robertson and Bode employed cyclohexane as the organic phase (3), while Schumacher *et al* employed octanol (10, 11). Using a small series of non-ionised sulphonamide derivatives, these investigators showed that as the lipophilicity of the solutes increased, as measured by the solute organic : aqueous partition coefficient, the rate of interfacial transfer increased (3, 10, 11). A two-phase transfer cell containing an aqueous : octanol system was used by Koprivc *et al* (13) to investigate the interfacial transport of a small series of non-ionised barbituric acid derivatives. Their results (13) supported the findings of Robertson and Bode (3) and Schumacher *et al* (10, 11).

Augustine and Swarbrick (14) used a Perrin-type apparatus (2) (Fig. 1.1c) that employed a variety of stirring arrangements. Their results showed that both cell design and agitation conditions employed

in two- and three-phase transfer cells significantly affect the magnitude and rank order of the experimentally observed interfacial transfer rate constants.

These two- and three-phase transfer cell (Fig. 1.1) studies (1 - 14) were largely confined to evaluating the effect of change of one physicochemical parameter, of either solute or solvent system, on the transfer kinetics of individual solutes (1 - 14). Such studies provided little insight into the fundamental processes that govern transfer of solutes across aqueous : organic interfaces. However, these investigations have established the chemical and physicochemical characteristics of the solute and solvent systems that influence the magnitude of the experimentally observed rates of solute transport.

Factors which control solute transfer between two immiscible phases were investigated by Lewis and Whitman (7), whose two-film theory essentially proposes that (a) the main barrier to transfer exists in two stagnant boundary layers adjacent to the interface, (b) these barriers, or resistances, are additive - the sum of the individual resistances offered to solute transfer are equivalent to the total resistance offered to solute transfer, and (c) the interface itself offers negligible resistance to solute transfer - the two phases are in equilibrium at the interface and the ratio of their concentration is the partition coefficient, K_D, for the solute under study. Gordon and Sherwood (6) used a two-phase system of water and butanol to study the transport of various solutes across the interface. Their studies (6) provided data that supported the two-film theory of Lewis and Whitman (7). Byron et al (8) employed a two-phase transfer cell containing equal volumes of a pre-equilibrated aqueous phase and light liquid petrolatum to study the kinetics of interfacial transport of a model solute (cyclohept-2-enone) in the presence and absence of competing degradation in the aqueous phase. Their results supported

the validity of the two-film theory (7) in the two-phase transfer cell with assumptions of no significant interfacial resistance, no thermal, electrical, and osmotic gradients, and steady-state diffusion in the two-phase transfer cell (8).

Recently, Waterbeemd et al (25 - 29) and Byron et al (24) independently derived equations which allowed solute transport kinetics in the two-phase transfer cell to be predicted from knowledge of some simply determined physicochemical characteristics of the solute and (defined) solvent systems.

Waterbeemd et al (25 - 29) investigated the transfer kinetics of a large series of non-ionised sulphonamide derivatives using a standardised two-phase transfer cell containing aqueous : octanol and aqueous : di-n-butylether systems stirred at 40 rpm and maintained at 20°C. Their results demonstrated that a characteristic relationship existed (Fig. 1.2) between log k_{obs} and log K_D, where k_{obs} refers to the experimentally observed forward, k_{12}, or reverse, k_{21}, apparent first-order rate constant for partitioning and K_D is the solute organic : aqueous partition coefficient. The authors concluded that each log k_{obs} versus log K_D curve comprised of three distinct regions (Fig. 1.2) (26, 28).

(a) a region for which log k_{obs} is linearly correlated with log K_D (regions $\vec{3}$ and $\overleftarrow{3}$).

(b) a parabolic middle part (regions $\vec{2}$ and $\overleftarrow{2}$).

(c) a region in which log k_{obs} remains constant (regions $\vec{1}$ and $\overleftarrow{1}$).

Where superscripts $\rightarrow$ and $\leftarrow$ refer to the forward and reverse rate constant for partitioning.

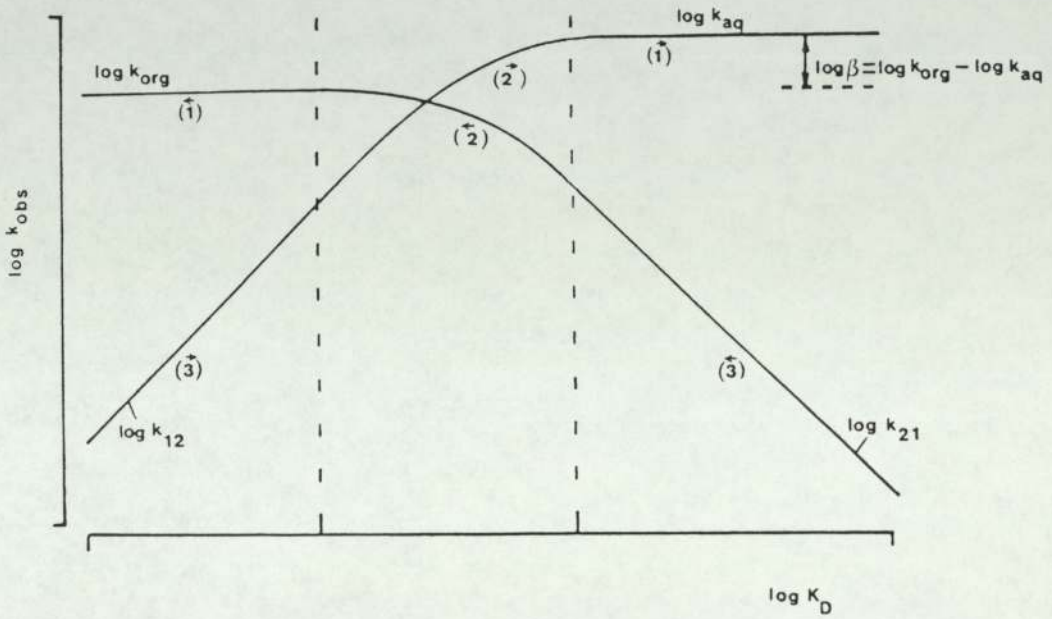

Figure 1.2 General form of a log k_{obs} versus log K_D plot comprising (1) a region for which log k_{obs} remains constant, (2) a parabolic middle region and (3) a region for which log k_{obs} is linearly correlated with log K_D. The system-dependent parameter β may be estimated from the difference of the two plateau regions (log k_{org} - log k_{aq}). Superscripts $\rightarrow$ and $\leftarrow$ refer to the forward and reverse partitioning process, respectively.

In order to mathematically describe the experimentally observed relationships between log k_{obs} and log K_D, the authors proposed a three-step model for interfacial transport (25, 28) in accord with Scheme 1.1.

Scheme 1.1

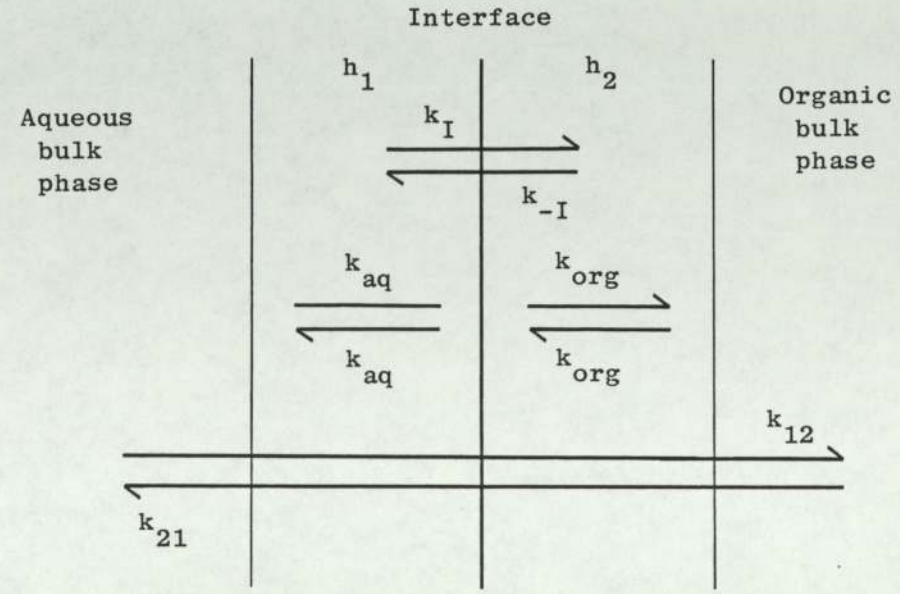

where h_1 and h_2 refer to stagnant diffusive boundary layers adjacent to the interface in the aqueous and organic phases respectively, k_I and k_{-I} are the forward and reverse "energy step rate constants" (interfacial resistances to mass transfer), k_{aq} and k_{org} refer to "diffusion rate constants" (permeability coefficients) in the aqueous and organic diffusive boundary layers respectively, and k_{12} and k_{21} represent the forward and reverse first-order rate constants for partitioning respectively, (25). Nomenclature in quotation marks are terms used by Waterbeemd et al (25) while bracketed terms are definitions more commonly used in the literature. With reference to Scheme 1.1 Waterbeemd et al (25, 28) proposed that solute transfer across the interface was controlled by three steps:

(1) a diffusion-controlled step through a stagnant layer adjacent to the interface.

(2) a de- and re-solvation step in the interface.

(3) a diffusion-controlled step through a second stagnant layer adjacent to the other side of the interface.

The authors applied a thermodynamic analysis to Scheme 1.1 (28) and derived six equations to describe the three distinct regions of each (forward and reverse) log k_{obs} versus log K_D curve. These equations were given as:

$$\log k_{12} = \log K_D + \log k_{org} \qquad [\text{region } \vec{3}] \qquad 1.1$$

$$\log k_{12} = -c\,(\log K_D)^2 + b \log K_D + x \qquad [\text{region } \vec{2}] \qquad 1.2$$

$$\log k_{12} = \log k_{aq} \qquad [\text{region } \vec{1}] \qquad 1.3$$

and

$$\log k_{21} = \log k_{org} \qquad [\text{region } \overleftarrow{1}] \qquad 1.4$$

$$\log k_{21} = (\log K_D)^2 + (b-1) \log K_D + x \qquad [\text{region } \overleftarrow{2}] \qquad 1.5$$

$$\log k_{21} = \log K_D + \log k_{aq} \qquad [\text{region } \overleftarrow{3}] \qquad 1.6$$

where square bracketed terms refer to the regions of curves in Fig. 1.2 and c, b and x are complex constants (28). Equations 1.1 through 1.3 describe the forward rate of transfer, k_{12}, while Eqs. 1.4 through 1.6 describe the reverse rate of transfer, k_{21}. To apply these equations, rate constants for forward and reverse interfacial transfer were empirically determined in a standardised two-phase transfer cell for a large series of solute homologues and analogues that displayed a wide range of partition coefficients, K_D. Experimentally observed values were then mathematically transformed into logarithmic form. Initially all transformed data points were treated as though they belonged to the parabolic middle part of the log k_{obs} / log K_D curves (region $\vec{2}$ and

$\overleftarrow{2}$; Fig. 1.2) and simultaneously curve fitted to Eqs. 1.2 and 1.5. The most lipophobic and lipophilic solutes were then omitted and the curve fitting process repeated until

(i) the coefficients b, c and x were equal in Eqs. 1.2 and 1.5.

(ii) none or only one of the included data points lay beyond the top of the parabola.

Equations 1.2 and 1.5 had restricted validity. Beyond the maxima of the parabola a maximum transport rate constant was experimentally observed. The maxima of the parabola was mathematically estimated and used in Eqs. 1.3 and 1.4 to describe solute transfer at the plateau region of the curve. Since by definition (8)

$$k_{12}/k_{21} = K_D \qquad 1.7$$

rearranging for k_{12} in Eq. 1.7 and logarithmic transformation gives Eq. 1.1. Similarly, rearrangement and a logarithmic transformation for k_{21} in Eq. 1.7 gives Eq. 1.6. Thus the lower linear regions of the log k_{obs} versus log K_D curve were defined by Eqs. 1.1 and 1.6 for the forward and reverse transfer processes, respectively. Hence, through a series of experimental determinations and mathematical curve fitting techniques Eqs. 1.1 through 1.6 were used to describe the experimentally observed dependence of log k_{obs} upon log K_D.

In addition to the thermodynamic approach, Waterbeemd et al (26, 28) applied a kinetic approach to describe solute transport in accord with Scheme 1.1. This approach yielded bilinear equations given by

$$\log k_{12} = \log K_D - \log\left[\frac{k_{org}(K_D + 1)}{k_{aq}}\right] + \log k_{org} \qquad 1.8$$

and

$$\log k_{21} = -\log \left[\frac{k_{org}}{k_{aq}} (K_D + 1) \right] + \log k_{org} \qquad 1.9$$

To apply these equations, rate constants for the forward and reverse partitioning process were empirically estimated for a large series of solute homologues and analogues that displayed a wide range of partition coefficient values. Experimentally observed values were then converted into logarithmic form and the transformed values fitted to Eqs. 1.8 and 1.9 using a curve fitting technique (28).

Waterbeemd and his co-workers employed a large series of sulphonamide derivatives ($n > 26$) (26) and, after exhaustive experimentation in the two-phase transfer cell, successfully fitted their logarithmically transformed partitioning data to the equations derived from both the thermodynamic (Eqs. 1.1 through 1.6) and kinetic approach (Eqs. 1.8 and 1.9) (26, 28).

From these empirical log k_{obs} versus log K_D profiles Waterbeemd et al (25 - 29) observed a characteristic solvent and system-dependent parameter, β, defined as the ratio of the plateau value for k_{12} at high values of K_D (region $\vec{1}$; Fig. 1.2) to the plateau value for k_{21} at low values for K_D (region $\overleftarrow{1}$; Fig. 1.2) (= k_{org} / k_{aq}). Direct measurement from log k_{obs} versus log K_D profiles (Fig. 1.2) provided the most accurate estimate for β (28). The authors used a two-phase aqueous : octanol system and compared the regression equations estimated for a large series of non-ionised sulphonamide derivatives to the regression equations estimated for a set of unrelated compounds of various molecular weights and structures (27). Because β could only be estimated with a relative standard deviation of ~10% (28) the authors observed that:

(a) the regression equations did not significantly differ

(b) β was a solute independent parameter, constant for a named solvent pair at a given temperature and stirring speed

(c) in a specified solvent pair under defined experimental conditions, all compounds behaved as belonging to one series with regard to their partitioning (28, 29).

Waterbeemd et al concluded that a knowledge of K_D for the solute and β for the solvent pair under study permitted a value for the logarithmic form of the first-order rate constant for partitioning to be predicted for a given solute in the standardised two-phase transfer cell (28, 29).

De Haan et al (30-32) empirically determined the transport kinetics and partition coefficients of a large series of non-ionised sulphonamide derivatives (25) across a variety of aqueous : organic interfaces. Organic phases chosen for study included n-hexane, cyclohexane, di-ethyl ether, di-isopropyl ether, di-n-butyl ether, n-octanol, cyclohexanol and oleyl alcohol. The authors observed bilinear relationships between log k_{obs} and log K_D of the type depicted in Fig. 1.2 and successfully fitted the logarithmic form of their experimentally observed values for the rate of solute transfer to the bilinear equations derived by Waterbeemd et al (26, 28) (Eqs. 1.8 and 1.9).

The investigations of Waterbeemd et al (25 - 29) and de Haan et al (30 - 32) provided a wealth of experimental evidence to support the validity of the equations derived by Waterbeemd et al (28) (Eqs. 1.1 through 1.9). However, implementation of these equations necessitates the availability and exhaustive experimental determination of the transport kinetics for each member of a large series of solute homologues and analogues [$n > 20$](28). The series must also display

partition coefficient values of sufficient range to estimate each of the three distinct regions of the tripartite log k_{obs} versus log K_D curve, in particular the plateau regions, to enable reliable estimates of β for the solvent system under investigation (28, 29).

Neither Waterbeemd et al (26 - 29) nor de Haan et al (30 - 32) describe methods that define the maximum or minimum values for K_D that ensure an accurate definition of each of the plateau regions of the log k_{obs} versus low K_D curve. In addition, the use of logarithmically transformed values of the rate constants for partitioning allowed specious conclusions to be drawn from the excellent agreement observed between logarithmically transformed rate constants and the equations derived by Waterbeemd et al (28, 29).

Byron et al (24) showed that in a symmetrically stirred two-phase transfer cell (Fig. 1.1a) the concentration of solute in the aqueous phase, C_1, at any time, t, may be written in terms of the solute partition coefficient, K_D, the initial aqueous phase concentration, C_1^o, and the observed first-order rate constant for partitioning, S ($= k_{12} + k_{21}$) as

$$C_1 = [C_1^o / (K_D + 1)][K_D e^{-St} + 1] \qquad 1.10$$

Assuming the validity of the two-film theory (7) and Fick's first law of diffusion, Byron et al (8) showed that the sum of the forward, k_{12}, and reverse, k_{21}, first-order rate constants in the two-phase transfer cell should be described by

$$(k_{12} + k_{21}) = S = \frac{D_1 D_2 A (K_D V_2 + V_1)}{V_1 V_2 (D_2 K_D h_1 + D_1 h_2)} \qquad 1.11$$

where subscripts 1 and 2 refer to the aqueous and organic phases, respectively and S is dependent on the solute diffusion coefficients

(D_1, D_2), the phase volumes (V_1, V_2), the diffusive boundary layer thicknesses at the interface (h_1, h_2) and the solute partition coefficient (K_D). Using the Wilke-Chang relationship for prediction of diffusion coefficients in dilute solution (33, 34) and the Levich equation (35, 36) for the prediction of diffusive boundary layer thicknesses adjacent to the aqueous : organic interface, Byron et al (24) showed that the diffusion coefficient ratio (D_1/D_2) and the diffusive boundary layer thickness ratio (h_1/h_2) in the two-phase transfer cell with symmetric stirring should be in accord with:

$$D_1/D_2 = (\eta_2/\eta_1) \quad [\,(\psi_1 M_1)/(\psi_2 M_2)\,]^{\frac{1}{2}} \qquad 1.12$$

and

$$h_1/h_2 = (D_1/D_2)^{1/3} \quad (\nu_1/\nu_2)^{1/6} \qquad 1.13$$

where η is solvent viscosity, ψ is the solvent association parameter (33), M is solvent molecular weight and ν refers to the kinematic viscosity of the solvent ($=\eta/\rho$, where ρ is density). Solving equations 1.12 and 1.13 for D_2 and h_2 and substituting into Eq. 1.11 gave

$$S = (D_1 A)/(V_1 h_1) \quad \left[\,(K_D + r)/\left[K_D + (R1)^{-2/3} \; (R2)^{1/6} \; (R3)^{1/3}\right]\right] \qquad 1.14$$

where A is interfacial area for solute transfer,

$r = V_1/V_2$, $R1 = \eta_1/\eta_2$, $R2 = \nu_2/\nu_1$ and

$R3 = (\psi_1 M_1)/(\psi_2 M_2)$. Equation 1.14 is a simplified form of the original equation derived by Byron et al (24) and allows prediction of the first-order rate constant for partitioning, S, in the two-phase transfer cell for any compound in a homologous series. The term $(D_1 A)/(V_1 h_1)$ is constant within a homologous series given fixed stirring conditions, constant temperature and aqueous phase volume in a standardised two-phase transfer cell (24). $(D_1 A)/(V_1 h_1)$ must be

first estimated experimentally for the system under study from a knowledge of the transfer kinetics of the parent compound. This estimation can be made by rearranging Eq. 1.14 to give

$$(D_1A)/(V_1h_1) = S\,[K_D + (R1)^{-2/3}\,(R2)^{1/6}(R3)^{1/3}]/(K_D + r) \qquad 1.15$$

Thus prediction of solute transfer kinetics as a function of K_D (Eq. 1.14) according to the method of Byron et al (24) necessitates the availability of a lead compound to allow the determination of its partition coefficient and partitioning kinetics in a chosen solvent pair. Viscometry and densiometry measurements on the mutually saturated binary solvent system under investigation (constant temperature) yield values for R1 and R2. The phase ratio, r , and molecular weights (M) of the solvents are known (37) while Wilke (33) quotes values for the association parameters ψ_1 and ψ_2. The term $(D_1A)/(V_1h_1)$ may then be determined using Eq. 1.15. Once estimated for the lead compound, $(D_1A)/(V_1h_1)$ may be used in Eq. 1.14 to calculate a value of S for any homologue related to the lead compound given either experimental determination or theoretical prediction (38, 39) of the homologue partition coefficient. Theoretically predicted values of S may then be used in Eq. 1.10 to define the C_1 versus time profiles for the specified homologue in the aqueous phase of a two-phase transfer cell given an assigned value for the initial aqueous phase concentration, C_1^o, and knowledge of the solute K_D.

Using a standardised two-phase transfer cell Byron et al (24) showed that the theory (Eq. 1.14) for the prediction of the first-order rate constant for partitioning $S\ (= k_{12} + k_{21})$ for any solute in a homologous series, held true for a series of non-ionised 5,5' - disubstituted barbituric acid derivatives (n = 6) in a pre-equilibrated octanol : aqueous (pH 5.0) buffer system maintained at 37°C and stirred symmetrically at 50 and 100 rpm. However, no further

proof has been forwarded to support the equation of Byron et al (24).

The approach of Byron et al (24) contrasts markedly to that of Waterbeemd et al (25 - 29). Byron et al's (24) approach necessitates the presence of a single lead compound alongside the empirical estimation of its transport kinetics and partition coefficient. Viscometric and densitometric measurements on the mutually saturated solvent system employed in the study are necessary to define the parameters of an equation that affords a continuous prediction of the first-order rate constant for partitioning as a function of the solute partition coefficient. In contrast, the approach of Waterbeemd et al (25 - 29) necessitates the availability of a large series of solute homologues and exhaustive experimentation to determine the transport rate constants of each individual member of the series in the defined two-phase system. In addition, rate constant values must be logarithmically transformed and a curve fitting technique employed to fit the transformed data to three separate equations which afford a discontinuous prediction of k_{obs} as a function of K_D.

Neither authors investigated or derived equations to predict a priori the effect of solute dissociation in the aqueous phase, or the effect of aqueous phase ionic strength, upon solute transport kinetics in the two-phase transfer cell. Such conditions prevail in the in vivo situation and their effect upon interfacial transport kinetics is of interest. In addition, neither authors provided a comprehensive description of the interrelationships that exist between kinetic and mass transport descriptors to afford a more complete definition of those factors which control mass transport kinetics across aqueous : organic interfaces.

This thesis has several aims. In Chapter 2 theoretical equations are derived which describe the interrelationships between interfacial

transport kinetics and mass transport descriptors in the two-phase transfer cell. The validity of these equations are experimentally investigated using a variety of solute homologues and solvent pairs. The importance of aqueous and organic diffusional resistance to solute transport is examined. A method is described to calculate a theoretical solute and solvent dependent ratio that enables estimation of the dominant diffusional resistance to which a given solute is subject during interfacial transfer in a particular solvent system. Variation of solute and solvent system allowed the predictive theory (Eq. 1.14) of Byron et al (24) to be tested under conditions where aqueous,organic or mixed diffusional control predominated. The predictive equation of Byron et al (24) is extended to account for solute ionisation in the aqueous phase of the two-phase transfer cell. Chapter 3 investigates the effect of aqueous phase pH and ionic strength upon interfacial transport kinetics. Transfer rate constants vary unpredictably with pH and fall significantly with increasing aqueous phase ionic strength. Results could not be explained by ionic strength induced variations in partition coefficient, pK_a or kinematic viscosity of the phases. The same solutes are studied in the rotating diffusion cell in Chapter 4. Transfer rate constants fall with increasing pH in accord with theoretical predictions and remain independent of aqueous phase ionic strength. In the rotating diffusion cell, which has a mechanically stabilized interface, aqueous diffusivities are unaffected by pH or ionic strength. Interfacial resistance to transfer are negligible for each solute studied. Interfacial instability, which was affected by the presence of ions in the aqueous phase, appears to be the reason for the unpredictable results in the two-phase transfer cell. Thus, the limitations of two-phase transfer cells in mass transfer studies and the information that could be provided by such cells are recognised.

CHAPTER TWO

PREDICTION OF INTERFACIAL TRANSFER KINETICS FOR NON-IONISED SOLUTES IN THE TWO-PHASE TRANSFER CELL

2.1 INTRODUCTION

The two-phase transfer cell is shown in Figure 1.1a. The interfacial transfer kinetics of non-ionised solute in the two-phase transfer cell is represented in Scheme 2.1 where C_1 and C_2 refer to solute concentrations in the aqueous and organic phases, respectively.

Scheme 2.1

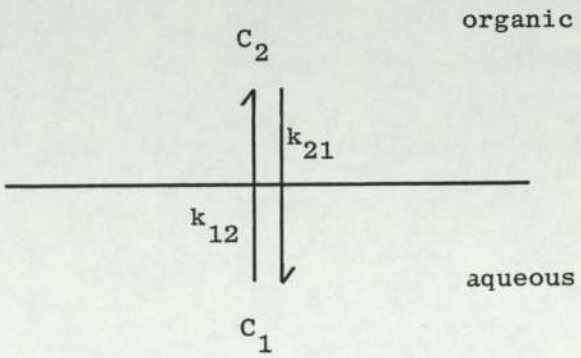

With symmetric stirring, using a paddle stirrer, (Fig. 1.1a) the forward, k_{12}, and reverse, k_{21}, rate constants for partitioning are apparent first-order (24). A solute may be introduced as a bolus at time t = 0 into the aqueous phase and its interfacial transfer kinetics estimated from C_1 versus time profiles obtained under previously standardised conditions. A first-order plot of ln $(C_1 - C_1^{\infty})$ versus time, t, according to

$$\ln (C_1 - C_1^{\infty}) = \ln (C_1^{o} - C_1^{\infty}) - (k_{12} + k_{21})\, t \qquad 2.1$$

provides a value for the apparent first-order rate constant for partitioning, S $(= k_{12} + k_{21})$ (24), where C_1^{o} and C_1^{∞} refer to the initial and final concentration of solute in the aqueous phase, respectively.

This Chapter is devoted to the development of theoretical equations which describe the interrelationships between interfacial

transport kinetics and mass transport descriptors in the two-phase transfer cell. The theories are tested by comparing partitioning rate constants, experimentally determined in a standardised two-phase transfer cell for three series of solute homologues across a variety of aqueous : organic interfaces, to the profiles predicted by the theoretical equations. In addition experimentally determined interfacial transfer kinetics are compared to those estimated from a predictive equation derived by Byron et al (24). The importance of aqueous and organic diffusional resistance to solute transfer is also examined. A method is described to calculate a theoretical solute and solvent dependent ratio that enables an estimation of the dominant diffusional resistance for a particular solute in a given solvent system. Variation of solute and solvent systems allowed the predictive theory of Byron et al (24) to be tested under conditions where aqueous, organic or mixed diffusional control predominated.

2.1.1 Theory

In the two-phase transfer cell transport kinetics are governed by the total diffusional resistance offered to solute transfer, R_T, where R_T is given by the sum of the individual resistances offered by the aqueous, R_{aq}, and organic, R_{org}, stagnant diffusive boundary layers adjacent to the interface of the length, h, as (24)

$$R_T = R_{aq} + R_{org}$$

$$= \frac{h_1}{D_1} + \frac{h_2}{D_2 K_D} \qquad 2.2$$

subscripts 1 and 2 refer to the aqueous and organic phases, respectively and D is the diffusion coefficient. The dependence of the first-order rate constant for partitioning, S, on the total diffusional resistance in the two-phase transfer cell was given by (8):

$$S = \left[\frac{1}{R_T}\right] \left[\frac{A\ (K_D V_2 + V_1)}{K_D V_1 V_2}\right] \qquad 2.3$$

In all the experiments performed in this Chapter the aqueous and organic phase volumes are equal ($V_1 = V_2 = V$; $r = V_1/V_2 = 1$) thus Eq. 2.3 becomes

$$S = \left[\frac{1}{R_T}\right] \left[\frac{A}{V}\right] \left[\frac{K_D + 1}{K_D}\right] \qquad 2.4$$

Individual values for the forward, k_{12}, and reverse, k_{21}, first-order rate constants can be derived since (8, 40)

$$K_D = k_{12}/k_{21} \qquad 2.5$$

and

$$S = k_{12} + k_{21} \qquad 2.6$$

Solving for k_{21} in Eq. 2.5, substituting into Eq. 2.6 and rearranging for k_{12} gives

$$k_{12} = \frac{S\ K_D}{K_D + 1} \qquad 2.7$$

Similarly, solving for k_{12} in Eq. 2.5, substituting into Eq. 2.6 and rearranging for k_{21} yields

$$k_{21} = \frac{S}{K_D + 1} \qquad 2.8$$

Thus substitution of Eq. 2.4 into Eqs. 2.7 and 2.8 allows the derivation of equations that show the dependence of the forward, k_{12}, and reverse, k_{21}, rate constants for partitioning, respectively, on the total diffusional resistance to solute transfer in the two-phase transfer cell (equal phase volumes) as

$$k_{12} = \left[\frac{1}{R_T}\right] \left[\frac{A}{V}\right] \qquad 2.9$$

and

$$k_{21} = \left[\frac{1}{R_T}\right] \left[\frac{A}{VK_D}\right] \qquad 2.10$$

Solving Eq. 2.2 for $1/R_T$ yields

$$\frac{1}{R_T} = \frac{D_1 D_2 K_D}{h_1 D_2 K_D + h_2 D_1} \qquad 2.11$$

Substituting Eq. 2.11 into Eqs. 2.9 and 2.10 and rearranging gives

$$k_{12} = \left[\frac{D_1 D_2}{h_1 D_2 + (h_2 D_1 / K_D)}\right] \left[\frac{A}{V}\right] \qquad 2.12$$

and

$$k_{21} = \left[\frac{D_1 D_2}{h_1 D_2 K_D + h_2 D_1}\right] \left[\frac{A}{V}\right] \qquad 2.13$$

respectively. Equations 2.12 and 2.13 show that individual values for k_{12} and k_{21} should rise and fall, respectively, with increasing K_D within a homologous series [assuming diffusion coefficients vary insignificantly within a homologous series (41) in a standardised two-phase transfer cell of known dimensions (where A, V, h_1 and h_2 are held constant throughout the study)]. However, substituting for $1/R_T$ from Eq. 2.11 into Eq. 2.4 and rearranging gives

$$S = \left[\frac{A}{V}\right] \left[\frac{D_1}{h_1}\right] \left[\frac{K_D + 1}{K_D + h_2 D_1 / h_1 D_2}\right] \qquad 2.14$$

Eq. 2.14 shows that dS/dK_D may be positive (when the ratio

$(h_2D_1/h_1D_2) > 1$, negative (when the ratio $(h_2D_1/h_1D_2) < 1$ or zero (when $(h_2D_1/h_1D_2) = 1$. Thus the apparent first-order rate constant for partitioning, $S(= k_{12} + k_{21}$; Scheme 2.1) may rise, fall or remain constant for a homologous series as the partition coefficient increases.

In two-phase systems, the importance of aqueous and organic diffusional resistances to solute transfer becomes clear upon examination of Eq. 2.2 at the two limits as $K_D \to \infty$ and $K_D \to 0$. According to Eq. 2.2 as $K_D \to \infty$, $R_T \to R_{aq}$ such that

$$R_T \ (K_D \to \infty) \quad \frac{h_1}{D_1} = R_{aq} \qquad 2.15$$

and as $K_D \to 0$, $R_T \to R_{org}$ such that

$$R_T \ (K_D \to 0) \to \frac{h_2}{D_2 K_D} = R_{org} \qquad 2.16$$

Equations 2.15 and 2.16 show that as $K_D \to \infty$ the resistance of the aqueous diffusive boundary layer dominates the total diffusional resistance to solute transfer, whereas as $K_D \to 0$ the resistance of the organic diffusive boundary layer dominates the total diffusional resistance to solute transfer.

Substitution of Eq. 2.15 into Eq. 2.4 as $K_D \to \infty$ gives

$$S \ (K_D \to \infty) \to \frac{D_1 A}{h_1 V} \quad (\to R_{aq}^{-1}) \qquad 2.17$$

and substitution of Eq. 2.16 into Eq. 2.4 as $K_D \to 0$ yields

$$S \ (K_D \to 0) \to \frac{D_2 A}{h_2 V} \quad (\to R_{org}^{-1}) \qquad 2.18$$

Equations 2.17 and 2.18 show that as $K_D \rightarrow \infty$, the first-order rate constant for partitioning S, is governed by the diffusional resistance offered to solute transfer by the aqueous diffusion boundary layer, while as $K_D \rightarrow 0$, the value of S is predominantly governed by the resistance offered to solute transfer by the organic diffusive boundary layer. The importance of aqueous and organic diffusional resistance as $K_D \rightarrow \infty$ and $K_D \rightarrow 0$ may also be examined for the individual values of k_{12} and k_{21}. Substitution of Eqs. 2.15 and 2.16 into Eq. 2.9 gives

$$k_{12\,(K_D \rightarrow \infty)} \rightarrow \frac{D_1 A}{h_1 V} \quad (\rightarrow R_{aq}^{-1}) \qquad 2.19$$

and

$$k_{12(K_D \rightarrow 0)} \rightarrow \frac{D_2 A K_D}{h_2 V} \quad (\rightarrow 0) \qquad 2.20$$

likewise, substitution of Eqs. 2.15 and 2.16 into Eq. 2.10 gives

$$k_{21\,(K_D \rightarrow \infty)} \rightarrow \frac{D_1 A}{h_1 V K_D} \quad (\rightarrow 0) \qquad 2.21$$

and

$$k_{21(K_D \rightarrow 0)} \rightarrow \frac{D_2 A}{h_2 V} \quad (\rightarrow R_{org}^{-1}) \qquad 2.22$$

Comparison of Eqs. 2.17 and 2.19 shows that as $K_D \rightarrow \infty$, $S \rightarrow k_{12}$. Similarly, Eqs. 2.18 and 2.22 show that as $K_D \rightarrow 0$, $S \rightarrow k_{21}$. However, Eqs. 2.20 and 2.21 show that values for k_{12} and k_{21} approach a minimum value as $K_D \rightarrow 0$ and $K_D \rightarrow \infty$ respectively.

As the limits of $K_D \rightarrow \infty$ and $K_D \rightarrow 0$ are approached, $R_T \rightarrow R_{aq}$ and R_{org}, respectively (Eqs. 2.15 and 2.16 respectively) and transport

kinetics are governed by a single diffusional resistance. However, for the case where K_D does not approach these limits, neither aqueous nor organic diffusional resistances may be expected to govern solute transfer kinetics independently of the other; both diffusional resistances would contribute to a greater or lesser extent, dependent on their relative importance. In this thesis the relative importance of each resistance will be defined in terms of their ratio, γ, through

$$\gamma = R_{aq} / R_{org} \qquad 2.23$$

In the case where the resistance of the organic diffusive boundary layer contributes insignificantly to the control of solute transfer say $\leqslant 0.05\ R_T$, the system may be said to possess "aqueous diffusional control", and the resistance ratio, γ, would yield a value of $\gamma \geqslant 20$. For the case where the aqueous diffusive boundary layer contributes insignificantly to the control of solute transfer ($R_{aq} \leqslant 0.05\ R_T$), the system may be said to possess "organic diffusional control" and be described by $\gamma \leqslant 0.05$. When both diffusional layers are of importance ($0.05 < \gamma < 20$), the system may be said to possess "mixed diffusional control".

Substituting values for R_{aq} and R_{org} from Eq. 2.2 into Eq. 2.23 and rearranging gives

$$\gamma = (h_1 D_2 K_D)/(h_2 D_1) \qquad 2.24$$

Prediction of absolute values for D_1, D_2, h_1 and h_2 in the two-phase transfer cell remains problematic. Wilke and Chang (33) developed an empirical equation to predict the diffusion coefficient of low molecular weight solutes in dilute solution. The Wilke equation :

$$D_{AB} = (7.4 \times 10^{-10})\ (\phi_B M_B)^{\frac{1}{2}}\ T\ (\eta V_A^{\ -0.6}) \qquad 2.25$$

predicts the diffusion coefficient (D_{AB}) of a diffusing solute (A) in

a specified solvent (B) at an absolute temperature (T) and takes into account the associating tendencies of the solvent molecules as an association parameter (ψ_B), the molecular weight of the solvent (M_B), and the molar volume of the solute as a liquid at its normal boiling point ($\bar{V}_A$). Typical association parameters were listed by Wilke and Chang (33). Experimental determinations of D_{AB} for numerous low molecular weight solutes of the type used in the present study in various solvents fell within 10% of the values predicted by Eq. 2.25 (33, 34, 42 - 44).

Levich (35, 36) introduced an equation permitting the prediction of the boundary layer thickness for diffusion adjacent to a rotating-disk electrode in a stationary fluid. Levich's equation was shown to hold true for systems of the type depicted in Fig. 1.1a (24, 45) and can be written for h_1 and h_2 such that

$$h_1 = 1.62\ (D_1 \nu_1)^{1/3}\ \ (\nu_1/\omega)^{\frac{1}{2}} \qquad 2.26$$

$$h_2 = 1.62\ (D_2 \nu_2)^{1/3}\ \ (\nu_2/\omega)^{\frac{1}{2}} \qquad 2.27$$

where ω is the angular velocity of one phase relative to the other.

In the two-phase transfer cell with symmetric stirring, the Wilke-Chang and Levich equations may be employed to describe ratios for the aqueous and organic diffusion coefficients and diffusive boundary layer thickness (Eqs. 1.12 and 1.13 respectively) (24). Substituting for D_1/D_2 from Eq. 1.12 and h_1/h_2 from Eq. 1.13 into Eq. 2.24 and rearranging yields

$$\gamma = (R1)^{2/3}\ (R2)^{-1/6}\ (R3)^{-1/3}\ K_D \qquad 2.28$$

Eq. 2.28 shows the resistance ratio, γ (= R_{aq}/R_{org}) to be directly proportional to the partition coefficient, K_D, of the solute in a specified solvent system. The system-dependent parameters R1 (= η_1/η_2),

R2 ($= \nu_2/\nu_1$) and R3 ($= \psi_1 M_1/\psi_2 M_2$) may be estimated empirically from viscometry and densitometry determinations, while molecular weights of the solvents are known (37) and association parameters are quoted by Wilke and Chang (33). Thus Eq. 2.28 is in a form that enables estimation of the resistance ratio, $\mathcal{V}$, from some simply determined system-dependent variables.

In this Chapter the determination of interfacial transfer kinetics are described for three series of solute homologues in a variety of aqueous : organic solvent systems in a standardised two-phase transfer cell of known dimensions (Fig. 1.1a). Experimentally determined transport kinetics are compared to those predicted from a theoretical equation (Byron et al (24); Eq. 1.14). Experimental determination of the partition coefficient of the solutes in each of the solvent systems under investigation allows an estimate for the individual values of the forward, k_{12}, and reverse, k_{21}, first-order rate constants for partitioning using Eqs. 2.7 and 2.8, respectively. These values are employed to test the validity of Eqs. 2.12 and 2.13 that predict a rise in k_{12} and fall in k_{21} when the value for the solute K_D increases as a homologous series is ascended. Those theories relating to the rise, fall, or constancy of S with increase in K_D, based on observations made upon Eq. 2.14, are tested by examination of S versus K_D plots. Values for the resistance ratio, $\mathcal{V}$, are estimated for each solute and solvent system under investigation, and used to describe the diffusional control that a specified solute is subject to during its interphase transfer. Octanol, chloroform and cyclohexane are chosen as the organic phases for study after theoretical values for R1, R2 and R3 were estimated (at 35°C) from viscometry and densitometry data extracted from the literature (46), solvent association parameters quoted by Wilke (33) and solvent molecular weights (37). The organic phases were considered to possess

the ideal physical properties to test the validity of Eq. 2.14, namely that the term K_D/ν [$= h_2D_1/h_1D_2 = (R1)^{-2/3}\ (R2)^{1/6}\ (R3)^{1/3}$] for octanol, chloroform and cyclohexane gave values of, > 1, < 1 and ~ 1 respectively, (Eq. 2.14). The three solute series under investigation (Table 2.1) were chosen because the range of K_D values for each series in the solvent pairs under study allowed the predictive equation of Byron et al (24) to be tested under conditions where aqueous, mixed or organic diffusional control predominated. It will be shown that the predictive equation of Byron et al (24) may be used to successfully predict transfer kinetics as a function of K_D under conditions where all three diffusional controls may be expected to govern interfacial transport.

2.2 EXPERIMENTAL

Molar absorptivities and isosbestic points for solute series A (Table 2.1) have been reported previously (23). Isosbestic points for solutes BI through BV (Table 2.1) were determined using stock solutions ~ 5 x 10^{-5} M prepared in double distilled water (DDW). Aqueous phase pH was altered with insignificant volume changes by the addition of 1 M HCl or 1 M NaOH, the pH values recorded (Model PHM 62, Radiometer, Copenhagen, Denmark) and the absorbance determined as a function of wavelength (Beckman ACTA V spectrophotometer, USA) between 325 and 200 nm using DDW as reference. λ_{max} values for solutes CI through CV were determined from stock solutions ~ 8 x 10^{-5} M prepared in DDW adjusted to pH 5.0 $\pm$ 0.1 (CII - CV) or pH 2.0 $\pm$ 0.1 (CI) (Model PHM62, Radiometer, Copenhagen, Denmark). The absorbance was determined for CI - CV as a function of wavelength between 350 and 200 nm (Beckman ACTA V Spectrophotometer, USA) using DDW adjusted to pH 5.0 or 2.0, as appropriate, for the reference solution. Isosbestic points (series B) and λ_{max} values (series C) are documented in Table 2.2. Molal absorptivities for solutes BI, BII - BV, CI and CII - CV at wavelengths 245 nm, 267.5 nm, 264 nm and 271 nm at pH values 5.0, 5.0, 2.0 and 5.0 respectively, were determined in accord with the method described below. Stock solutions of derivatives BI - BV and CI - CV (Table 2.1) were prepared, in DDW adjusted to pH, to give concentrations in the range 0 - 1.0 x 10^{-4} M. The solutions were maintained at 37°C (Model Grant Water Bath, Grant Instruments Ltd., Cambridge, England) and pumped (Model RPD Lab. pump, Fluid Metering Inc., N.Y.) through a flow cell in a U.V. spectrophotometer (Model CE 272, Cecil Instruments, Cambridge, England). The absorbance for each solute, at each respective wavelength and pH value reported above, were determined at each concentration employed in the study using DDW as a reference (37°C). The absorbance of at least ten

TABLE 2.1

Structure and source of the solutes used in the study.

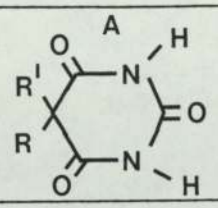

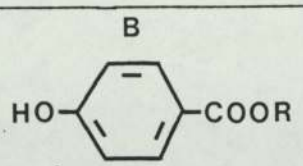

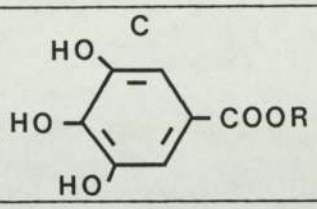

Series	Compound	R	R'	Source
A	I	CH_3CH_2-	CH_3CH_2-	a
	II	$CH_2 = CHCH_2$-	$CH_2 = CHCH_2$-	b
	III	$CH_2 = CHCH_2$-	$(CH_3)_2CH$-	b
	IV	$CH_2 = CHCH_2$-	$(CH_3)_2CHCH_2$-	c
	V	$CH_2 = CHCH_2$-	$CH_3CH_2CH(CH_3)$-	b
	VI	$CH_2 = CHCH_2$-	$CH_3(CH_2)_2CH(CH_3)$-	b
B	I	H-		d
	II	CH_3-		d
	III	CH_3CH_2-		d
	IV	$CH_3(CH_2)_2$-		d
	V	$CH_3(CH_2)_3$-		d
C	I	H-		d
	II	CH_3-		e
	III	CH_3CH_2-		e
	IV	$CH_3(CH_2)_2$-		d
	V	$CH_3(CH_2)_3$-		e

a. Hopkins and Williams, Essex, England.
b. Ganes Chemical Works, Carlstadt, N.J., U.S.A.
c. Sterling-Winthrop Research Institute, Rensselader, N.Y., U.S.A.
d. Sigma Chemical Company, St. Louis, MO., U.S.A.
e. Fluka A.G., Chem Fabric, Buchs, Switzerland.

TABLE 2.2

Aqueous phase pH, pK_a, wavelength employed for spectral analysis and molar absorptivity of the solutes used in the study.

Compound[a]	pK_a[b]	pH[c]	Wavelength	Molar absorptivity ($\pm$ SD)[e]
AI	7.88	5.0	222.5[g]	3902[i]
AII	7.60	5.0	222.5[g]	5256[i]
AIII	7.81	5.0	222.5[g]	4600[i]
AIV	7.66	5.0	222.5[g]	4313[i]
AV	7.82	5.0	222.5[g]	4659[i]
AVI	7.90	5.0	222.5[g]	4538[i]
BI	4.24	2.0	245.0[g]	10859 $\pm$ 130
BII	8.22	5.0	267.5[g]	11374 $\pm$ 58
BIII	8.28	5.0	267.5[g]	11495 $\pm$ 15
BIV	8.23	5.0	267.5[g]	11702 $\pm$ 38
BV	8.22	5.0	267.5[g]	11911 $\pm$ 65
CI	4.23[f]	2.0	264.0[h]	7625 $\pm$ 45
CII	7.78[f]	5.0	271.0[h]	9796 $\pm$ 48
CIII	7.83[f]	5.0	271.0[h]	9886 $\pm$ 67
CIV	7.84[f]	5.0	271.0[h]	10059 $\pm$ 42
CV	7.85[f]	5.0	271.0[h]	10018 $\pm$ 44

a. Table 2.1

b. Determined by titration at 37°C; ionic strength = 0.3M KCl.

c. $\pm$ 0.1; 37°C; Model PHM62, Radiometer, Copenhagen, Denmark.

d. 37°C; path length 1.0 CM; pH = column 3.

e. Ref. (49).

f. Ref. (50).

g. isosbestic point.

h. λ_{max}.

i. Ref. (23).

different concentrations were determined in triplicate for each derivative. Rectilinear plots of absorbance versus molal concentration were subject to least squares regression analysis (47) [correlation coefficient > 0.999 ($n \geq 10$)] and displayed insignificant intercepts on the absorbance axis at zero concentration. The molar absorptivities, M_a, of each member of series B and C are documented in Table 2.2 and were determined according to

$$M_a = (Abs)_\lambda / C_1 \qquad 2.29$$

where $(Abs)_\lambda$ refers to the absorbance value at the wavelength used for spectral analysis, λ, and C_1 refers to the aqueous phase molal concentration. Molal absorptivities for solutes BI through BV were shown to change insignificantly in the presence of organic phase saturation using either octanol, chloroform or cyclohexane (Spectrograde, Fisons Ltd, Loughborough., England) as the organic phase.

pK_a values for series A and B at constant ionic strength (0.3 M) using potassium chloride (A.R. Grade, Fisons Ltd., Loughborough, England) were estimated in triplicate at 37°C. Stock solutions approximately 5×10^{-3} M were prepared for solutes AI through AVI and BI through BIV, and approximately 2.5×10^{-3} M for solute BV in 0.3 M KCl solution. Prior to titration, 35 ml aliquots of the stock solution were equilibrated at 37 ± 0.1°C (Model Churchill Water Bath, Churchill Instruments Ltd., England) in a jacketed glass cell. The solutions were titrated at 37°C using a combined titration assembly (Model TTA 60, Radiometer, Copenhagen, Denmark) and autoburette (Model ABU12, Radiometer, Copenhagen, Denmark) using 0.1M NaOH (Model TTT 2, Radiometer, Copenhagen, Denmark) as the titrant. Changes in pH were recorded (Model SBR 3 Titrigraph, Radiometer, Copenhagen, Denmark) as a function of alkali added. Volume changes were insignificant and each pK_a estimated from plots of pH versus volume

added according to the method of Albert et al (48). Values for pK_a are documented in Table 2.2. pK_a values were shown to be independent of titrant composition and organic phase saturation of the aqueous phase.

The kinetics of transfer were studied for three series of non-ionised solutes [A (5, 5' - disubstituted barbituric acids), B (1 - alkyl monosubstituted parahydroxybenzoic acids) and C (3, 4, 5 - alkyl substituted trihydroxybenzoic acids); Table 2.1] in the two-phase transfer cell (Fig. 1.1a) containing equal volumes of aqueous and organic phases($V_1 = V_2 = V = 90$ ml). The two-phase transfer cell used in the study (Fig. 1.1a) was made of glass with an internal diameter of 6.0 cm, internal height of 7.5 cm and employed a double bladed glass paddle stirrer of diameter 3.7 cm, individual blade width of 0.8 cm and inter-blade distance of 2.8 cm, positioned 1.4 cm from the interface in each phase. Organic phases comprised either octanol, chloroform or cyclohexane (Spectrograde, Fisons Ltd., Loughborough, England) pre-equilibrated with an aqueous phase of 0.3 molal potassium chloride (A.R. Grade, Fisons Ltd., Loughborough, England) adjusted to pH by the addition of 1 M HCl or 1 M NaOH prior to solute introduction. Values for pH were chosen to ensure all solutes were insignificantly ionised (< 1%) and are documented in Table 2.2. During a transfer experiment pH varied < 0.1 pH unit thereby eliminating the need for buffers in the system. Pre-equilibration was effected by stirring for > 8 hrs prior to solute introduction. During a transfer experiment the phases were stirred symmetrically (Model RZR 50, Heidolph, West Germany) at 100 $\pm$ 0.5 rpm. Solutes were introduced as a 1 ml bolus into either the aqueous (methanolic bolus; aqueous : octanol and aqueous : chloroform systems) or organic (chloroform bolus; aqueous : cyclohexane systems) phase in concentrations to produce absorbances in the aqueous phase ranging 0 to 0.9 absorbance units. The aqueous phase

was pumped (Model RPD lab. pump, Fluids Metering Inc., Oyster Bay, N.Y.) through a flow cell in a spectrophotometer (Model CE 272, Cecil Instruments Cambridge, England). The concentration in the aqueous phase (C_1) was continuously monitored by automatically recording (Model J.J. CR453 recorder, J.J. Lloyd Instruments Ltd., Southampton, England) the absorption as a function of time at wavelengths according to Table 2.2. Control experiments monitoring solute absorbances in the absence of the organic phase at 37 $\pm$ 0.1°C showed that solutes series A, B and C were stable for the time course of a kinetic determination ($<$2% degradation during a 5 hour period). A temperature of 37 $\pm$ 0.1°C was maintained throughout a kinetic run.

Organic : aqueous partition coefficients, K_D, and their concentration dependence in each solvent pair were estimated in triplicate for each solute at 37°C. Values of K_D were determined by equilibrating the solute by shaking (Grant Water Bath, Grant Instruments Ltd., Cambridge, England) for $>$24 hours at 37 $\pm$ 0.1°C in each of the previously defined solvent systems. Initial concentrations in the aqueous phase at time t = 0, C_1^o, were adjusted to represent the range of concentrations found in the transfer cell experiments. The phase ratio, r' (organic/aqueous), was adjusted such that the concentration in the aqueous phase at time t = ∞, C_1^∞, gave absorbance values $>$0.05 absorbance units and varied from between 500 and 0.1 dependent upon the lipophilicity of the solute under study. Initial and final solute concentrations in the aqueous phase were determined spectrophotometrically (Model CE 272, Cecil Instruments, Cambridge, England) and K_D calculated from

$$K_D = \left[(C_1^o - C_1^\infty)\, r'\right] / C_1^\infty \qquad 2.30$$

Values for k_{12} and k_{21} were estimated from knowledge of the transfer kinetics and partition coefficient of the solute at 37°C using Eqs. 2.7 and 2.8, respectively.

The viscosities and densities of each of the mutually saturated solvent systems employed in the study were determined in triplicate relative to water at 37 $\pm$ 0.1°C using an Ostwald U-tube viscometer and a 25 cm^3 specific gravity bottle. Mean values for η and ρ enabled estimation of R1 (= η_1/η_2, where η is viscosity) and R2 (= ν_2/ν_1, where $\nu = \eta/\rho$ and ρ is density). Association parameters, ψ, (33) and molecular weights, M, of the pre-equilibrated aqueous and organic phases were assigned values as if they were pure solvents and enabled estimation of R3 (= $\psi_1 M_1/\psi_2 M_2$).

The theoretical dependence of S (= $k_{12} + k_{21}$) upon K_D was determined for each system using Eq. 1.14 after calculating an average value for the cell constant $(D_1A)/(V_1h_1)$ from estimates of $(D_1A)/(V_1h_1)$ for each solute : solvent system under study using Eq. 1.15. Theoretical values were compared to those experimentally determined from the negative log : linear slopes of plots of ln (transferable concentration) versus time based on Eq. 2.1 after least squares regression analysis (47).

2.3 RESULTS AND DISCUSSION

The sum of the forward and reverse first-order rate constants for partitioning, S (= $k_{12} + k_{21}$; Scheme 2.1) have been determined for each compound in solute series A, B and C (Table 2.1) in a standardised two-phase transfer cell (Fig. 1.1a) containing equal volumes of an aqueous and organic phase. S values were estimated from first-order plots of ln (transferable concentration) versus time based on Eq. 2.1 and were linear for > 95% of the partitioning process, for all solutes studied, in each solvent system at 37°C, 100 rpm (see Appendix C for a worked example). Observed terminal slopes, S_{obs}, are documented in Table 2.3 for series A in aqueous : octanol, aqueous : chloroform and aqueous : cyclohexane systems and for series B and C in an aqueous : octanol system. The terminal slopes (S_{obs}) were determined in each case by least squares regression analysis (correlation coefficient > 0.999, n $\geq$ 10).

In order to test the predictive theory (Eq. 1.14) derived by Byron et al (24) a cell constant, $(D_1A)/(V_1h_1)$, was estimated for each solute in each of the solvent systems under investigation using Eq. 1.15, from knowledge of the partitioning kinetics, S_{obs}, and partition coefficient of the solute (Table 2.3) and the system-dependent variables R1, R2 and R3 (Table 2.4). Partition coefficients were shown to be concentration independent over the range employed for a kinetic run (Table 2.5). Theoretical values for S were generated using Eq. 1.14 with the coefficient $(D_1A)/(V_1h_1)$ held constant at their mean values at 37°C, 100 rpm (Table 2.6) and are recorded as S_{th} in Table 2.3. The percent error involved when determining S from Eq. 1.14 (S_{th}) as opposed to experimentally in the two-phase transfer cell (S_{obs}) at 37°C, 100 rpm is shown in Table 2.3 to be < 10%.

TABLE 2.3

Organic/aqueous phase partition coefficients and theoretical and experimental estimates for S (= $k_{12} + k_{21}$) for each solute studied in the transfer cell (100 rpm, 37°C).

COMPOUND[a]	ORGANIC PHASE	γ [b]	K_D [c]	S_{obs} [d]	S_{th} [e]	PERCENT ERROR[f]
AI		1.6	0.82	3.37	3.31	- 1.8
AII		5.9	2.98	2.88	2.75	- 4.5
AIII	CHLOROFORM	6.9	3.51	2.52	2.71	+ 7.5
AIV		17	8.35	2.53	2.54	+ 0.4
AV		21	10.4	2.47	2.53	+ 2.0
AVI		103	52.2	2.53	2.43	- 4.0
AI		0.003	0.003	3.40	3.39	- 0.3
AII		0.008	0.007	3.57	3.39	- 5.0
AIII	CYCLOHEXANE	0.016	0.014	3.28	3.38	+ 3.0
AIV		0.047	0.041	3.48	3.37	- 3.2
AV		0.069	0.061	3.32	3.36	+ 1.2
AVI		0.25	0.222	3.15	3.31	+ 5.1
AI		1.4	4.8	7.20	7.19	- 0.1
AII		4.2	14.4	8.10	8.81	+ 8.8
AIII	OCTANOL	8.5	29.1	9.68	9.44	- 2.5
AIV		20	69.6	10.0	9.86	- 1.4
AV		25	84.9	10.3	9.92	- 3.7
AVI		70	239	9.87	10.1	+ 2.3
BI		8.7	29.9	6.85	7.53	+ 9.9
BII		23	79.2	7.98	7.89	- 1.1
BIII	OCTANOL	68	235	8.38	8.05	- 3.9
BIV		244	837	8.30	8.11	- 2.3
BV		527	1809	8.25	8.12	- 1.6
CI		0.5	1.64	3.85	3.48	- 9.6
CII		1.7	5.69	4.97	4.90	- 1.4
CIII	OCTANOL	4.7	16.3	5.60	5.86	+ 4.6
CIV		21	71.9	6.32	6.46	+ 2.2
CV		71	242	6.23	6.61	+ 6.1

a. Table 2.1; A, B and C refer to compound series.

b. Equation 2.28.

c. Observed, mean of 3 determinations.

d. $(k_{12} + k_{21})$ based on kinetic analysis; Eq. 2.1; $sec^{-1} \times 10^4$.

e. Equation 1.14; expressed in $sec^{-1} \times 10^4$.

f. $100\ (S_{th} - S_{obs})/S_{obs}$.

TABLE 2.4

Physicochemical data for mutually saturated aqueous and organic phases employed in the study, 37°C.

Parameter	organic phase[a]		
	chloroform	cyclohexane	octanol
η_1 (poise x 10^{-2})	0.711	0.687	0.697
η_2 (poise x 10^{-2})	0.491	0.704	4.423
ν_1 (= η/ρ)	0.706	0.682	0.691
ν_2 (= η/ρ)	0.337	0.923	5.40
ρ_1 (g.cm^{-3})	1.007	1.008	1.008
ρ_2 (g.cm^{-3})	1.456	0.763	0.819
ϕ_1[b]	2.6	2.6	2.6
ϕ_2[b]	1.0	1.0	1.0
M_1[b]	18.02	18.02	18.02
M_2[b]	119.38	84.16	130.23
R1 (= η_1/η_2)	1.448	0.976	0.158
R2 (= ν_2/ν_1)	0.478	1.354	7.810
R3 (= $\phi_1 M_1/\phi_2 M_2$)	0.392	0.557	0.359
$(R1)^{-2/3}$	0.781	1.016	3.422
$(R2)^{1/6}$	0.884	1.052	1.409
$(R3)^{1/3}$	0.732	0.823	0.711
$[(R1)^{-2/3}(R2)^{1/6}(R3)^{1/3}]$	0.506	0.879	3.428

a. Saturated with aqueous phase.

b. Pure solvent.

TABLE 2.5

The effect of initial concentration upon the organic : aqueous equilibrium partition coefficient, K_D, for solute AIII in aqueous : octanol, aqueous : chloroform and aqueous : cyclohexane systems. The results are typical of each of the solute : solvent systems employed in the present study.

Organic phase	Initial concentration in aqueous phase M	Equilibrium partition coefficient[a] (mean $\pm$ SD[b])
Octanol	1.12×10^{-4}	28.3 ± 0.31
	8.7×10^{-5}	28.9 ± 0.21
	7.0×10^{-5}	30.1 ± 0.48
Chloroform	1.2×10^{-4}	8.29 ± 0.12
	7.5×10^{-5}	8.45 ± 0.18
	6.2×10^{-5}	8.32 ± 0.11
Cyclohexane	1.1×10^{-4}	0.014 ± 0.0006
	9.1×10^{-5}	0.013 ± 0.006
	7.1×10^{-5}	0.014 ± 0.014

a. Organic/aqueous.

b. Standard deviation (49).

TABLE 2.6

Estimates for the coefficient $(D_1A)/(V_1h_1)$ for each solute : solvent system under study 37°C, 100 rpm.

Compound[a]	Organic Phase	$(D_1A)/(V_1h_1)$[b]	Average $(D_1A)/(V_1h_1)$ $\pm$ SD[c]
AI		2.45	
AII		2.52	
AIII	Chloroform	2.24	2.41
AIV		2.40	($\pm$ 0.11)
AV		2.36	
AVI		2.51	
AI		2.99	
AII		3.14	
AIII	Cyclohexane	2.89	2.98
AIV		3.08	($\pm$ 0.11)
AV		2.94	
AVI		2.84	
AI		10.2	
AII		9.38	
AIII	Octanol	10.5	10.2
AIV		10.3	($\pm$ 0.44)
AV		10.6	
AVI		9.97	
BI		7.39	
BII		8.22	8.13
BIII	Octanol	8.47	($\pm$ 0.43)
BIV		8.32	
BV		8.26	
CI		7.40	
CII		6.78	6.68
CIII	Octanol	6.39	($\pm$ 0.44)
CIV		6.53	
CV		6.29	

a. Table 2.1.

b. Eq. 1.5; $sec^{-1} \times 10^{4}$.

c. Standard deviation (49).

Figure 2.1 shows the experimental dependence of S upon K_D for series C in an aqueous : octanol system (✪), and series A in an aqueous : chloroform (□) and aqueous : cyclohexane system (●). The solid profiles of S versus K_D in Fig. 2.1 are theoretical curves generated using Eq. 1.14 with $(D_1A)/(V_1h_1)$ held constant at their previously estimated mean values (Table 2.6). Figure 2.1 and Table 2.3 show the excellent agreement between theory and experiment and attest to the validity of Eq. 1.14 in describing solute transfer kinetics in the two-phase transfer cell.

Figure 2.1 also shows how S may rise (series C; aqueous : octanol), fall (series A; aqueous : chloroform) or remain constant (series A; aqueous : cyclohexane) with increasing K_D as a homologous series is ascended. These observations are in accord with those based upon Eq. 2.14 which theoretically predicts such relationships.

Eq. 2.12 and 2.13 theoretically predict that the individual values for the forward, k_{12}, and reverse, k_{21}, first-order rate constants for partitioning should rise (Eq. 2.12) and fall (Eq. 2.13), respectively with increasing K_D as a homologous series is ascended. This is irrespective of those observations based upon Eq. 2.14 that show S (= $k_{12} + k_{21}$) may rise, fall or remain constant with increasing K_D. In order to test these theories, (Eqs. 2.12 and 2.13), theoretical solutions for k_{12} and k_{21} were derived from Eq. 1.14 to allow the generation of theoretical profiles of k_{12} and k_{21} as a function of K_D in an analogous manner to the generation of S versus K_D profiles using Eq. 1.14 of Byron et al (24). Assuming $V_1 = V_2 = V$ ($r = 1$), substitution of S from Eq. 1.14 into equations 2.7 and 2.8, and rearranging gives

$$k_{12} = [(D_1A)/(V_1h_1)]\left[K_D/[K_D + (R1)^{-2/3}(R2)^{1/6}(R3)^{1/3}]\right]$$

$$= [(D_1A)\ (V_1h_1)][1/(1 + \nu^{-1})] \qquad 2.31$$

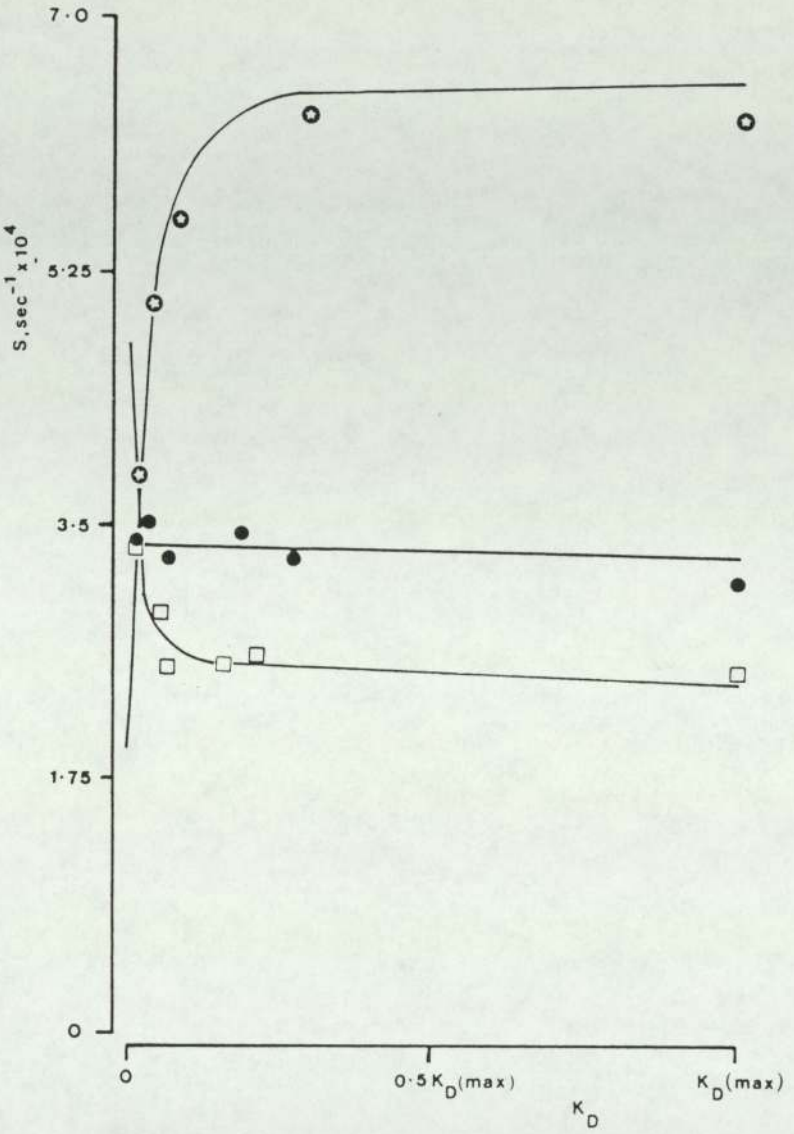

Figure 2.1 Theoretical (solid curves; Eq. 1.14) and experimental dependence of S on K_D for (✪) series C in octanol : aqueous, (●) series A in cyclohexane : aqueous and (□) series A in chloroform : aqueous systems at 100 rpm, 37°C. The term K_D (max) is the largest observed partition coefficient for the solute series in the solvent under investigation (Table 2.3). The abcissa axis (K_D) is linear.

and

$$k_{21} = [(D_1A)/(V_1h_1)] \left[1/ [K_D + (R1)^{-2/3}(R2)^{1/6}(R3)^{1/3}] \right]$$

$$= [(D_1A)/(V_1h_1)] [1/K_D \ (1 + \gamma^{-1})] \qquad 2.32$$

Eqs. 2.31 and 2.32 are now in a form that allow generation of theoretical curves of k_{12} and k_{21} as a function of K_D in an analogous manner to the generation of S versus K_D profiles using Eq. 1.14, namely $(D_1A)/(V_1h_1)$ values for each solute : solvent system are estimated after rearrangement of Eqs. 2.31 and 2.32 to give

$$(D_1A)/(V_1h_1) = k_{12} \ [K_D + (R1)^{-2/3}(R2)^{1/6}(R3)^{1/3}]/K_D$$

$$= k_{12} \ (1 + \gamma^{-1}) \qquad 2.33$$

and

$$(D_1A)/(V_1h_1) = k_{21}[K_D + (R1)^{-2/3}(R2)^{1/6}(R3)^{1/3}]$$

$$= k_{21} [K_D \ (1 + \gamma^{-1})] \qquad 2.34$$

Mean values for the coefficient $(D_1A)/(V_1h_1)$ are estimated for each series in each of the solvent systems, held constant, and used in Eqs. 2.31 and 2.32 to generate theoretical values for k_{12} and k_{21}, respectively as a function of K_D or γ (directly proportional to K_D; Eq. 2.28). For a given solute in a specified solvent system Eqs. 1.15, 2.33 and 2.34 provide the same value for $(D_1A)/(V_1h_1)$ given either S, k_{12} or k_{21}, respectively and the system-dependent variables r, K_D, R1, R2 and R3.

Figure 2.2 shows the agreement between the theoretical (Eqs. 2.31 and 2.32 using mean $(D_1A)/(V_1h_1)$ values as documented in Table 2.6 and experimental [$k_{12} = (S_{obs} \ K_D)/(K_D + 1)$; $k_{21} = S_{obs}/(K_D + 1)$; Table 2.7] dependence of k_{12} and k_{21} upon γ (directly proportional to K_D; Eq. 2.28; Table 2.3) for solute series A in aqueous : octanol (✱),

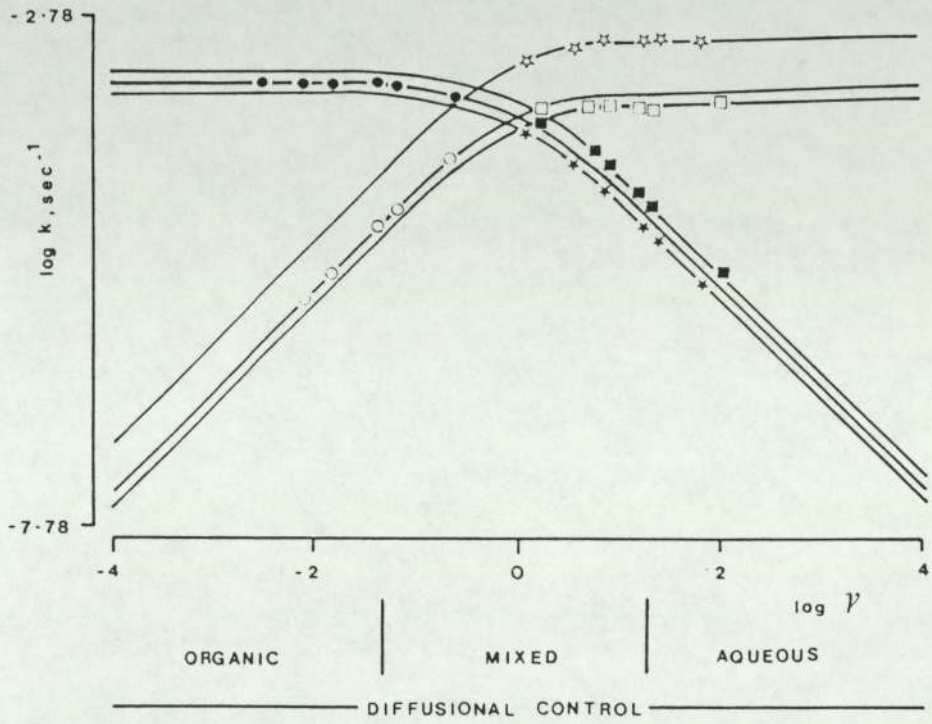

Figure 2.2 Theoretical (solid curves, Eqs. 2.31 and 2.32) and experimental dependence of the first-order forward, k_{12} (open symbols), and reverse, k_{21} (closed symbols), rate constants for partitioning for series A (Table 2.1) in (☆) octanol : aqueous, (○) cyclohexane : aqueous and (□) chloroform : aqueous systems upon the resistance ratio, ν (proportional to K_D), at 100 rpm, 37°C.

TABLE 2.7

Estimates for k_{12} and k_{21} for series A (Table 2.1) in each of the solvent systems employed in the study.

Compound[a]	Organic phase	log P[b]	k_{12}[c]	log k_{12}	k_{21}[d]	log k_{21}
AI		0.20	1.52	- 3.818	18.5	- 3.733
AII		0.77	2.16	- 3.666	7.24	- 4.140
AIII	chloroform	0.84	1.96	- 3.708	5.59	- 4.253
AIV		1.23	2.26	- 3.646	2.71	- 4.567
AV		1.83	2.25	- 3.648	2.17	- 4.664
AVI		2.01	2.48	- 3.606	0.48	- 5.319
AI		- 2.52	1.02	- 3.991	33.9	- 3.469
AII		- 2.09	2.48	- 3.606	35.4	- 3.451
AIII	cyclohexane	- 1.79	4.53	- 3.344	32.3	- 3.491
AIV		- 1.33	0.14	- 4.854	33.4	- 3.476
AV		- 1.16	0.19	- 4.721	31.3	- 3.504
AVI		- 0.60	0.57	- 4.244	25.8	- 3.588
AI		0.15	5.97	- 3.224	12.4	- 3.907
AII		0.67	7.57	- 3.121	5.26	- 4.279
AIII	octanol	0.93	9.37	- 3.028	3.22	- 4.492
AIV		1.30	9.90	- 3.004	1.42	- 4.848
AV		1.39	10.2	- 2.991	1.19	- 4.924
AVI		1.85	9.82	- 3.008	0.42	- 5.377

a. Table 2.1.

b. Eq. 2.28.

c. Eq. 2.31; $sec^{-1} \times 10^{4}$.

d. Eq. 2.32; $sec^{-1} \times 10^{5}$.

aqueous : chloroform (■) and aqueous : cyclohexane (●) systems. For presentation purposes rate constants and γ are expressed in logarithmic form. Plots of log k_{obs} (where $k_{obs} = k_{12}$ or k_{21}) versus log K_D are more frequently used to present this type of data. However, because the regions of organic, aqueous and mixed diffusional control are dependent upon the resistance ratio, γ ($= (R1)^{2/3} (R2)^{-1/6} (R3)^{-1/3} K_D$) and not K_D alone, the use of γ as the independent variable in Fig. 2.2 enables these regions to be displayed in a system-independent fashion. Thus the abcissa of Fig. 2.2 shows the three distinct regions of diffusional control, described previously, for each solvent system at 37°C. Figure 2.2 clearly demonstrates how k_{12} and k_{21} rise and fall, respectively with increasing K_D, independent of the solvent employed in the study, despite earlier observations (cf Fig. 2.1 and Table 2.3) that theoretical and experimentally determined values of S ($= k_{12} + k_{21}$); Scheme 2.1) for series A (Table 2.1) may rise (aqueous : octanol), fall (aqueous : chloroform) or remain constant (aqueous : cyclohexane) as the partition coefficient increases. The observed rise in k_{12} and fall in k_{21} with increase in K_D as a homologous series is ascended are in accord with those theoretically predicted by 2.12 and 2.13, respectively.

Values for γ in the two-phase transfer cell, ≤ 0.05, ≥ 20 or in the range 0.05 - 20 imply organic, aqueous or mixed diffusional control respectively. Table 2.3 documents values for γ for each solute : solvent system investigated in the present study. Table 2.3 shows cases of organic diffusional (solutes AI through AIV in aqueous : cyclohexane system) aqueous diffusional (solutes AV and AVI in aqueous : chloroform system, solutes AIV - AVI, BII - BV and CIV - CV in aqueous : octanol system) and mixed diffusional control (remaining solute : solvent systems). Thus the theory for dependence of S upon K_D (Eq. 1.14) (24) has been tested and shown to hold true

under conditions where each of the diffusional controls are expected to predominate.

The introduction of γ as a means of estimating the diffusional resistance a particular solute is subject to during interfacial transfer in a specified solvent pair, allows definition for the maximum and minimum K_D values required in a solute series to implement the approach of Waterbeemd et al (28). Values for K_D within a solute series should be chosen such that values for γ range ≤ 0.05 (organic diffusional control) and ≥ 20 (aqueous diffusional control) to allow the plateau regions k_{org} and k_{aq}, respectively, and consequently β, to be defined. Waterbeemd et al terms k_{aq}, k_{org} and β (25 - 29) are equivalent to $k_{12(K_D \to \infty)}$ (Eq. 2.19), $k_{21(K_D \to 0)}$ (Eq. 2.22) and γ/K_D [$= (R1)^{2/3}\ (R2)^{-1/6}\ (R3)^{-1/3}$] respectively, in this Chapter.

Examination of Eq. 2.28 shows the term γ to be dependent upon both solvent (densities, viscosities, association parameters and molecular weights of aqueous and organic phases) and solute (K_D) parameters. In this Chapter, experimental verification of the theory for dependence of S upon K_D (Eq. 1.14) using solute series A, B and C (Table 2.1) involved changes in solvent system dependent parameters to allow the theory (Eq. 1.14) to be tested under conditions where organic, aqueous or mixed diffusional control were expected to predominate. Ideally, Eq. 1.14 should also be tested under conditions where values for γ indicate aqueous, organic and mixed diffusional control, when solvent system parameters are held constant.

Waterbeemd et al (28) employed a two-phase transfer cell containing equal volumes of aqueous and organic (either octanol or di-n-butyl ether) phases to investigate the transport kinetics of a large series of closely related sulphonamide derivatives (Table 2.8) at 40 rpm, 20°C. log (transport rate constants) determined by

TABLE 2.8

Structures, organic/aqueous partition coefficients and $(D_1A)/(V_1h_1)$[b] values for solutes studied by Waterbeemd et al (28) in the two-phase transfer cell 20°C, 40 rpm.

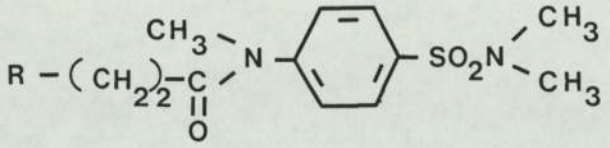

Compound	R	Octanol		di-n-butyl ether	
		K_D[a]	$(D_1A)/(V_1h_1)$[b]	K_D[a]	$(D_1A)/(V_1h_1)$[b]
W1	$SOCH_3$	0.213	3.72	0.007	6.36
W2	$CONH_2$	0.275	3.71	0.009	6.04
W3	$NHCOCH_3$	0.444	3.86	0.018	6.25
W4	OH	0.548	4.49	0.023	6.05
W	OSO_2CH_2	0.855	4.35	0.042	6.65
W6	CN	0.962	4.00	0.041	7.15
W7	$COCH_3$	1.58	3.95	0.085	7.90
W8	$OCOCH_3$	1.80	3.89	0.115	8.10
W9	NO_2	1.98	4.28	0.157	6.11
W10	OCH_3	2.16	3.39	0.139	8.23
W11	CO_2CH_2	2.67	3.79	0.199	8.12
W12	H	5.12	3.88	0.436	11.4
W13	$OCOC_2H_5$	5.89	3.14	0.527	8.04
W14	SCN	6.84	3.02	0.518	8.72
W15	$CO_2C_2H_5$	6.92	3.22	0.679	8.05
W16	C_2H	7.52	3.24	1.98	10.1
W17	Cl	9.52	2.92	1.27	10.5
W18	SCH_3	9.86	2.87	0.98	9.97
W19	Br	13.5	2.97	1.91	9.47
W20	CH_3	15.4	2.87	1.52	10.1
W21	$n\text{-}OC_3H_7$	18.3	2.16	1.90	8.62
W22	I	24.8	2.51	4.10	9.57
W23	C_2H_5	42.8	2.39	4.97	10.1
W24	C_6H_5	54.1	2.57	20.2	9.69
W25	$-C_3H_7$	143	2.37	25.9	9.54
W26	$-C_4H_9$	509	2.32	164	9.47
W27	$-C_5H_{11}$	1227	2.15	627	8.89
Average			3.26		8.49
$\pm$ SD[c]			$\pm$ 0.501		$\pm$ 1.54

a. organic/aqueous.

b. Eq. 1.15.

c. Standard deviation (49).

Waterbeemd et al (28) are documented in Tables 2.9 and 2.10 for the aqueous : octanol and aqueous : di-n-butyl ether systems, respectively. Also documented are resistance ratio values, $\mathcal{Y}$, and theoretical values for log k_{12} and log k_{21} generated using Eqs. 2.31 and 2.32, respectively with $(D_1A)/(V_1h_1)$ held at their mean values as shown in Table 2.8. Values for K_D and the physicochemical data necessary to employ Eqs. 2.31 and 2.32 are documented in Tables 2.8 and 2.11, respectively (28). Figures 2.3 and 2.4 show the theoretical (solid profiles; Eqs. 2.31 and 2.32) and experimental[(✱) k_{12} and (✲) k_{21}] dependence of log k_{obs} on log $\mathcal{Y}$ for the sulphonamide series in aqueous : octanol and aqueous : di-n-butyl ether systems, respectively. Figures 2.3 and 2.4 show the agreement between the theoretical and experimental estimates of log k_{obs}. The % errors involved in estimating theoretical values for log k_{obs} (Eqs. 2.31 and 2.32) as opposed to experimentally in the two-phase transfer cell 40 rpm, 20°C are shown in Tables 2.9 and 2.10 to be $< 5\%$. These errors compare favourably to those observed by Waterbeemd et al (28) for the prediction of log k_{obs} values as a function of log K_D using their methods. Tables 2.9 and 2.10 attest to the validity of Eqs. 2.31 and 2.32, typical errors between theory and experiment frequently ranged $< 2\%$. Tables 2.9 and 2.10 and Figs. 2.3 and 2.4 show cases of organic diffusional, aqueous diffusional and mixed diffusional control. Thus the predictive theory has been tested and shown to hold true under conditions where each of the diffusional controls are expected to predominate when either the solute or solvent system-dependent parameters in $\mathcal{Y}$ are held constant.

TABLE 2.9 Theoretical and experimental estimates for k_{12} and k_{21} and the resistance ratio, γ, in the aqueous : octanol system 20°C, 40 rpm.

Compound[a]	γ[b]	log γ	log $k_{12(obs)}$[c]	log $k_{12(th)}$[d]	% error[e]	log $k_{21(obs)}$[c]	log $k_{21(th)}$[f]	% error[e]
W1	0.046	- 1.33	-4.777	-4.836	1.2	-4.106	-4.165	1.4
W2	0.06	- 1.22	-4.672	-4.727	1.2	-4.113	-4.166	1.3
W3	0.09	- 1.04	-4.459	-4.534	1.7	-4.111	-4.182	1.7
W4	0.12	- 0.92	-4.315	-4.455	3.2	-4.056	-4.19	3.5
W5	0.19	- 9.72	-4.160	-4.287	3.0	-4.092	-4.219	3.1
W6	0.21	- 0.68	-4.154	-4.245	2.2	-4.136	-4.228	2.2
W7	0.35	- 0.46	-3.996	-4.076	2.0	-4.190	-4.275	2.0
W8	0.39	- 0.40	-3.957	-4.033	1.9	-4.217	-4.289	1.8
W9	0.44	- 0.36	-3.886	-4.004	3.0	-4.182	-4.301	2.8
W10	0.48	- 0.32	-3.962	-3.978	0.4	-4.296	-4.312	0.4
W11	0.59	- 0.22	-3.852	-3.918	1.7	-4.277	-4.345	1.6
W12	1.13	0.05	-3.687	-3.762	2.0	-4.396	-4.471	1.7
W13	1.29	0.11	-3.750	-3.734	0.4	-4.520	-4.503	0.3
W14	1.50	0.18	-3.742	-3.707	-0.9	-4.577	-4.542	-0.8
W15	1.52	0.18	-3.710	-3.715	0.1	-4.550	-4.492	-1.3
W16	1.65	0.22	-3.695	-3.692	-0.1	-4.571	-4.569	-0.1
W17	2.09	0.32	-3.703	-3.656	-1.2	-4.686	-4.635	-1.1
W18	2.17	0.34	-3.806	-3.651	-3.9	-4.693	-4.645	-1.0
W19	2.97	0.47	-3.653	-3.613	-1.1	-4.784	-4.743	-0.8
W20	3.39	0.53	-3.654	-3.599	-1.5	-4.841	-4.787	-1.1
W21	4.03	0.61	-3.656	-3.582	-2.0	-4.919	-4.845	-1.5
W22	5.46	0.74	-3.673	-3.559	-3.1	-5.067	-4.954	-2.2
W23	9.42	0.97	-3.672	-3.530	-3.9	-5.303	-5.161	-2.7
W24	11.9	1.08	-3.624	-3.522	-2.8	-5.357	-5.255	-1.9
W25	32	1.50	-3.640	-3.501	-3.8	-5.795	-5.656	-2.4
W26	90	1.95	-3.640	-3.492	-4.1	-6.252	-6.103	-2.4
W27	270	2.43	-3.670	-3.488	-4.9	-6.759	-6.577	-2.7

a. Table 2.8. b. Eq. 2.28. c. Ref. (28). d. Eq. 2.31. e. 100 $(S_{th} - S_{obs})/S_{obs}$. f. Eq. 2.32.

TABLE 2.10 Theoretical and experimental estimates for k_{12} and k_{21} and the resistance ratio, γ, in the aqueous : di-n-butyl ether system 20°C, 40 rpm.

Compound[a]	γ[b]	log γ	log $k_{12(obs)}$[c]	log $k_{12(th)}$[d]	% error[e]	log $k_{21(obs)}$[c]	log $k_{21(th)}$[f]	% error[e]
W1	0.013	- 1.89	-6.099	-5.973	-2.1	-3.944	-3.818	-3.2
W2	0.016	- 1.79	-6.012	-5.865	-2.4	-3.967	-3.819	-3.7
W3	0.033	- 1.48	-5.702	-5.702	-2.3	-3.957	-3.826	-3.3
W4	0.042	- 1.38	-5.614	-5.469	-2.5	-3.976	-3.831	-3.6
W5	0.076	- 1.12	-5.328	-5.219	-2.0	-3.951	-3.842	-2.7
W6	0.075	- 1.12	-5.304	-5.231	-1.3	-3.916	3.844	-1.8
W7	0.15	- 0.82	-4.976	-4.945	-0.6	-3.905	-3.874	-0.7
W8	0.21	- 0.68	-4.855	-4.834	-0.4	-3.915	-3.895	-0.5
W9	0.29	- 0.54	-4.807	-4.724	-1.7	-4.003	-3.920	-2.1
W10	0.25	- 0.60	-4.781	-4.767	-0.3	-3.924	-3.910	-0.3
W11	0.36	- 0.44	-4.665	-4.649	-0.3	-3.966	-3.948	-0.4
W12	0.79	- 0.1	-4.299	-4.424	2.9	-3.938	-4.064	3.1
W13	0.96	- 0.02	-4.404	-4.466	2.2	-4.127	-4.118	1.4
W14	0.94	- 0.03	-4.374	-4.384	0.2	-4.088	-4.098	0.2
W15	1.23	0.09	-4.352	-4.329	-0.5	-4.184	-4.161	-0.5
W16	1.96	0.29	-4.172	-4.251	1.9	-4.205	-4.285	1.9
W17	2.31	0.36	-4.132	-4.227	2.3	-4.236	-4.331	2.2
W18	1.78	0.25	-4.192	-4.264	1.7	-4.187	-4.255	1.6
W19	3.47	0.54	-4.132	-4.183	1.2	-4.414	-4.464	1.1
W20	2.76	0.44	-4.130	-4.207	1.9	-4.314	-4.388	1.7
W21	3.45	0.54	-4.176	-4.184	0.2	-4.454	-4.462	0.2
W22	7.45	0.87	-4.072	-4.126	1.3	-4.683	-4.739	1.2
W23	9.04	0.96	-4.044	-4.116	1.8	-4.740	-4.812	1.5
W24	37	1.57	-4.023	-4.081	1.4	-5.329	-5.387	1.1
W25	47	1.67	-4.030	-4.082	1.3	-5.444	-5.495	0.9
W26	298	2.47	-4.023	-4.073	1.2	-6.240	-6.288	0.7
W27	1139	3.06	-4.053	-4.071	1.2	-6.850	-6.869	0.3

a. Table 2.8. b. Eq. 2.28. c. Ref. (28). d. Eq. 2.31. e. $100\ (S_{th} - S_{obs})/S_{obs}$. f. Eq. 2.32.

TABLE 2.11

Physiocochemical data[a] for mutually saturated aqueous and organic phases at 20°C (28).

Parameter	organic solvent: octanol	organic solvent: di-n-ethyl ether
η_1 (poise x 10^{-2})	1.002	1.002
η_2 (poise x 10^{-2})	8.892	0.700
ν_1 (= η/ρ)	1.004	1.004
ν_2 (= η/ρ)	10.77	0.911
ρ_1 g.cm^{-3}	0.9982	0.9982
ρ_2 g.cm^{-3}	0.8256	0.7684
ψ_1	2.6	2.6
ψ_2	1.0	1.0
M_1	18.02	18.02
M_2	130.23	130.23
R1 (= η_1/η_2)	0.113	1.430
R2 (= ν_2/ν_1)	10.73	0.907
R3 (= $\psi_1 M_1/\psi_2 M_2$)	0.359	0.359
$(R1)^{-2/3}$	4.290	0.787
$(R2)^{1/6}$	1.490	0.984
$(R3)^{1/3}$	0.711	0.711
$[(R1)^{-2/3}(R2)^{1/6}(R3)^{1/3}]$	4.545	0.550

a. Ref. (28).

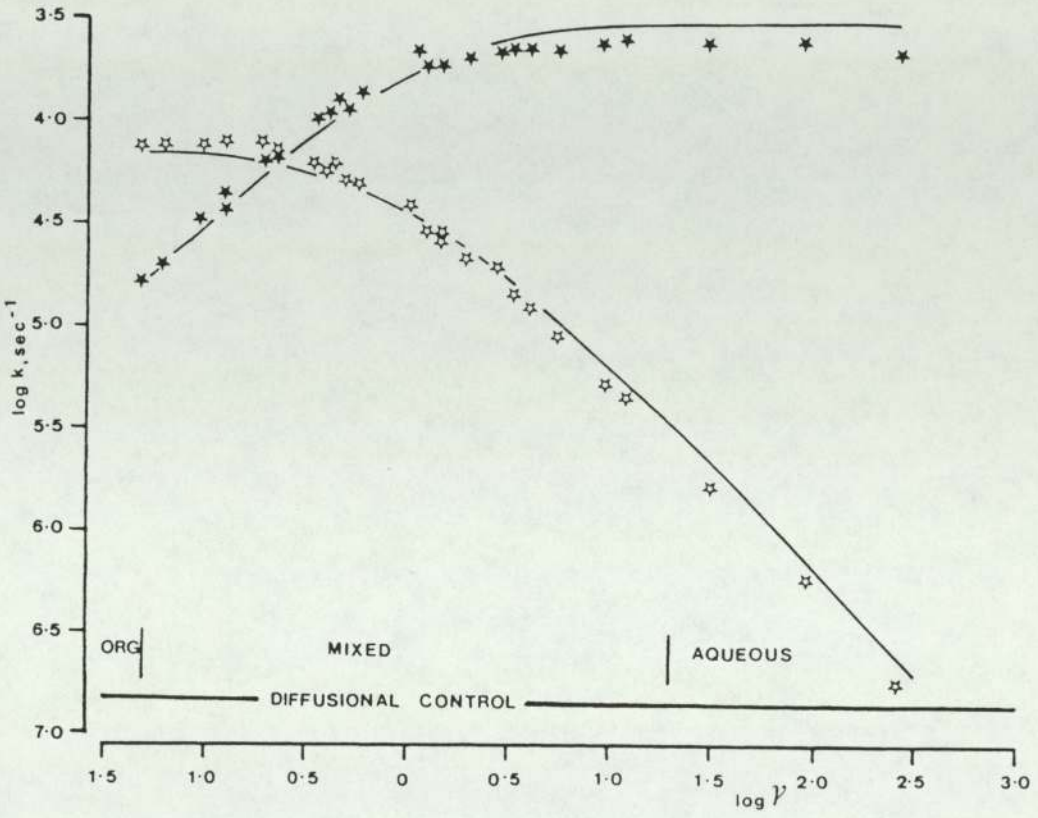

Figure 2.3 Theoretical (solid curves; Eqs. 2.31 and 2.32) and experimental dependence of the apparent first-order forward, k_{12} (closed symbols), and reverse, k_{21} (open symbols), rate constants for partitioning for solutes W1 - W27 (Table 2.8) in an aqueous : octanol system on the resistance ratio, Ψ (proportional to K_D), at 40 rpm, 20°C.

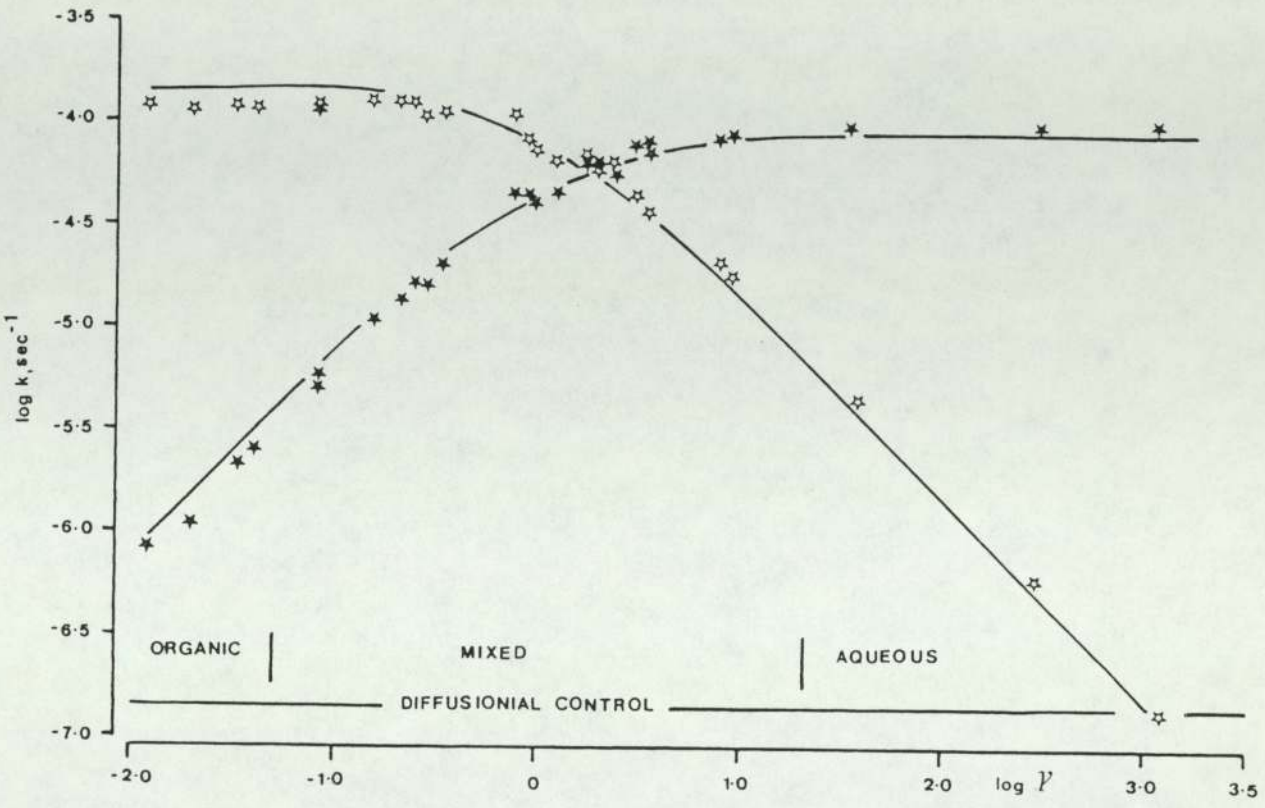

Figure 2.4 Theoretical (solid curves; Eqs. 2.31 and 2.32) and experimental dependence of the apparent first-order forward, k_{12} (closed symbols), and reverse, k_{21} (open symbols), rate constants for partitioning for solutes W1 - W27 (Table 2.8) in an aqueous : di-n-butyl ether system on the resistance ratio, Y (proportional to K_D), at 40 rpm, 20°C.

CHAPTER THREE

SOLUTE IONISATION AND AQUEOUS PHASE IONIC STRENGTH EFFECTS IN THE TWO-PHASE TRANSFER CELL

3.1 INTRODUCTION

Few authors have investigated mass transport kinetics across aqueous : organic interfaces of solutes subject to differing degrees of ionisation in the aqueous phase (1, 51, 52). Doluisio and Swintosky employed an inverted Y-tube apparatus (aqueous : cyclohexane : aqueous) to investigate the rate of solute transfer of salicylic acid from a donor aqueous phase in which pH was varied (1, 51). The same apparatus and organic phase was used by Lamy to study the transport kinetics of a variety of weak acids and bases (52). Their studies showed that essentially only the non-ionised solute partitioned (1, 51, 52). The magnitude of the experimentally observed transport rate constant, S, was shown to be dependent upon the forward, k_{12}, and reverse, k_{21}, first-order rate constants for partitioning and the fraction of non-ionised solute in the aqueous phase, fn, in accord with Eq. 3.1 (1, 52, 53).

$$S = k_{12}\, fn + k_{21} \qquad 3.1$$

The fraction of non-ionised solute in the aqueous phase of a two-phase transfer cell, fn, may be described by the Henderson-Hasselbach equation (53) which, for a weakly acidic monoprotic acid states

$$fn = C_{1n}/(C_{1n} + C_{1i}) = 1/(1 + 10^{pH-pK_a}) \qquad 3.2$$

where, C_{1n} and C_{1i} refer to the concentration in the aqueous phase of the non-ionised and ionised species, respectively. Thus, given values for the first-order forward and reverse partitioning rate constants and pK_a of the solute, it should be possible to define the characteristic sigmoidal dependence of S as a function of pH for that solute using Eq. 3.1. However, given a large series of solute homologues, prediction of the transport kinetics of any member of that series at a specified pH using Eq. 3.1 would necessitate exhaustive

experimentation to estimate the individual values for k_{12} and k_{21} of each homologue.

This Chapter documents the development of a predictive theory which allows transport rate constants of structurally related compounds to be predicted, at any specified aqueous phase pH, from knowledge of the transport kinetics, pK_a and partition coefficient of the lead compound, the pH of the aqueous phase and the partition coefficient and pK_a of the homologue. The theory is tested by comparing partitioning rate constants of a variety of weakly acidic solutes, experimentally determined in a standardised two-phase transfer cell in which aqueous phase pH is varied, to theoretical profiles generated by the predictive equation.

3.1.1 THEORY

When an ionising solute is allowed, by variation of the aqueous phase pH to possess a degree of dissociation, and assuming that only the non-ionised species may partition, then its partitioning kinetics should accord with Scheme 3.1.

Scheme 3.1

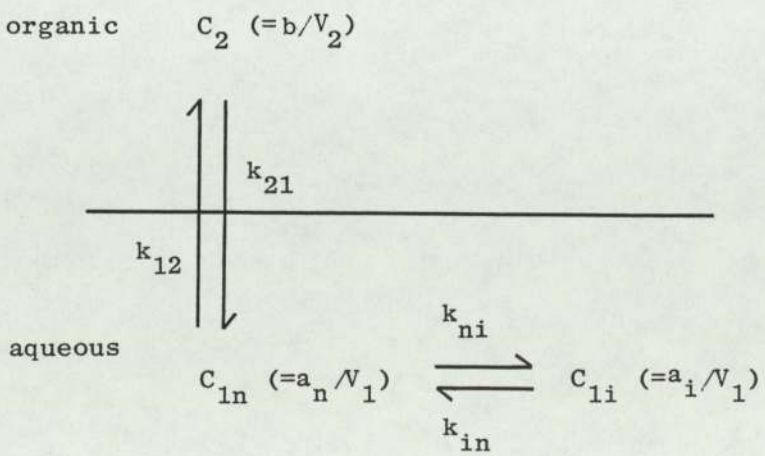

Scheme 3.1 represents simultaneous first-order partitioning of non-ionised solute with reversible aqueous phase ionisation to a non-partitioning species in the two-phase transfer cell (Figure 1.1a). Symbols k_{12} and k_{21} represent apparent first-order forward and reverse rate constants for partitioning of the non-ionised species, respectively, and k_{in} and k_{ni} refer to the forward and reverse rate constants for solute ionisation, respectively. In the organic phase of volume V_2, solute exists in the non-ionised form in an amount, b, corresponding to a concentration C_2. Solute concentrations of the non-ionised and ionised forms in the aqueous phase of volume, V_1, C_{1n} and C_{1i}, respectively, correspond to amounts a_n and a_i, respectively, and the total aqueous concentration $C_1 = a/V_1$ where a is the total amount of solute ($= a_n + a_i$), and $(a_n + a_i)/V_1 = C_{1n} + C_{1i}$.

Assuming initial conditions at time t = 0 are such that $C_1 = C_1^o$ and $C_2 = 0$, where C_1^o refers to the initial concentration in the aqueous phase ($= C_{1n}^o + C_{1i}^o$), then the amounts of solute are, according to the definition above, a ($= a_n^o + a_i^o$) $= a^o$, b = 0, where a^o is the initial amount in the aqueous phase at time t = 0.

The dependence of the apparent first-order rate constant for partitioning, S, upon pH (partial solute ionisation in the aqueous phase alone; Scheme 3.1) can be derived by writing

$$d(a_n + a_i)/dt = da/dt = -fn\, k_{12}\, a + k_{21} b \qquad 3.3$$

which is true because the ionisation equilibrium is so rapidly achieved in the aqueous phase. This rate equation is directly analogous to that describing an A to B reversible transfer and integrates (54) to give

$$(a - a^\infty) = (a^o - a^\infty) e^{-(k_{12} fn + k_{21})t} \qquad 3.4$$

Where a^∞ refers to the final amount of solute in the aqueous phase.

Division of both sides of Eq. 3.4 by V_1 and taking natural logarithims provides the first-order rate equation in terms of concentration

$$\ln (C_1 - C_1^{\infty}) = \ln (C_1^{o} - C_1^{\infty}) - (k_{12}fn + k_{21})\, t \qquad 3.5$$

Thus, a first-order plot of $\ln (C_1 - C_1^{\infty})$ versus time, t, is linear with a negative slope, S, where

$$S = k_{12}fn + k_{21} \qquad 3.6$$

A solute may be introduced as a bolus into the aqueous phase of a two-phase transfer cell at time t = 0 and its transfer kinetics, S ($= k_{12}fn + k_{21}$), estimated from C_1 versus time profiles under conditions of varying aqueous phase pH using Eq. 3.5.

When a transfer experiment conforms to Scheme 3.1, the solute is a stable weak acid and is introduced as a bolus to the aqueous phase of a two-phase transfer cell, then the flux, J, of the solute from the bulk of the aqueous phase to the bulk of the organic phase may be given by

$$J = \frac{db}{dt} = -\frac{d(a_n + a_i)}{dt} = \frac{A}{R_T}\left[C_{1n} - C_2/K_D\right] \qquad 3.7$$

where the flux, J, across an interfacial area, A, is limited by the total diffusional resistance, R_T, offered to solute transfer by the stagnant diffusive boundary layers, h, adjacent to the interface such that (8)

$$R_T = \frac{h_1}{D_1} + \frac{h_2}{D_2 K_D} \qquad 3.8$$

provided that the interface itself offers no resistance to solute transfer. Solving Eq. 3.2 for C_{1n} and substituting into Eq. 3.7 gives

$$\frac{-d(a_n + a_i)}{dt} = \frac{A}{R_T} \left[fn(C_{1n} + C_{1i}) - C_2/K_D \right] \qquad 3.9$$

Observing that $C_2 = b/V_2 = a^o - (a_n + a_i)/V_2$ where $a^o = a_n^o + a_i^o$ = initial amount of solute entered into the aqueous phase at time t = 0, and that $C_1 = C_{1n} + C_{1i} = (a_n + a_i)/V_1 = a/V_1$, Eq. 3.13 may be written in terms of amount. Thus

$$\frac{-d(a_n + a_i)}{dt} = \frac{-da}{dt} = \frac{A}{R_T} \left[\frac{fna}{V_1} - \frac{(a^o - a)}{K_D V_2} \right] \qquad 3.10$$

Integration of Eq. 3.10 using Laplace transforms (55) with respect to time, t, from t = 0 to t = t, and substitution of a^∞ for $(a_n^\infty + a_i^\infty)$ $= a^o V_1/(K_D V_2 fn + V_1)$ and S for $A(K_D V_2 fn + V_1)/R_T K_D V_1 V_2$ gives

$$\ln(a - a^\infty) = \ln(a^o - a^\infty) - St \qquad 3.11$$

which may also be written as

$$a - a^\infty = (a^o - a^\infty).e^{-St} \qquad 3.12$$

Dividing by V_1 allows conversion of Eq. 3.12 to concentration

$$(C_1 - C_1^\infty) = (C_1^o - C_1^\infty).e^{-St} \qquad 3.13$$

Thus a plot of $\ln(C_1 - C_1^\infty)$ versus time is linear with a negative slope, S, defined by

$$S = \frac{A(K_D V_2 fn + V_1)}{R_T K_D V_1 V_2} \qquad 3.14$$

Rearrangement of Eq. 3.14 gives

$$S = \frac{A\ fn}{R_T V_1} + \frac{A}{R_T K_D V_2} \qquad 3.15$$

Byron et al (8) showed that

$$k_{12} = A/R_T V_1 \qquad 3.16$$

and

$$k_{21} = A/R_T K_D V_2 \qquad 3.17$$

Substitution of k_{12} for $A/R_T V_1$ from Eq. 3.16 and k_{21} for $A/R_T K_D V_2$ from Eq. 3.17 into Eq. 3.15 gives Eq. 3.1. Thus both kinetic analysis and diffusive analysis of Scheme 3.1 show that when an ionising solute is allowed, by variation of the aqueous phase pH, to possess a significant degree of dissociation in the aqueous phase of a two-phase transfer cell, its interfacial transfer kinetics should accord with Eq. 3.1.

Substitution of R_T from Eq. 3.8 into Eq. 3.14 and rearranging gives

$$S = \frac{D_1 D_2 A \ (K_D V_2 fn + V_1)}{V_1 V_2 \ (D_2 K_D h_1 + D_1 h_2)} \qquad 3.18$$

It follows from Eq. 3.18 that if this theory and its attendant assumptions hold true for the two-phase transfer cell, given values for D_1, D_2, V_1, V_2, h_1, h_2, A, K_D, aqueous phase pH and pK_a of the solute then S (= k_{12} fn + k_{21}; Scheme 3.1) should be theoretically predictable as a function of aqueous phase pH (fn) when ionising solutes are subject to differing degrees of dissociation in the aqueous phase. The interfacial area, A, phase volumes V_1 and V_2 and the aqueous phase pH may be kept constant throughout an experiment using a standardised two-phase transfer cell. The pK_a and K_D of a given solute in a specified solvent system at fixed temperatures may be determined empirically. Indeed, both pK_a and K_D values may be predicted even for unsynthesized analogues (38, 39, 56) from a knowledge of the pK_a and K_D of a lead compound and its substituents.

However, prediction of absolute values for D_1, D_2, h_1 and h_2 remains problematic in the two-phase transfer cell. Because Eq. 3.18 is analogous to that derived by Byron et al (24) for prediction of transfer kinetics of non-ionised solutes in the two-phase transfer cell, if the only diffusing species are in the non-ionised form, (assumption; Scheme 3.1) then a similar approach to that employed by Byron et al (24) may be used to overcome the problem of estimating values for D_1, D_2, h_1 and h_2. Chapter 1 has discussed the approach of Byron et al (24). The agreement between theoretical and experimental values for S in Chapter 2 for a number of non-ionised solute series across a variety of aqueous : organic solvent systems attests to the validity of the Byron et al approach (24). Substituting for D_1/D_2 and h_i/h_2 from Eqs. 1.12 and 1.13 respectively, into Eq. 3.18 and rearranging gives

$$S = \left[\frac{D_1 A}{V_1 h_1}\right] \left[\frac{(K_D\ fn + r)}{K_D + (R1)^{-2/3}\ (R2)^{1/6}\ (R3)^{1/3}}\right] \qquad 3.19$$

Equation 3.19 is now in a form that enables prediction of S ($= k_{12}\ fn + k_{21}$; Scheme 3.1) for a solute at a specified aqueous phase pH. In an analogous way to the predictive equation of Byron et al (24) for prediction of non-ionised solute transfer kinetics in the two-phase transfer cell, the prediction of solute transfer in the presence of ionisation (Eq. 3.19) necessitates an estimation of the term $(D_1A)/(V_1h_1)$ from a knowledge of the transfer kinetics, organic : aqueous partition coefficient and pK_a of the solute, the pH of the aqueous phase and some simply determined system-dependent parameters. This estimation can be made by rearranging Eq. 3.19 to give

$$\frac{D_1 A}{V_1 h_1} = \frac{S\ [\ K_D + (R1)^{-2/3}\ (R2)^{1/6}\ (R3)^{1/3}\ ]}{(K_D\ fn + r)} \qquad 3.20$$

With fixed stirring conditions, constant temperature and constant aqueous phase volume, $A/(V_1 h_1)$ should be independent of the solute under consideration. Moreover, since only the non-ionised solute partitions, the diffusion coefficient of the chosen solute should remain independent of aqueous phase pH. The term $(D_1 A)/(V_1 h_1)$ can thus be considered constant for a given solute at each aqueous phase pH, once estimated under defined conditions in the two-phase transfer cell. Therefore Eq. 3.19 can be used to calculate S (= k_{12} fn + k_{21}; Scheme 3.1) as a function of pH (fn; Eq. 3.2) for a given solute under conditions of varying aqueous phase pH. Given the theoretical estimation of K_D and pK_a, prediction of partitioning kinetics as a function of pH should be possible, for any member of a homologous series (assuming D_1 changes insignificantly within a homologous series (41)), without exhaustive experimentation. This theory, as it pertains to a variety of weakly acidic monoprotic acids, has been evaluated in an aqueous : octanol two-phase system in which aqueous phase pH is varied. Octanol was chosen as the organic phase for investigation since the aqueous : octanol system is the most widely employed system in two-phase partitioning studies (10 - 12, 24 - 32). In each of the systems under investigation it is assumed that the ion contributing to the aqueous phase ionic strength and pH partition insignificantly into the organic phase (57, 58). In addition the degrees of aqueous phase saturation of the organic phase and organic phase saturation of the aqueous phase are assumed to remain unaffected by varying amounts of inorganic ions in the aqueous phase (59).

3.2 EXPERIMENTAL

Transport kinetics were investigated under conditions of varying aqueous phase pH and ionic strength in a standardised two-phase transfer cell (Fig. 1.1a) for barbitone, 5, 5'-diallylbarbituric acid, 5-allyl, 5'-isopropylbarbituric acid, 5-allyl, 5'-isopentylbarbituric acid, methyparahydroxybenzoate and ethylparahydroxybenzoate. Transfer kinetics determined under conditions of differing aqueous phase ionic strength were estimated according to Section 2.2, with the following modifications. The organic phase (90 ml) was octanol (Spectrograde, Fisons Ltd., Loughborough, England) preequilibrated with an aqueous phase (90 ml) comprising either potassium chloride, sodium chloride, calcium chloride or orthophosphate buffer (A.R. Grade, Fisons Ltd., Loughborough, England) solutions adjusted to pH 5.0 with molalities in the range 0 - 2.0 M. In the case of ionic strength studies employing orthophosphate buffers the aqueous phase was manufactured according to Table 3.1.

For the case of the ionisation studies, the two-phase transfer cell contained equal volumes of aqueous and organic phase such that $V_1 = V_2 = V = 100$ ml ($r = 1$) and was made of glass with an internal diameter of 6.6 cm and internal height = 8.4 cm. The cell employed a double bladed paddle stirrer of diameter 3.7 cm, individual blade width of 0.8 cm and inter-blade distance of 2.8 cm positioned 1.4 cm from the interface in each phase. A perspex lid prevented excessive evaporation losses. The organic phase comprised octan-1-ol (Spectrograde, Fisons Ltd., Loughborough, England) preequilibrated with an aqueous phase comprising either 0.3 molal orthophosphate buffer (Table 3.2) or 0.3 molal potassium chloride solutions in which aqueous phase pH were maintained constant ($\pm$ 0.2 pH unit) using a pH stat technique. In the 0.3 molal potassium chloride aqueous : octanol

TABLE 3.1

Composition of orthophosphate buffers employed in the study[a]. The final volume of each buffer solution was 1000 ml. Column 1 documents the ionic strength of the final solution.

Ionic[b] strength	KH_2PO_4[c] (g)	$Na_2HPO_4.12H_2O$[c] (g)	pH[d]
0.1	12.92	0.5405	4.84
0.2	25.84	1.0809	4.82
0.3	38.76	1.6214	4.86
0.4	51.68	2.7020	4.85
0.8	103.36	4.3237	4.89

a. Adapted from reference (60).

b. Aqueous phase; Molal.

c. A.R. Grade, Fisons Ltd., Loughborough, England.

d. $37 \pm 0.1^{o}C$; Model PHM62 Standard pH meter, Radiometer, Copenhagen, Denmark.

TABLE 3.2

The composition of 0.3 molal orthophosphate buffer solutions[a] used in the study. The final volumes of all buffer solutions was 1000 ml. The ionic strength of these solutions was 0.3 M.

KH_2PO_4[b] (g)	$Na_2HPO_4.12H_2O$[b] (g)	$Na_3PO_4.H_2O$[c] (g)	pH[d]
40.8000	-	-	4.34
38.7600	1.6214	-	4.86
27.6000	11.5399	-	5.85
16.2750	21.4371	-	6.38
7.0650	29.6513	-	6.92
3.2138	33.0134	-	7.31
0.8400	35.1608	-	7.98
-	35.7914	-	9.10
-	30.8592	3.6575	10.71

a. Adapted from ref. (60).

b. A.R. Grade, Fisons Ltd., Loughborough, England.

c. Analar Grade, BDH Chemicals Ltd., Poole, England.

d. 37 $\pm$ 0.1°C; Model PHM62 Standard pH meter, Radiometer, Copenhagen, England.

systems, after preequilibration of the two phases, a combined glass electrode (Model GK2401C, Radiometer, Copenhagen, Denmark) and titrant feed nozzle were entered through the organic phase into the aqueous phase and positioned adjacent to the lower blade of the stirrer. Initial pH was adjusted using 1M HCL or 1M NaOH and the selected pH of the transfer experiment set on the pH stat (Model SBR3 Titratigraph, Radiometer, Copenhagen, Denmark). The pH stat and titrant feed nozzle were interconnected via an autoburette (Model ABU12 Autoburette, Radiometer, Copenhagen, Denmark). Experiments were initiated by the introduction of the solute as a 1 ml methanolic bolus into the aqueous phase. Readjustment of initial pH and occasional overshoot were monitored and manually adjusted by addition of 1M HCL or 1M NaOH. In all other cases pH stat and autoburette monitored and maintained pH constant by addition of 0.1M NaOH via titrant feed nozzle. For the 0.3 molal orthophosphate buffer : octanol systems, experiments were initiated by the introduction of 1ml methanolic bolus into the aqueous phase and pH maintained constant throughout a kinetic run by the intrinsic buffer components. The remaining experimental conditions necessary to estimate transport kinetics of the chosen solutes as a function of aqueous phase pH applied to both buffered and non-buffered systems and were according to the method described in Section 2.2, 100 rpm, 37°C.

Organic : aqueous true, $K_D (= C_2^{\infty}/C_1^{\infty})$, and apparent, $(K_D)_{app} = C_2^{\infty}/(C_{1n}^{\infty} + C_{1i}^{\infty})$, equilibrium partition coefficients were determined in triplicate as described in Section 2.2 at 37° ± 0.1°C, using octanol (Spectrograde, Fisons Ltd., Loughborough, England) as the organic phase. Aqueous phases comprised either potassium chloride, sodium chloride or calcium chloride solutions (adjusted to pH 5.0 with molalities in the range 0 - 2.0 M) or 0.3 M orthophosphate buffer systems of varying pH (Table 3.2).

Values for the forward, k_{12}, and reverse, k_{21}, partitioning rate constants were estimated from knowledge of the transport kinetics and partition coefficient of the solutes at pH 4.34 (0.3 M orthophosphate buffer system) or pH 4.0 (0.3 M KCl solution) using Eqs. 2.7 and 2.8 respectively.

The pK_a values for barbitone were determined in accord with Section 2.2. Aqueous phase ionic strength and ion type were adjusted to represent the range employed in the transfer experiments.

Viscosities and densities of the mutually saturated solvent systems employed in the study were determined in triplicate at 37°C. as described in Section 2.2.

Values for the ratios R1 (= η_1/η_2) and R2 (= ν_2/ν_1) were determined from knowledge of the densities and viscosities of the aqueous and organic phases. Association parameters, ψ, and molecular weights, M, of the preequilibrated aqueous and organic phases were assigned as if they were pure solvents (Table 2.4) and enabled estimation of R3 (= $\psi_1 M_1/\psi_2 M_2$). A value for the coefficient $(D_1A)/(V_1h_1)$ was determined using Eq. 3.20 for each solute based upon r = 1 and knowledge of the K_D and transport kinetics of that solute at a chosen pH. Values for $(D_1A)/(V_1h_1)$ were held constant and used in Eq. 3.19 to predict S as a function of aqueous phase pH. Theoretical values were compared to those determined experimentally from the negative log : linear slopes of plots of ln $(C_1 - C_1^{\infty})$ versus time based on Eq. 3.5.

3.3 RESULTS AND DISCUSSION

Experimental estimates of S as a function of aqueous phase pH in the standardised two-phase transfer cell [octanol : aqueous (0.3 M orthophosphate buffer) system, 100 rpm, 37°C] are documented as S_{obs} in Table 3.3 for barbitone (AI), 5, 5'-diallylbarbituric acid (AII), 5-allyl, 5-isopentylbarbituric acid (AIII), methylparahydroxybenzoate (BII) and ethylparabydroxybenzoate (BIII). Bracketed terms refer to Table 2.1. S values were estimated from first-order plots of ln $(C_1 - C_1^{\infty})$ versus time based on Eq. 3.5 (see Appendix C) and were linear for > 95% of the partitioning process for each solute under study at 100 rpm, 37°C. The slopes were determined in each case by least squares regression analysis (correlation coefficient > 0.999, $n \geq 10$). In order to test the theory developed in Section 3.1.1, cell dependent constants $(D_1A)/(V_1h_1)$ were determined using Eq. 3.20 from knowledge of the partitioning kinetics (Table 3.3) and partition coefficient (Tables 2.3 and 3.8) of each solute at pH 4.34, with the system-dependent constants r, R1, R2 and R3 assigned values of 1, 0.177, 7.70 and 0.359, respectively. The theoretical dependence of S upon pH according to Eq. 3.19, with $(D_1A)/(V_1h_1)$ assigned as documented in Table 3.4 (their values at pH 4.34), are shown as the solid profiles in Figures 3.1 through 3.5 for barbitone, 5, 5'-diallylbarbituric acid, 5-allyl, 5'-isopropylbarbituric acid, methylparahydroxybenzoate and ethylparahydroxybenzoate, respectively. It is clear from inspection of these figures that the predictive theory as developed in Section 3.1.1, which describes the dependence of S upon mass transport descriptors when solutes are subject to differing degrees of dissociation in the aqueous phase of the two-phase transfer cell, is inappropriate for the solute : solvent systems investigated in the present study.

TABLE 3.3

Experimental estimates of S at various aqueous phase pH in the two-phase transfer cell, octanol : aqueous (0.3 M orthophosphate buffer[a]) 100 rpm, 37°C, for barbitone (pK_a = 7.88), 5, 5'-diallylbarbituric acid (pK_a = 7.60), 5-allyl, 5'-isopropylbarbituric acid (pK_a = 7.81), methylparahydroxybenzoate (pK_a = 8.22) and ethylparahydroxybenzoate (pK_a = 8.28).

pH[b]	S_{obs} (sec^{-1} x 10^4)[c]				
	barbitone	5, 5'-diallyl-barbituric acid	5-allyl, 5'-isopropyl-barbituric acid	methyl parahydroxy-benzoate	ethyl parahydroxy-benzoate
4.34	7.39	7.92	8.98	9.35	9.22
4.86	7.90	7.63	7.85	8.14	7.58
5.85	7.70	4.49	5.23	5.47	5.35
6.38	7.59	5.76	6.42	4.01	3.89
6.92	5.78	-	-	5.24	5.24
7.31	6.86	5.50	6.10	4.02	4.12
7.98	4.40	7.66	9.39	6.24	6.62

a. Table 3.2.

b. Aqueous phase; 37°C.

c. Kinetic analysis; Eq. 3.5.

TABLE 3.4

Experimental estimates of the forward, k_{12}, and reverse, k_{21}, first-order rate constants for partitioning in the two-phase transfer cell octanol : aqueous (pH 4.34; 0.3 M orthophosphate buffer) 100 rpm, 37°C for barbitone, 5, 5'-diallylbarbituric acid, 5-allyl, 5'-isopropylbarbituric acid, methylparahydroxybenzoate and ethylparahydroxybenzoate.

Compound	pK_a	S ($sec^{-1} \times 10^4$)	$(D_1A)/(V_1h_1)$ ($sec^{-1} \times 10^4$)	k_{12}[b] ($sec^{-1} \times 10^4$)	k_{21}[c] ($sec^{-1} \times 10^4$)
barbitone	7.88	7.39	9.74	6.28	1.11
5, 5'-diallylbarbituric acid	7.60	7.92	9.04	7.4	0.51
5-allyl, 5'-isopropylbarbituric acid	7.81	8.98	9.61	8.69	0.29
methylparahydroxybenzoate	8.22	9.35	9.60	9.23	0.12
ethylparahydroxybenzoate	8.28	9.22	9.29	9.19	0.30

a. Table 2.2.

b. Eq. 2.7; pH 4.34.

c. Eq. 2.8; pH 4.34.

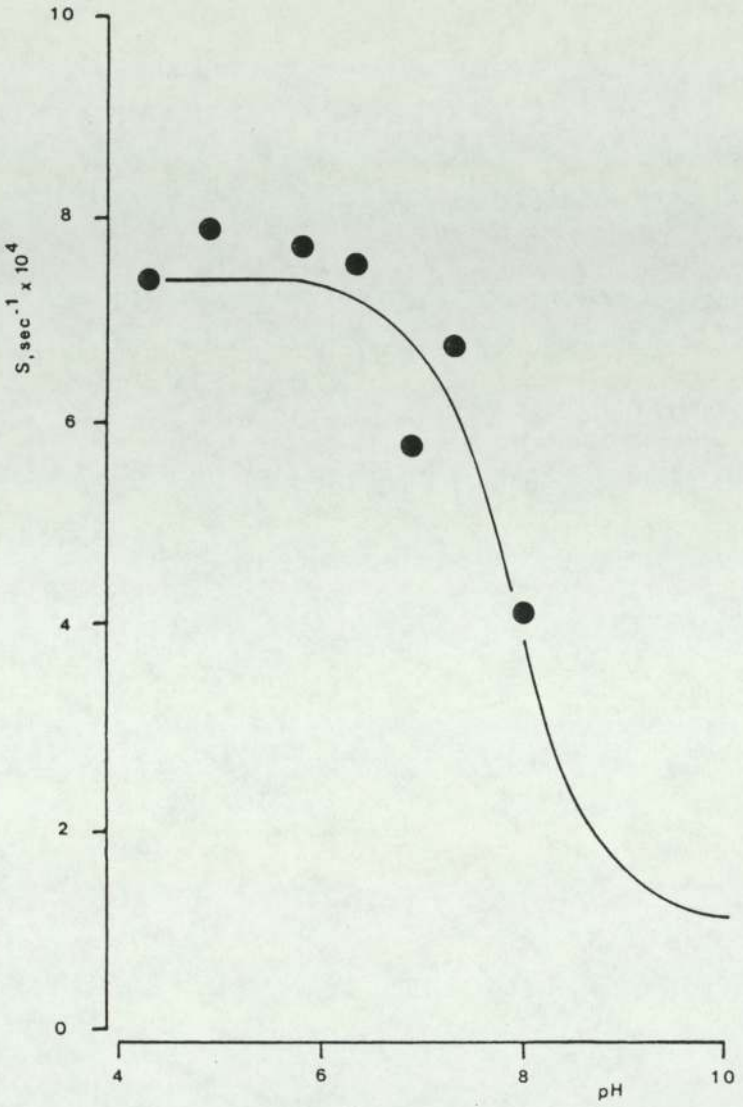

Figure 3.1 Theoretical (solid profile; Eq. 3.19) and experimental (symbols) dependence of S on pH in the two-phase transfer cell (octanol : aqueous 0.3 M orthophosphate buffer) for barbitone (pK_a = 7.88) 100 rpm, 37°C.

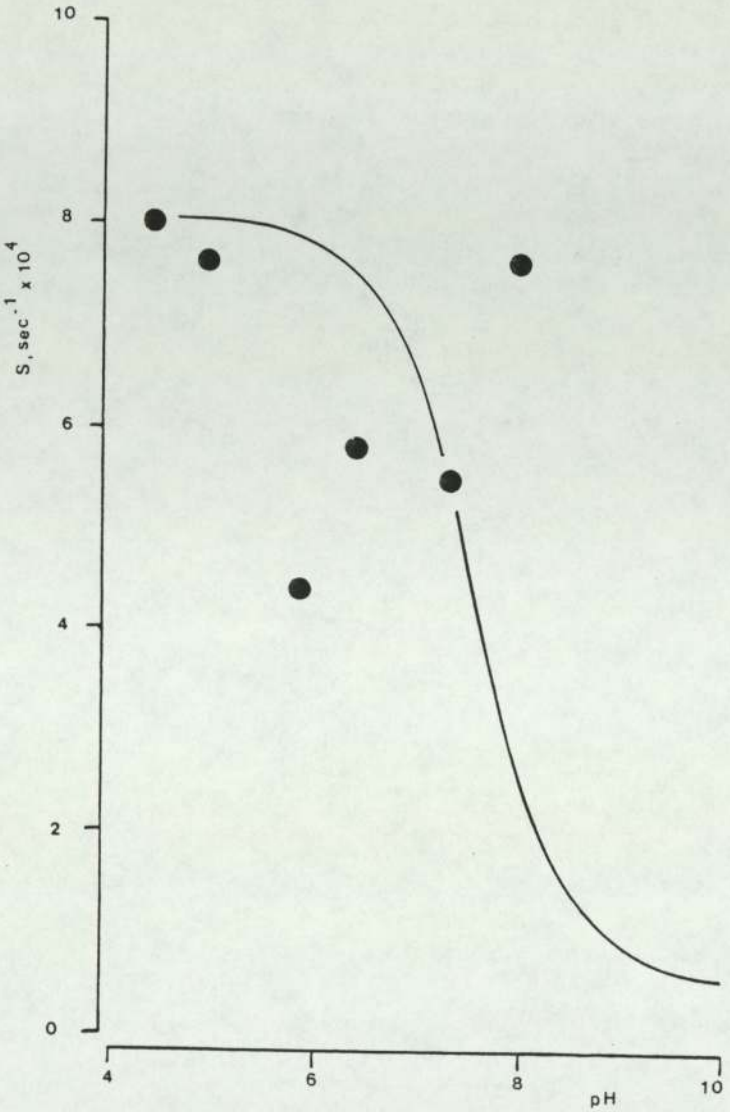

Figure 3.2 Theoretical (solid profile; Eq. 3.19) and experimental (symbols) dependence of S on pH in the two-phase transfer cell (octanol : aqueous 0.3 M orthophosphate buffer) for 5, 5'-diallyl-barbituric acid (pK_a = 7.60) 100 rpm, 37°C.

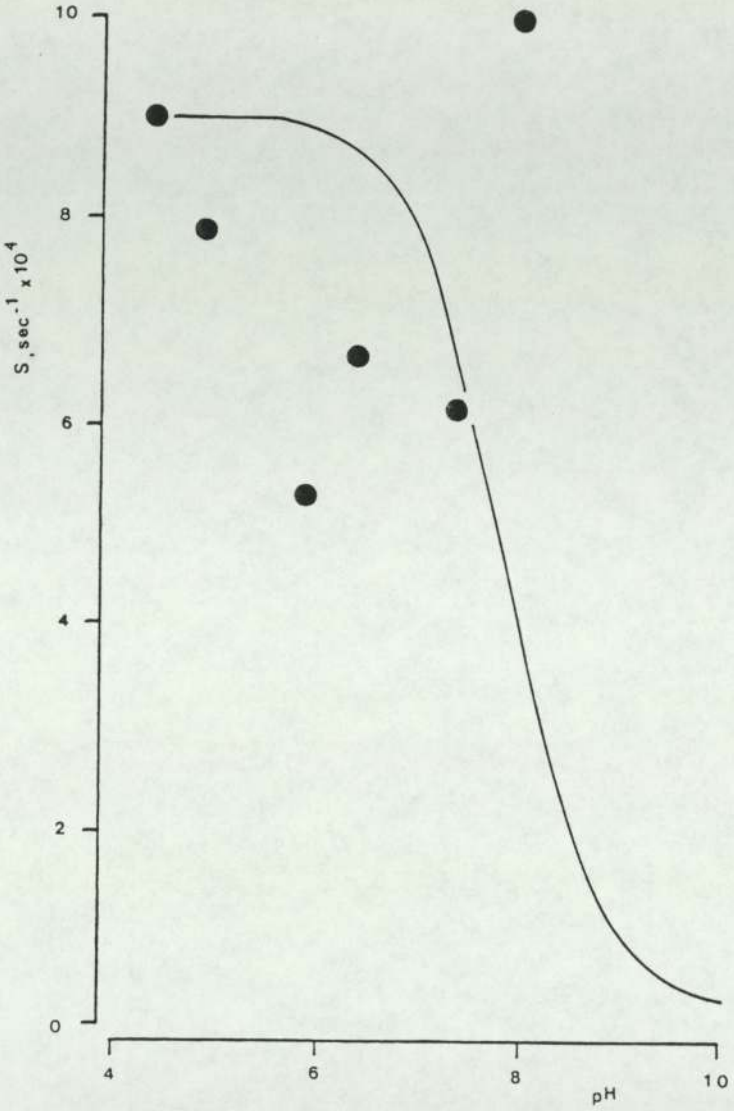

Figure 3.3 Theoretical (solid profile; Eq. 3.19) and experimental (symbols) dependence of S on pH in the two-phase transfer cell (octanol : aqueous 0.3 M orthophosphate buffer) for 5-allyl, 5'-isopropylbarbituric acid (pK_a = 7.81) 100 rpm, 37°C.

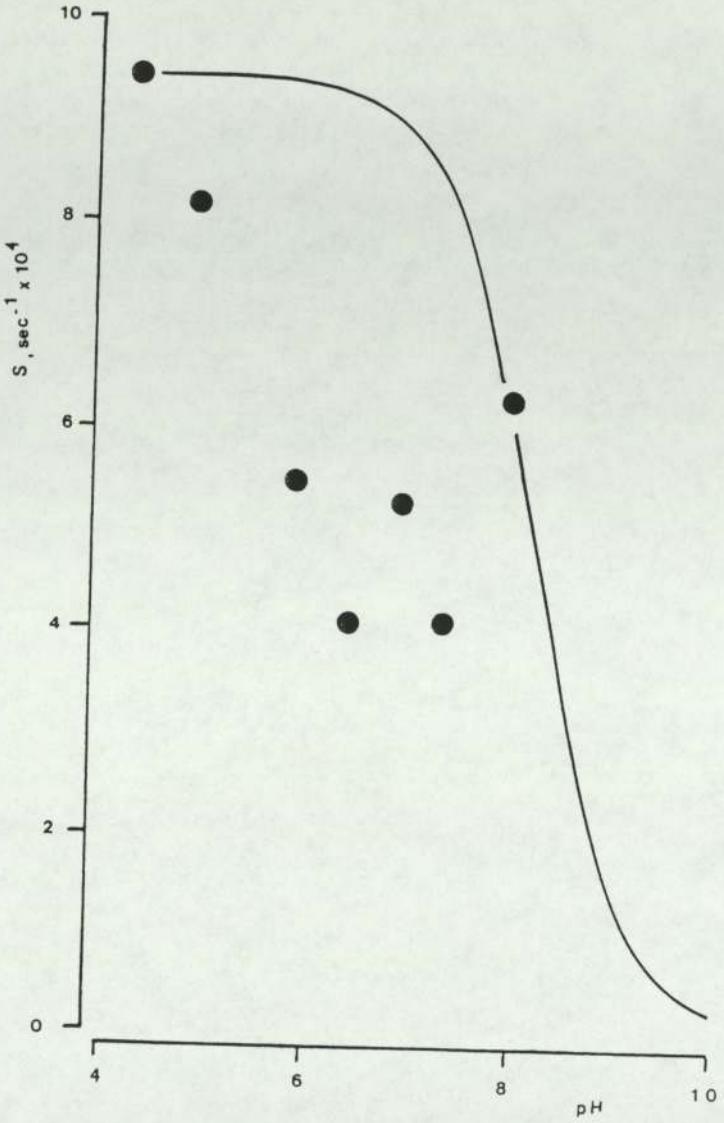

Figure 3.4 Theoretical (solid profile; Eq. 3.19) and experimental (symbols) dependence of S on pH in the two-phase transfer cell (octanol : aqueous 0.3 M orthophosphate buffer) for methylparahydroxybenzoate (pK_a = 8.22) 100 rpm, 37°C.

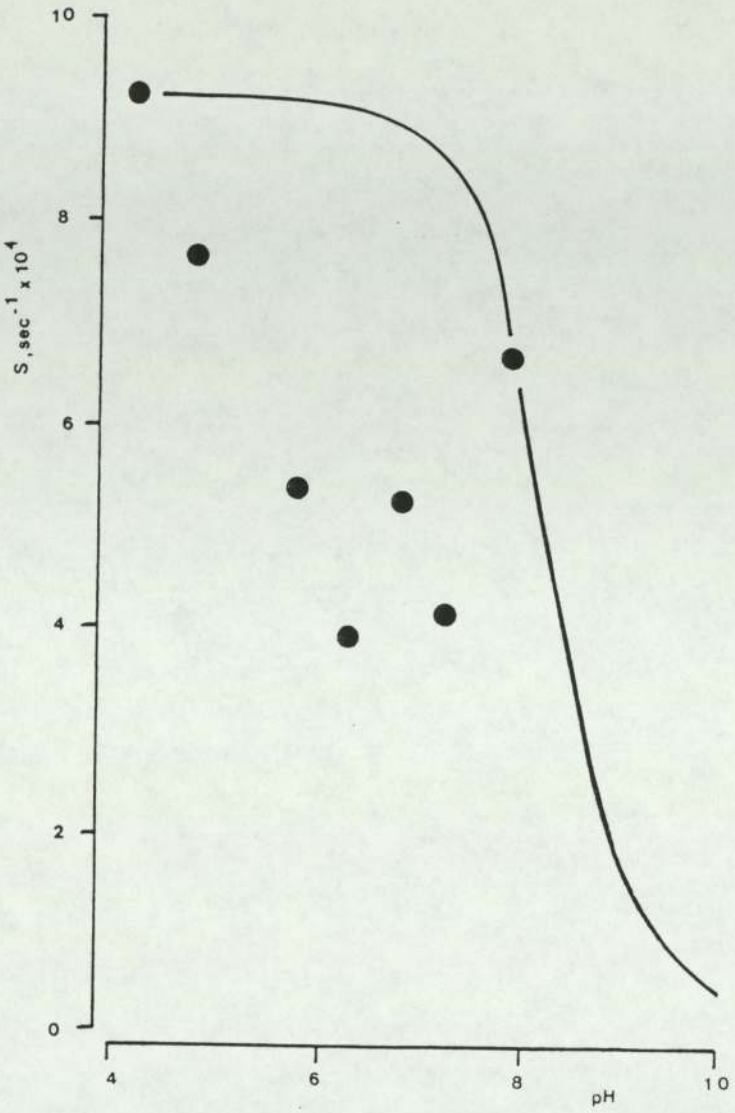

Figure 3.5 Theoretical (solid profile; Eq. 3.19) and experimental (symbols) dependence of S on pH in the two-phase transfer cell (octanol : aqueous 0.3 M orthophosphate buffer) for ethylparahydroxybenzoate (pK_a = 8.24) 100 rpm, 37°C.

Section 3.1 also documents the theoretical dependence of S upon the individual rate constants for partitioning, k_{12} and k_{21}, under conditions of varying aqueous phase pH in the two-phase transfer cell (Eq. 3.1). Values for the forward, k_{12}, and reverse, k_{21}, first-order rate constants for partitioning, of each solute under study at pH 4.34, are shown in Table 3.4 and were estimated from the transport kinetics (Table 3.3) and partition coefficient (Tables 2.3 and 3.8) of each solute at pH 4.34 (fn = 1) using Eqs. 2.7 and 2.8, respectively. Figure 3.6 shows a comparison of the theoretical dependence of S upon pH generated using Eq. 3.19 (solid curve), to theoretical values of S generated using Eq. 3.1 (open squares) for barbitone in the two-phase transfer cell aqueous : octanol 100 rpm, 37°C. The solid profile in Figure 3.6 was generated, as described above, using Eq. 3.19 with $(D_1A)/(V_1h_1)$ held constant at 9.74×10^{-4} sec^{-1} (its value at pH 4.34). Theoretical values of S in Figure 3.6 (symbols) were generated using Eq. 3.1 from knowledge of k_{12} and k_{21} at pH 4.34 as documented in Table 3.4. It is clear from inspection of Figure 3.6, that values for S predicted by Eqs. 3.19 and 3.1 are identical. It follows that Eq. 3.1 predicts the same S versus pH profiles as those documented in Figures 3.1 - 3.5 which were generated using Eq. 3.19.

Reasons for the poor agreement between theory and experiment as shown in Figures 3.1 - 3.5 have been investigated and are discussed below.

Experimental errors involved in determining S, from first-order plots of $\ln (C_1 - C_1^{\infty})$ versus time based on Eq. 3.5, in the present study under conditions of partial ionisation of the solute in the aqueous phase are shown in Table 3.5 to be < 8%. Typical replicates were usually within 5% of each other. One major problem associated with estimating transport rate constants in the two-phase transfer cell

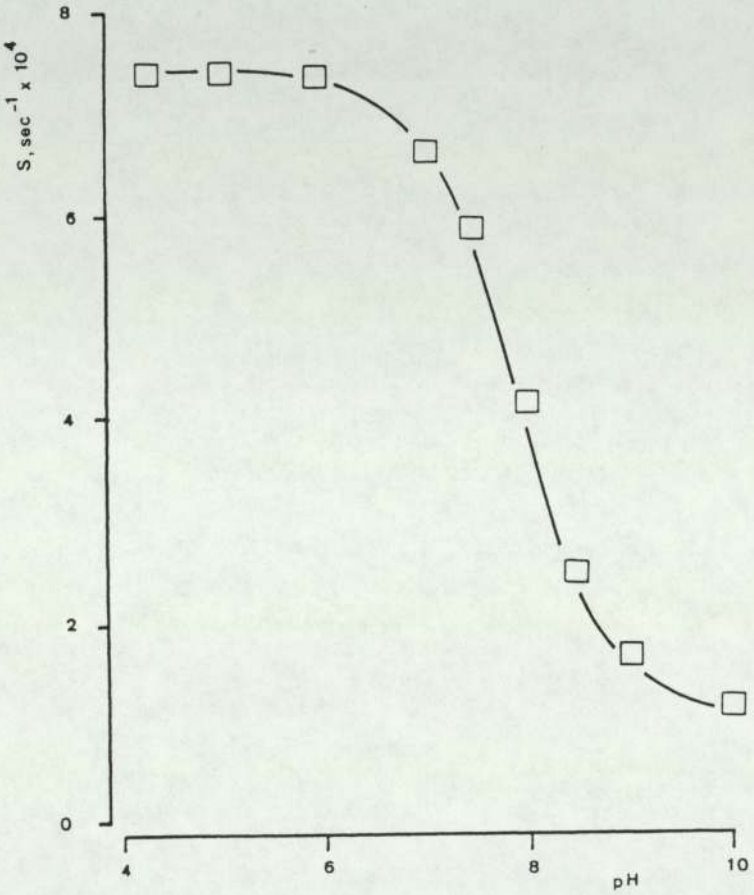

Figure 3.6 Comparative profiles of predicted values for S as a function of aqueous phase pH for barbitone (pK_a = 7.88) in the two-phase transfer cell (octanol : aqueous 0.3 M orthophosphate buffer) 100 rpm, 37°C, using Eq. 3.19 (solid profile) and Eq. 3.1 (symbols).

TABLE 3.5

Experimental replicates of S[a] in the two-phase transfer cell octanol : aqueous 100 rpm, 37°C under conditions of varying aqueous phase pH.

Solute	pH[b]	fn[c]	Experiment number						mean ± SD[d]	
			1	2	3	4	5	6		
barbitone	7.31	0.79	7.31	6.77	6.92	6.44	–	–	6.86	0.36
5, 5'-diallyl-barbituric acid	4.34	1.0	8.03	7.85	7.95	7.86	-	-	7.92	0.08
5-allyl, 5'-isopropyl-barbituric acid	4.86	1.0	7.82	7.63	7.68	7.58	7.48	8.92	7.85	0.54
	6.38	0.98	6.45	6.35	6.01	6.45	6.60	6.68	6.42	0.23
	7.31	0.89	6.15	6.35	5.80	-	-	-	6.10	0.28

a. Based on kinetic analysis; Eq. 3.5; $sec^{-1} \times 10^4$.

b. 37°C.

c. Eq. 3.2.

d. Ref. (49).

from plots of ln $(C_1 - C_1^{\infty})$ versus time (Eq. 3.5), is the accurate experimental determination of the equilibrium concentration of the solute in the aqueous phase at time $t = \infty$, C_1^{∞}. However, several authors have reported methods for estimating the rate constant of a first-order reversible process that do not require a knowledge of the final concentration of the reacting species (61 - 64). These methods are applicable to partitioning processes of the type depicted in Scheme 3.1 (65). Tables 3.6 and 3.7 document theoretical estimates of S using these methods (61 - 64) for each solute and pH employed in the present study (columns 4, 5 and 6) together with values of S estimated from first-order plots of ln $(C_1 - C_1^{\infty})$ versus time (column 3). Tables 3.6 and 3.7 show the good agreement between rate constants estimated by these methods (C_1^{∞} unknown) and those estimated from plots of ln $(C_1 - C_1^{\infty})$ versus time using experimentally observed values for C_1^{∞}. Tables 3.5 - 3.7 attest to the reproducibility and the pattern of results for S versus pH, shown in Figures 3.1 - 3.5.

The assumptions required to derive the theory in Section 3.1.1 are described in the following paragraphs. Likely deviations from these assumptions are discussed and reasons are proposed for the observed deviation between theory and experiment.

In order for the theory to hold true the solute must conform to Scheme 3.1. The solute must remain stable for the time course of a kinetic run, must neither dissociate or associate in the organic phase and the ionised solute must remain confined to the aqueous phase. Control experiments monitoring the absorbance of methylparahydroxybenzoate at 267.5 nm, in the absence of organic phase at 37°C, showed the solute to be stable (< 2% degredation) during a 7 hour period at pH 10.77 (0.3 m orthophosphate buffer; Table 3.2) and at pH 2.0 (0.1 M HCl adjusted to ionic strength (0.3 M) using potassium

TABLE 3.6

Estimates of S (sec^{-1} x 10^{4}) from kinetic analysis of C_1 versus time profiles with and without (Guggenheim, Kezdy-Swinbourne and Hartley analysis) knowledge of C_1^{∞} for barbitone, 5, 5' diallybarbituric acid and 5-allyl, 5'-isopropylbarbituric acid in the two-phase transfer cell octanol : aqueous (0.3 M orthophosphate buffer) 100 rpm, 37°C

Compound	pH[a]	Method of analysis			
		known C_1^{∞}[b]	Guggenheim[b]	Kezdy-Swinbourne[d]	Hartley[e]
barbitone	4.34	7.39	7.64	7.66	7.72
	4.86	7.90	7.82	7.87	7.78
	5.85	7.70	7.45	7.47	7.57
	6.38	7.59	6.98	6.83	6.68
	6.92	5.78	6.21	6.21	6.25
	7.31	6.75	6.86	6.84	6.85
	7.98	4.04	4.29	4.36	4.30
5, 5'-diallyl-barbituric acid	4.34	8.01	8.07	7.92	8.12
	4.86	7.63	7.89	7.93	7.87
	5.85	4.49	4.75	4.74	4.73
	6.38	5.76	5.87	5.87	5.85
	6.92	-	-	-	-
	7.31	5.50	5.69	5.65	5.70
	7.98	7.66	7.41	7.36	7.48
5-allyl, 5'-isopropyl-barbituric acid	4.34	8.98	8.07	8.09	8.08
	4.86	7.85	7.97	7.94	7.97
	5.85	5.23	4.84	4.83	4.92
	6.38	6.63	5.61	5.93	5.85
	6.92	-	-	-	-
	7.31	6.06	6.36	6.39	6.26
	7.98	9.39	8.46	8.35	8.40

a. Aqueous phase; 37°C.

b. Eq. 3.5.

c. Ref. (61).

d. Ref. (62, 63).

e. Ref. (64).

TABLE 3.7

Estimates of S (sec^{-1} x 10^{4}) from kinetic analysis of C_1 versus time profiles with and without (Guggenheim, Kezdy-Swinbourne and Hartley analysis) knowledge of C_1^{∞} for methylparahydroxybenzoate and ethylparahydroxybenzoate in the two-phase transfer cell octanol : aqueous (0.3 M orthophosphate buffer) 100 rpm, 37°C.

Compound	pH[a]	Method of analysis			
		known C_1^{∞}[b]	Guggenheim[c]	Kezdy-Swinbourne[d]	Hartley[e]
methyl-parahydroxy-benzoate	4.34	9.35	9.29	9.28	9.32
	4.86	8.14	7.83	7.79	7.83
	5.85	5.47	5.47	5.48	5.42
	6.92	5.24	5.22	5.21	5.20
	7.31	4.02	4.06	4.08	4.09
	7.98	6.24	5.99	5.95	5.97
ethyl-parahydroxy-benzoate	4.34	9.22	9.04	9.15	8.99
	4.86	7.58	7.65	7.61	7.68
	5.85	5.35	5.33	5.35	5.29
	6.38	3.89	3.81	3.83	3.89
	6.92	5.24	4.76	4.73	4.78
	7.31	4.12	4.09	4.11	4.11
	7.98	6.62	6.52	6.44	6.45

a. Aqueous phase; 37°C.

b. Eq. 3.5.

c. Ref. (61).

d. Ref. (62, 63).

e. Ref. (64).

chloride). Control experiments monitoring the absorbance of barbitone at 222.5 nm in the absence of organic phase at 37°C, showed that at pH 5.0, 6.96, 7.91 (1/15 M Sørensens phosphate buffer (65), 10.81 (0.1 M sodium hydroxide) and 5.0 (0.3 M KCl), the solute remained stable (< 1% degradation) over the time course of a kinetic run. A number of authors have investigated the chemical stability of various 1-alkyl-parahydroxybenzoate (66-68) and barbiturates (69 - 71) at different temperatures, aqueous phase ionic strengths and pH values. Their results support those documented above and suggest that each solute under study remained stable throughout the duration of a kinetic run at each pH employed in the study.

In accord with Scheme 3.1 the true partition coefficient, K_D, may be described by

$$K_D = \frac{C_2}{C_{1n}} \qquad 3.21$$

and the apparent partition coefficient, (K_D) app, through

$$(K_D)\ \text{app} = \frac{C_2}{C_{1n} + C_{1i}} \qquad 3.22$$

The fraction of non-ionised solute, fn, in the aqueous phase of a two-phase transfer cell at any specified pH, may be described through the Henderson-Hasselbach equation (53) which, for a weakly acidic monoprotic acid states:-

$$pH = pk_a - \log \frac{C_{1n}}{C_{1i}} \qquad 3.23$$

Rearranging Eq. 3.23 for C_{1i} and substituting into Eq. 3.22, followed by substitution of C_2/C_{1n} for K_D from Eq. 3.21 gives

$$(K_D)\ app = K_D\ fn \qquad 3.24$$

where $fn = 1/(10^{pH - pK_a} + 1)$ (Eq. 3.2). Given the validity of Scheme 3.1, with insignificant ionised solute partitioning, a plot of (K_D) app versus fn according to Eq. 3.24 should be linear with an insignificant intercept and slope equal to the true partition coefficient, K_D, of the solute. Mean experimentally observed values (n = 3), for the true and apparent octanol/aqueous equilibrium partition coefficients for barbitone, 5-allyl, 5'-isopropylbarbituric acid and ethylparahydroxy-benzoate, are documented in Table 3.8. Figures 3.7 - 3.9, show the theoretical (solid profile; Eq. 3.24) and experimental (symbols) dependence of (K_D) app on fn. Theoretical profiles were generated using Eq. 3.24 with values for the true K_D held constant at 5.66, 30.5 and 299 (the mean of their values at each pH that dictated fn = 1; Table 3.8) for barbitone, 5-allyl, 5'-isopropylbarbituric acid and ethylparahydroxybenzoate, respectively, and fn from knowledge of the pK_a of the solute (7.88, 7.81 and 8.28, respectively) and pH of the aqueous phase using Eq. 3.2. Figures 3.7 through 3.9 show the good agreement between theory (Eq. 3.24) and experiment and suggest that the ionised species remain confined to the aqueous phase. With reference to Eq. 3.24 the values for (K_D) app shown in Table 3.8 were subject to least squares regression analysis (47). In each case correlation coefficients were > 0.99 (n = 5), each solute displayed insignificant intercepts and gave slopes of 5.56, 32.4, and 311 which compare favourably with the true partition coefficients of barbitone (5.66), 5-allyl, 5'-isopropylbarbituric acid (30.5) and ethylparahydroxy-benzoate (299), respectively. The linearity of the data, absence of intercepts and good agreement between slope and partition coefficient data are consistent with Scheme 3.1 and suggest that the ionised moiety remained a non-partitioning species. These observations were supported by control experiments monitoring partition coefficients and

TABLE 3.8

Experimentally observed octanol/aqueous partition coefficients for barbitone, 5-allyl, 5'-isopropylbarbituric acid and ethylparahydroxybenzoate at various aqueous phase pH.

pH[a]	barbitone		5-allyl,5'-isopropyl-barbituric acid		ethylparahydroxy-benzoate	
	fn^b	$(K_D)_{app}^c$	fn^b	$(K_D)_{app}^c$	fn^b	$(K_D)_{app}^c$
4.34	1	5.63	1	29.9	1	307
4.84	1	5.73	1	30.6	1	302
5.85	1	5.62	1	30.9	1	289
6.38	0.97	5.39	0.96	28.4	0.98	278
6.92	0.90	4.90	0.89	25.7	0.95	266
7.31	0.79	4.52	0.76	22.0	0.89	245
7.98	0.44	2.46	0.39	9.94	0.63	171

a. Aqueous phase; 37°C.

b. Eq. 3.2.

c. Organic/aqueous.

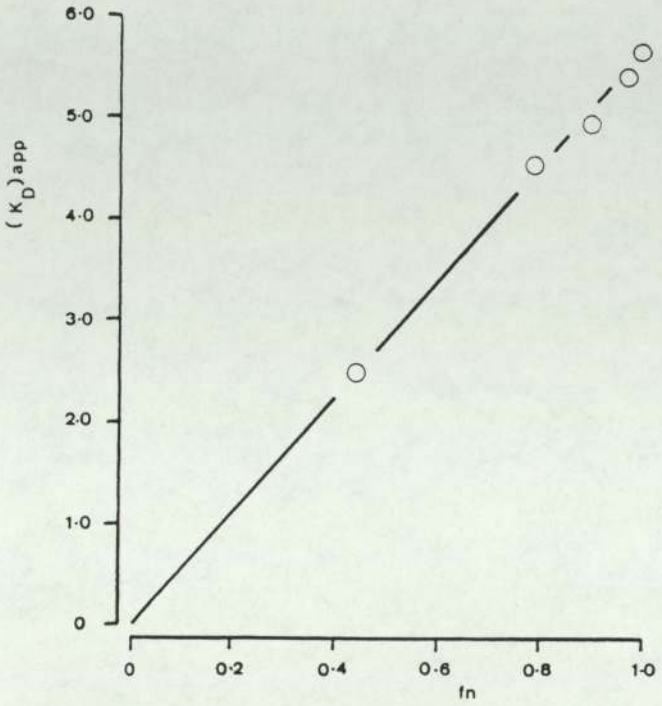

Figure 3.7 Theoretical (solid profile; Eq. 3.24) and experimental (symbols) dependence of the apparent organic (octanol)/aqueous equilibrium partition coefficient, (K_D) app, on pH (fn; Eq. 3.2) for barbitone (pK_a = 7.88), 37°C.

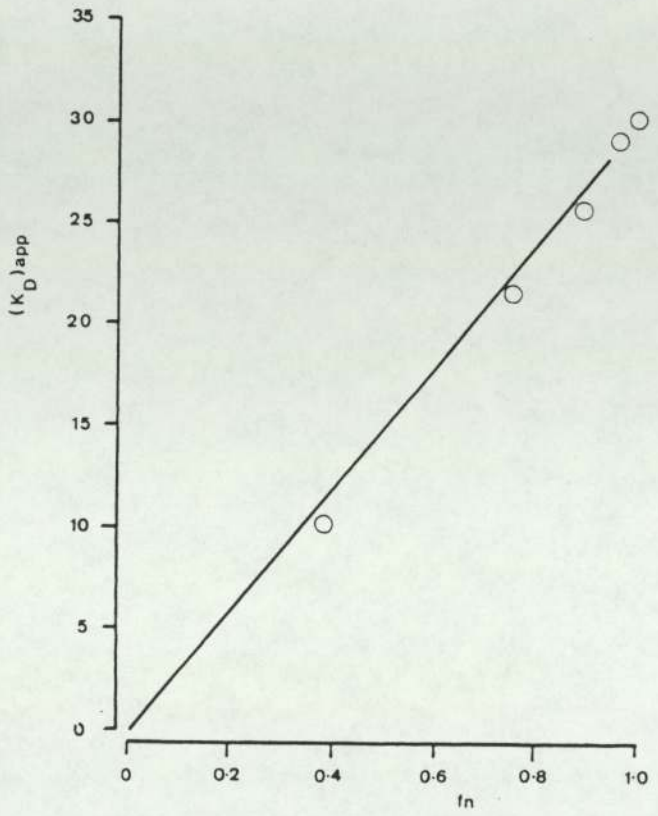

Figure 3.8 Theoretical (solid profile; Eq. 3.24) and experimental (symbols) dependence of the apparent organic (octanol)/aqueous equilibrium partition coefficient, (K_D) app, on pH (fn; Eq. 3.2) for 5-allyl, 5'-isopropylbarbituric acid (pK_a = 7.81), 37°C.

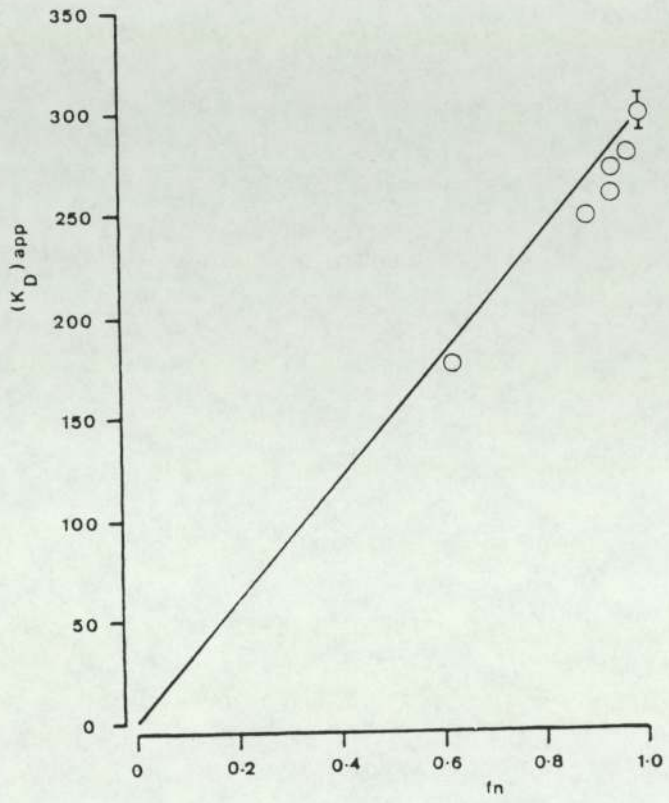

Figure 3.9 Theoretical (solid profile; Eq. 3.24) and experimental (symbols) dependence of the apparent organic (octanol)/aqueous equilibrium partition coefficient, (K_D) app, on pH (fn, Eq. 3.2) for ethylparahydroxybenzoate (pK_a = 8.28), 37°C.

partitioning kinetics at a value for pH that dictated essentially only the presence of ionised solute (pH 10.71; Table 3.2) aqueous : octanol 100 rpm, 37°C. These studies showed insignificant partitioning (< 0.5%) of the ionised solute from the aqueous phase. Furthermore in Chapter 2 it was shown that each solute studied in this Chapter were unlikely to exist as any other than the non-ionised monomer in the organic phase. These studies suggest that each solute under investigation are likely to conform to Scheme 3.1.

Other assumptions that were necessary in order to develop the theory in Section 3.1.1 required that the interface itself offered an insignificant resistance to solute transfer and that the total diffusional resistance to solute transfer was defined by the sum of the resistance offered by the aqueous, R_{aq}, and organic, R_{org}, phases through (8)

$$R_T = R_{aq} + R_{org} \qquad 3.25$$

where, with reference to Eq. 3.8

$$R_{aq} = \frac{h_1}{D_1} \qquad 3.26$$

and

$$R_{org} = \frac{h_2}{D_2 K_D} \qquad 3.27$$

DeMeere et al (72) has shown that in two-phase systems of the type depicted in Fig. 1.1a, under conditions of partial ionisation if it is assumed that only non-ionised solute may partition, a more accurate definition of R_{org} may be given by

$$R_{org} = \frac{h_2}{fn\ D_2 K_D} \qquad 3.28$$

If it is also assumed that the permeability of the ionised and non-ionised species is the same in the aqueous phase, then R_{aq} may be defined through Eq. 3.26. Substitution of R_{aq} and R_{org} from Eqs. 3.26 and 3.28, respectively, into Eq. 3.25 gives

$$R_T = \frac{h_1}{D_1} + \frac{h_2}{fn\ D_2 K_D} \qquad 3.29$$

Rearranging Eq. 3.29 gives

$$R_T = \frac{h_1\ fn\ D_2\ K_D + h_2\ D_2}{D_1\ D_2\ f_n\ K_D} \qquad 3.30$$

Thus in accord with the theories of DeMeere et al (72), Eq. 3.30 is now in a form that provides a more accurate definition of the total diffusional resistance to solute transfer, R_T, under conditions of partial ionisation. If equation 3.30 is now employed in the place of Eq. 3.8 to define the total diffusional resistance, R_T, and substituted into Eq. 3.14 then

$$S = \frac{D_1\ D_2\ A\ fn\ (K_D V_2 fn + V_1)}{V_1 V_2\ (h_1\ fn\ D_2\ K_D + h_2\ D_1)} \qquad 3.31$$

Rearrangement and subsequent simplification of Eq. 3.31 gives

$$S = \frac{D_1 A\ (K_D\ fn + [V_1/V_2])}{V_1 h_1\ (K_D + [h_2 D_1/h_1 D_2]/fn)} \qquad 3.32$$

Substitution of D_1/D_2 and h_1/h_2 from Eqs. 1.12 and 1.13, respectively, into Eq. 3.32 gives

$$S = \left[\frac{D_1 A}{V_1 h_1}\right]\left[\frac{(K_D\ fn + r)}{K_D + (R1)^{-2/3}\ (R2)^{1/6}\ (R3)^{1/3}\ (fn)^{-1}}\right] \qquad 3.33$$

Eq. 3.33 was derived in an analogous manner to Eq. 3.19 and may be used in an identical way to generate theoretical estimates for S as a

function of aqueous phase pH. In order to test Eq. 3.33 theoretical values of S as a function of aqueous phase pH were generated using Eq. 3.33 and compared to (a) theoretical values predicted by Eq. 3.19 and (b) experimental values determined for barbitone in the two-phase transfer cell under conditions of varying aqueous phase pH (Table 3.3) 100 rpm, 37°C. Figure 3.10 shows the experimental (symbols) and theoretical (solid profile; Eq. 3.19, hatched profile ; Eq. 3.33) dependence of S on pH for barbitone octanol : aqueous(orthophosphate buffer) 100 rpm, 37°C (Table 3.3). Experimental values (symbols) and the theoretical solid profile (Eq. 3.19) documented in Fig. 3.10 are identical to those shown in Fig. 3.1 and were generated as described previously. The hatched profile (Eq. 3.33) in Figure 3.10, was generated following estimation of a cell constant, $(D_1A)/(V_1h_1)$, for barbitone at pH 4.34 using Eq. 3.34 after rearrangment of Eq. 3.33 to give

$$\frac{D_1A}{V_1h_1} = \frac{S\left[K_D + (R1)^{-2/3}\ (R2)^{1/6}\ (R3)^{1/3}\ (fn)^{-1}\right]}{(K_D + r)} \qquad 3.34$$

Values for K_D, fn, R1, R2 and R3 at pH 4.34 were estimated as 5.66, 1.0, 0.177, 1.384 and 0.359, respectively. The term $(D_1A)/(V_1h_1)$ was then held constant at 9.76×10^{-1} sec^{-1} and used in Eq. 3.33 to predict S as a function of aqueous phase pH (fn; Eq. 3.2). It is clear from inspection of Figure 3.10 that Eqs. 3.33 (hatched profile) and 3.19 (solid profile) predict different profiles for the dependence of S upon pH in the two-phase transfer cell. However, it is also clear from Figure 3.10 that neither Eq. 3.19 or its amended form (Eq. 3.33) fully account for the experimentally observed dependence of S upon aqueous phase pH observed in this Chapter.

Significant diffusional resistances to interfacial transfer have been reported for some solutes at the organic : aqueous interface

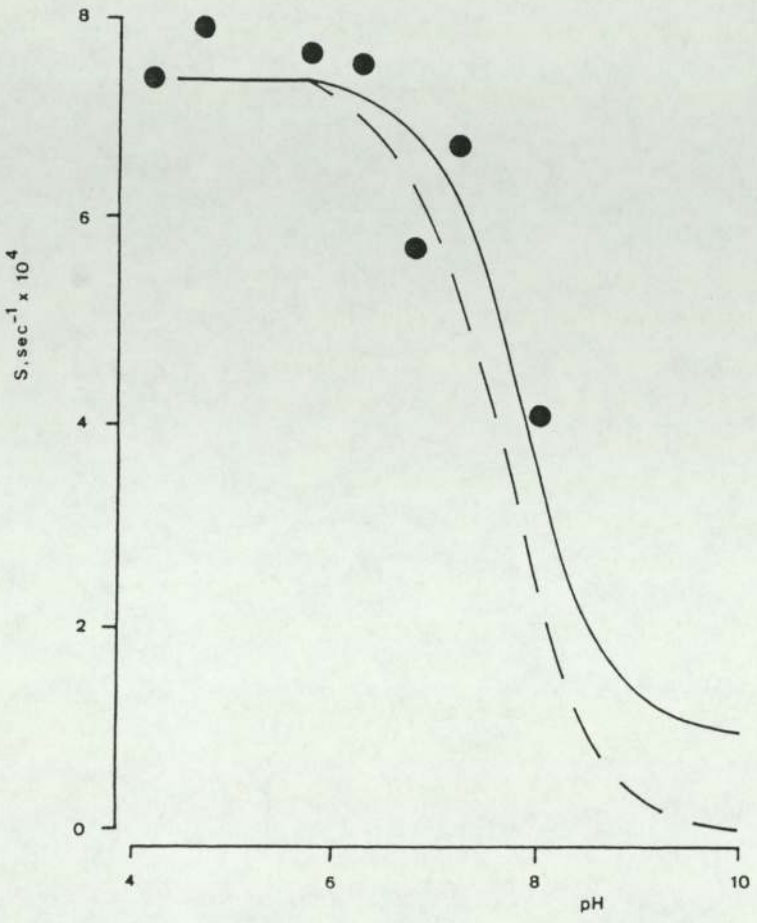

Figure 3.10 Theoretical (solid profile; Eq. 3.19 and hatched profile: Eq. 3.33) and experimental (symbols) dependence of S on pH in the two-phase transfer cell (octanol : aqueous 0.3 M orthophosphate buffer) for barbitone (pK_a = 7.88) 100 rpm, 37°C.

(73 - 80). However, the agreement between theory and experiment for the transfer of non-ionised solutes in the two-phase transfer cell in Chapter 2 suggests that no significant interfacial resistance to solute transfer occurs at the octanol : aqueous interface for any of the solute : solvent systems employed in this Chapter (assumption; Eq. 1.9). It is not within the scope of this Chapter to investigate further the existence of interfacial resistance to solute transfer, however, this subject is considered in detail in the following Chapter.

The remaining assumptions necessary to derive the theory and Eq. 3.19 required that diffusion coefficients and boundary layers adjacent to the aqueous : octanol interface remained unaffected by the changes in buffer components that are necessary to alter aqueous phase pH. Buffer systems often comprise a variety of different ions (81). In the present study orthophosphate buffers of constant ionic strength were employed as the aqueous phase. However, as shown in Table 3.9, the relative proportions of each ion vary according to the pH of the aqueous phase (60). Previous studies in the two-phase transfer cell with partial ionisation (82) employed Sørensen phosphate buffers as the aqueous phase in which pH and ionic strength varied. Plots of S versus pH from these studies showed even larger deviations from theory than those represented by the closed symbols in Figs. 3.1 - 3.5.

Experimental estimates for S as a function of aqueous phase pH under conditions of constant ionic strength and type in the aqueous phase in the standardised two-phase transfer cell (octanol : aqueous 100 rpm, 37^{o}C) are documented as S_{obs} in Tables 3.10 and 3.11 for barbitone, 5, 5'-diallybarbituric acid, 5-allyl, 5'-isopropylbarbituric acid, methlylparahydroxybenzoate and ethylparahydroxybenzoate. In this case aqueous phase ionic strength was maintained constant (0.3 M) using potassium chloride and pH maintained by pH stat. S values were

TABLE 3.9

Variation in concentration of the ion content of orthophosphate buffers (0.3 M) at various aqueous phase pH.

pH	K^+ concentration (molal)	$H_2PO_4^-$ concentration (molal)	Na^+ concentration (molal)	$HPO^=$ concentration (molal)	ionic strength (molal)
4.20	0.3	0.3	-	-	0.3
4.60	0.297	0.297	0.00374	0.0018	0.3
5.00	0.285	0.285	0.009	0.0045	0.3
5.40	0.267	0.267	0.021	0.011	0.3
5.80	0.231	0.231	0.047	0.023	0.3
6.00	0.203	0.203	0.063	0.032	0.3
6.50	0.119	0.119	0.1197	0.059	0.3
7.00	0.052	0.052	0.165	0.083	0.3
7.40	0.0236	0.0236	0.183	0.092	0.3
8.00	0.006	0.006	0.195	0.098	0.3
8.80	0.0011	0.0011	0.201	0.101	0.3

TABLE 3.10

Experimental estimates of S for barbitone, 5, 5'-diallylbarbituric acid and 5-allyl, 5'-isopropylbarbituric acid in an octanol : aqueous (0.3 M KCl) system in the two-phase transfer cell 100 rpm, 37°C.

Compound	pH[a]	fn[b]	S[c] ($sec^{-1} \times 10^{4}$)
barbitone	4.0	1	5.75
	5.0	1	5.67
	5.4	1	5.21
	6.0	0.98	4.47
	6.5	0.96	3.15
	6.9	0.91	3.56
5,5'-diallyl-barbituric acid	4.0	1	6.55
	5.0	1	6.65
	6.0	0.97	6.34
	6.3	0.95	5.78
	6.9	0.83	4.12
5-allyl, 5'-isopropyl-barbituric acid	4.0	1	7.09
	5.0	1	7.39
	5.5	1	6.77
	6.0	0.98	5.56
	6.3	0.97	4.83
	6.9	0.89	5.02
	7.7	0.56	3.19
	8.1	0.34	3.16

a. Aqueous phase; 37°C.

b. Eq. 3.2.

c. Kinetic analysis; Eq. 3.5.

TABLE 3.11

Experimental estimates of S for methylparahydroxybenzoate and ethylparahydroxybenzoate in an octanol : aqueous (0.3 M KCl) system in the two-phase transfer cell 100 rpm, 37°C.

Compound	pH[a]	fn[b]	S[c] ($sec^{-1} \times 10^{4}$)
methylparahydroxybenzoate	4.0	1	7.70
	5.0	1	7.03
	6.0	1	7.55
	6.2	1	7.12
	6.6	0.98	5.54
	7.7	0.77	4.43
ethylparahydroxybenzoate	4.0	1	7.05
	5.0	1	7.07
	5.4	1	6,97
	6.0	0.99	5.67
	6.5	0.98	4.94
	6.9	0.96	5.03
	7.6	0.83	4.48

a. Aqueous phase; 37°C.

b. Eq. 3.2.

c. Kinetic analysis; Eq. 3.5.

estimated from first-order plots of ln $(C_1 - C_1^{\infty})$ versus time based on Eq. 3.5 (correlation coefficient > 0.999, n ≥ 10) and are shown in Figures 3.11 - 3.15 as the closed symbols. In order to test the theory developed in Section 3.1.1 (Eq. 3.19) and its amended form derived in Section 3.4 (Eq. 3.33), cell dependent constants $(D_1A)/(V_1h_1)$ were determined using Eqs. 3.20 and 3.34, respectively from knowledge of the partitioning kinetics (Tables 3.10 and 3.11) and partition coefficient (Tables 2.3), for each solute at pH 4.0, with the system-dependent constants r, R1, R2 and R3 assigned values of 1, 0.158, 7.810 and 0.359 respectively. The theoretical dependence of S upon pH according to Eqs. 3.19 and 3.33 were generated with $(D_1A)/(V_1h_1)$ assigned values of 8.16, 7.58, 7.66, 7.93 and 7.12 x 10^{4} sec^{-1} (their values for both equations at pH 4.0) for barbitone, 5, 5'-diallylbarbituric acid, 5-allyl, 5'-isopropylbarbituric acid, methyl-parahydroxybenzoate and ehtylparahydroxybenzoate, respectively and shown as the solid (Eq. 3.19) and hatched (Eq. 3.33) profiles in Figures 3.11 - 3.15. Figures 3.11 through 3.15 show how values for S in the absence of buffer fall with increasing pH (symbols) but remain poorly described by either Eqs. 3.19 or 3.33 (solid and hatched profiles, respectively).

Earlier determinations of S as a function of aqueous phase pH in the two-phase transfer cell employed 0.3 M orthophosophate buffers to maintain pH constant at a given value. In such systems the ionic strength of each individual ion varied simultaneously with pH (Table 3.9). Plots of S versus pH from these studies (Figures 3.1 - 3.5), showed even larger deviations from theory (Eqs. 3.1 or 3.19) than those determined in the presence of 0.3 M KCl solutions (Figs. 3.11 - 3.15). The contrast between plots of S versus pH in the presence (Figs. 3.1 - 3.5) and absence (Figs 3.11 - 3.15) of buffer components, suggest that the ionic content of the aqueous phase affects the apparent transport

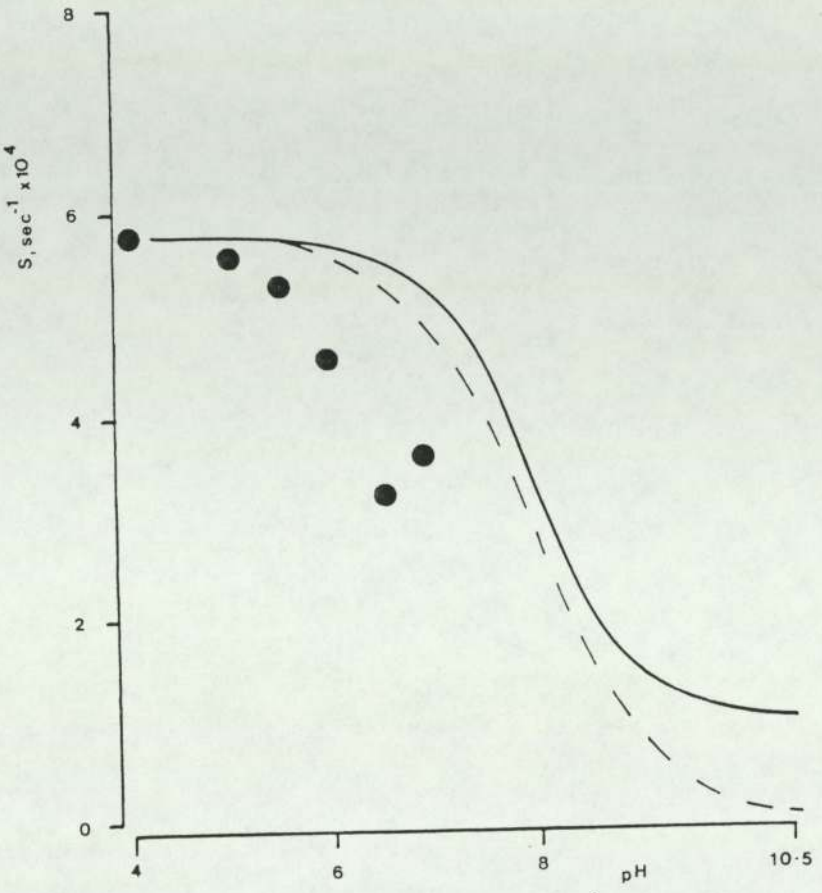

Figure 3.11 Theoretical (solid profile; Eq. 3.19 and hatched profile; Eq. 3.33) and experimental (symbols) dependence of S on pH in the two-phase transfer cell (octanol : aqueous 0.3 M KCl) for barbitone (pK_a = 7.88) 100 rpm, 37°C.

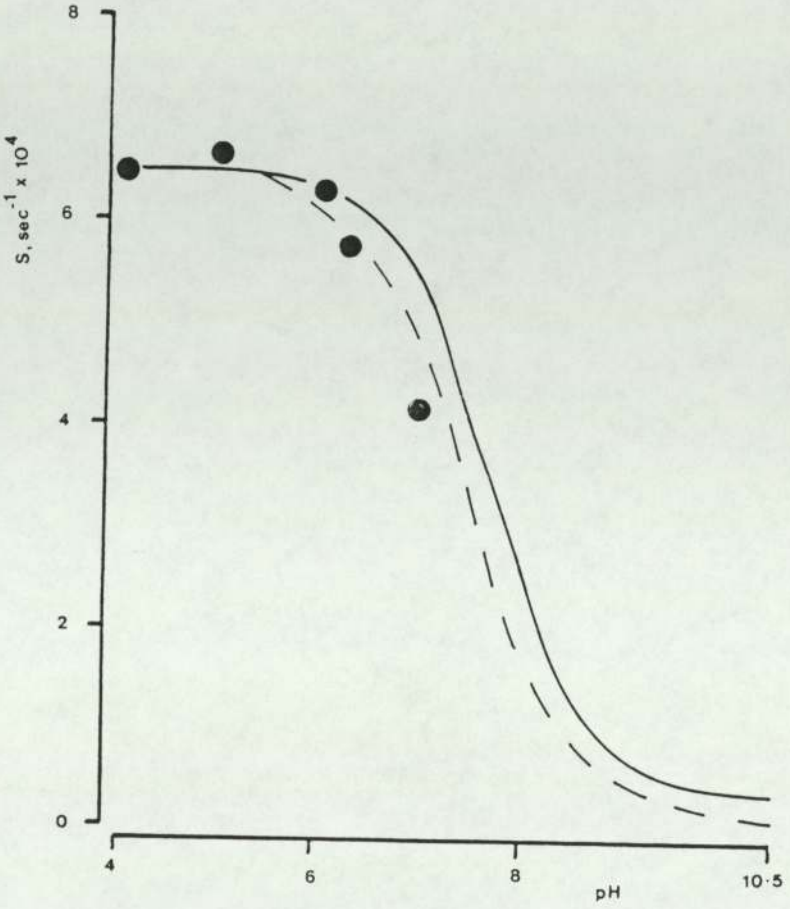

Figure 3.12 Theoretical (solid profile; Eq. 3.19 and hatched profile; Eq. 3.33) and experimental (symbols) dependence of S on pH in the two-phase transfer cell (octanol : aqueous 0.3 M KCl) for 5, 5'-diallylbarbituric acid (pK_a = 7.60) 100 rpm, 37°C.

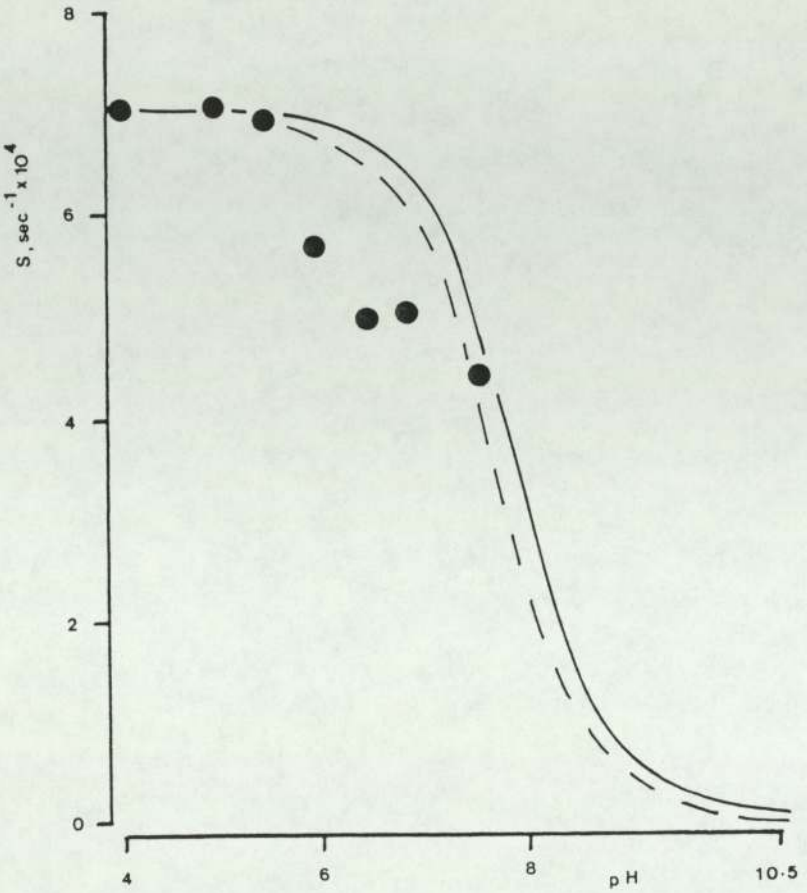

Figure 3.13 Theoretical (solid profile; Eq. 3.19 and hatched profile; Eq. 3.33) and experimental (symbols) dependence of S on pH in the two-phase transfer cell (octanol : aqueous 0.3 M KCl) for 5-allyl, 5'-isopropylbarbituric acid (pK_a = 7.81) 100 rpm, 37°C.

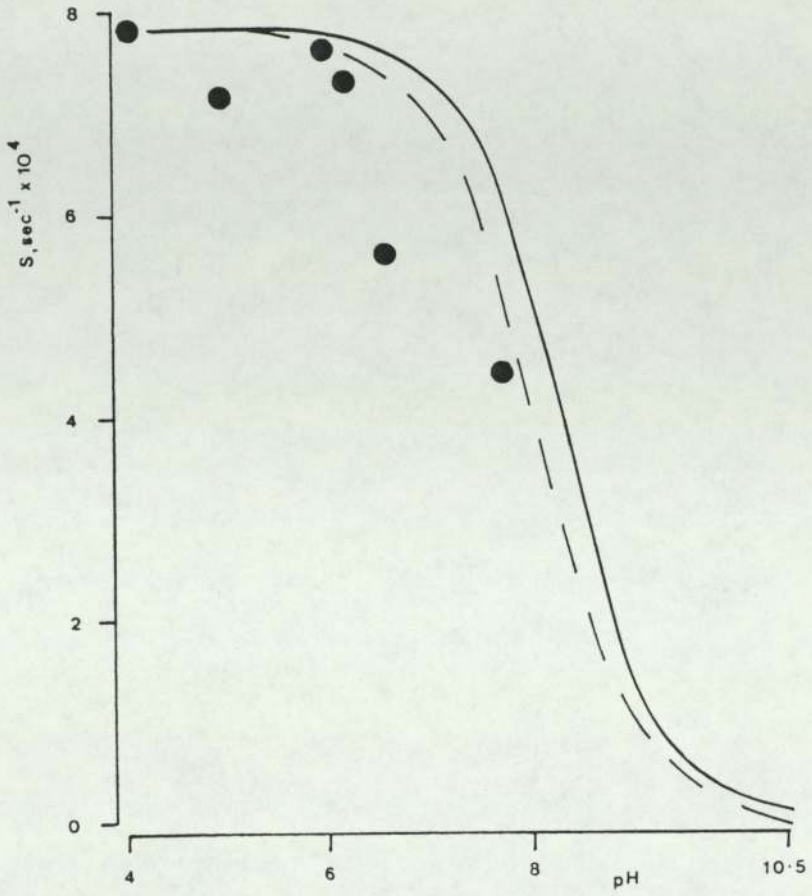

Figure 3.14 Theoretical (solid profile; Eq. 3.19 and hatched profile; Eq. 3.33) and experimental (symbols) dependence of S on pH in the two-phase transfer cell (octanol : aqueous 0.3 M KCl) for methlyparahydroxy-benzoate (pK_a = 8.22) 100 rpm, 37°C.

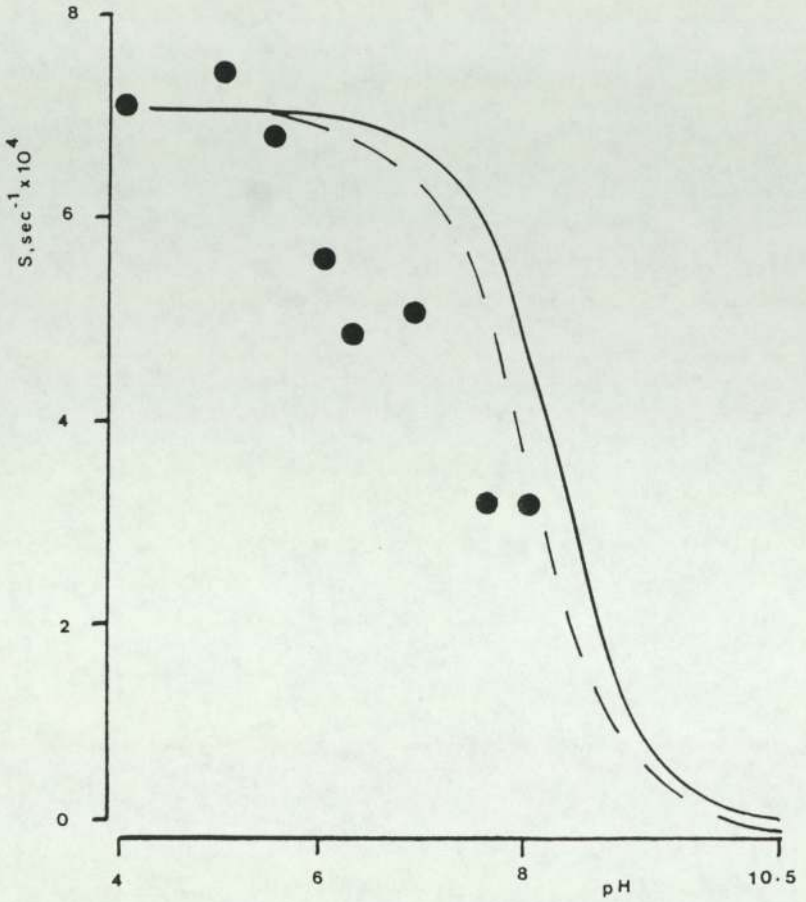

Figure 3.15 Theoretical (solid profiles; Eq. 3.19 and hatched profiles; Eq. 3.33) and experimental (symbols) dependence of S on pH in the two-phase transfer cell (octanol : aqueous 0.3 M KCl) for ethyl-parahydroxybenzoate (pK_a = 8.24) 100 rpm, 37^{o}C.

kinetics of the solute, even in the effective absence of ionisation. These observations prompted further studies to establish the effect of aqueous phase ionic strength upon the transport kinetics of solutes, essentially non-ionised in the aqueous phase of the two-phase transfer cell, in an attempt to resolve the conflict with theory.

Tables 3.12 and 3.13 and Figures 3.16 and 3.17 document values for S, in the effective absence of ionisation (pH = 5.0), for barbitone, 5, 5'-diallylbarbituric acid and 5-allyl, 5'-isopentyl-barbituric acid, as a function of aqueous phase ionic strength and type. It is clear from inspection of these figures that the ionic content of the aqueous phase affects the apparent transport kinetics of the non-ionised solute. The solid profiles in Figures 3.16 and 3.17 (overlay) represent theoretical values of S generated by using the non-ionised predictive theory of Byron et al (24) (Eq. 1.9). Theoretical values for S were generated using Eq. 1.9 from knowledge of the transport kinetics and partition coefficient of the solute at zero ionic strength. The cell constants $(D_1A)/(V_1h_1)$ were estimated for each solute at zero ionic strength using Eq. 1.10 with values for R1, R2 and R3 held constant at their experimentally determined values shown in Table 3.14. Values for $(D_1A)/(V_1h_1)$ were then held constant at 1.12, 1.01 and 1.08 $sec^{-1} \times 10^4$ for barbitone, 5, 5'-diallyl-barbituric acid and 5-allyl, 5'-isopentylbarbituric acid, respectively, and used in Eq. 1.9 to generate theoretical values for S. Figures 3.16 and 3.17 show that the theory for non-ionised solute transfer [Byron et al (24); Eq. 1.9] in the two-phase transfer cell is not appropriate for predicting values of S in systems in which aqueous phase ionic strength is varied.

Inspection of Figure 3.16 shows how the partitioning kinetics of barbitone, essentially non-ionised at pH 5.0, remains effectively

TABLE 3.12

Experimental estimates for S, S_{obs}, for barbitone under conditions of varying aqueous phase ionic strength and ion type in the two-phase transfer cell (aqueous : octanol) 100 rpm, 37°C.

Aqueous phase[a] ion type	Aqueous phase ionic strength[b]	K_D[c]	ν[d]	S_{obs}[e]
NaCl	0	4.43	1.2	7.53
	0.1	4.58	1.3	7.47
	0.3	4.91	1.4	7.02
	0.5	5.24	1.5	7.45
	1.0	6.10	1.8	7.08
	2.0	6.74	2.0	6.70
$CaCl_2$	0	4.43	1.2	7.53
	0.1	4.36	1.3	7.03
	0.3	4.62	1.3	7.47
	0.5	4.91	1.4	6.98
	1.0	5.45	1.6	6.85
	2.0	6.53	1.9	6.93
KCl	0	4.43	1.2	7.53
	0.1	4.60	1.3	7.40
	0.3	4.80	1.4	7.20
	0.5	5.00	1.5	7.40
	1.0	5.79	1.7	7.43
	2.0	6.61	2.0	7.15
orthophosphate buffer[f]	0	4.43	1.2	7.53
	0.1	4.78	1.4	6.64
	0.2	5.28	1.6	6.62
	0.3	5.66	1.6	6.23
	0.4	5.72	1.7	5.46
	0.8	6.00	1.8	4.18

a. Saturated with octanol.
b. Molal, adjusted to pH 5.0.
c. Mean of 3 determinations.
d. Eq. 2.28.
e. $(k_{12} + k_{21})$ based on kinetic analysis (Eq. 2.1); $(sec^{-1} \times 10^4)$.
f. Table 3.1.

TABLE 3.13

Experimental estimates of S, S_{obs}, for barbitone, 5,5'-diallylbarbituric acid and 5-allyl, 5'-isopentylbarbituric acid under conditions of varying aqueous phase ionic strength in the two-phase transfer cell (aqueous : octanol) 100 rpm, 37°C.

Compound[a]	Aqueous phase ionic strength[b]	K_D[c]	ν[d]	S_{obs}[e]
barbitone	0	4.43	1.2	7.53
	0.1	4.60	1.3	7.40
	0.3	4.80	1.4	7.20
	0.5	5.00	1.5	7.40
	1.0	5.79	1.7	7.43
	2.0	6.61	2.0	7.15
5,5'-diallyl-barbituric acid	0	12.9	3.5	8.48
	0.1	14.0	4.1	8.58
	0.3	14.6	4.3	8.10
	0.5	15.6	4.6	8.28
	1.0	18.1	5.3	7.67
	2.0	22.7	6.8	7.43
5-allyl, 5'-isopentylbarbituric acid	0	221	60.7	10.7
	0.1	229	66.6	10.3
	0.3	239	69.7	9.87
	0.5	266	77.8	9.80
	1.0	287	84.4	8.95
	2.0	355	106	8.37

a. Table 2.1.

b. Molal; ion type KCl adjusted to pH 5.0.

c. Mean of three determinations.

d. Eq. 2.28.

e. $(k_{12} + k_{21})$ based on kinetic analysis (Eq. 2.1); $sec^{-1} \times 10^4$.

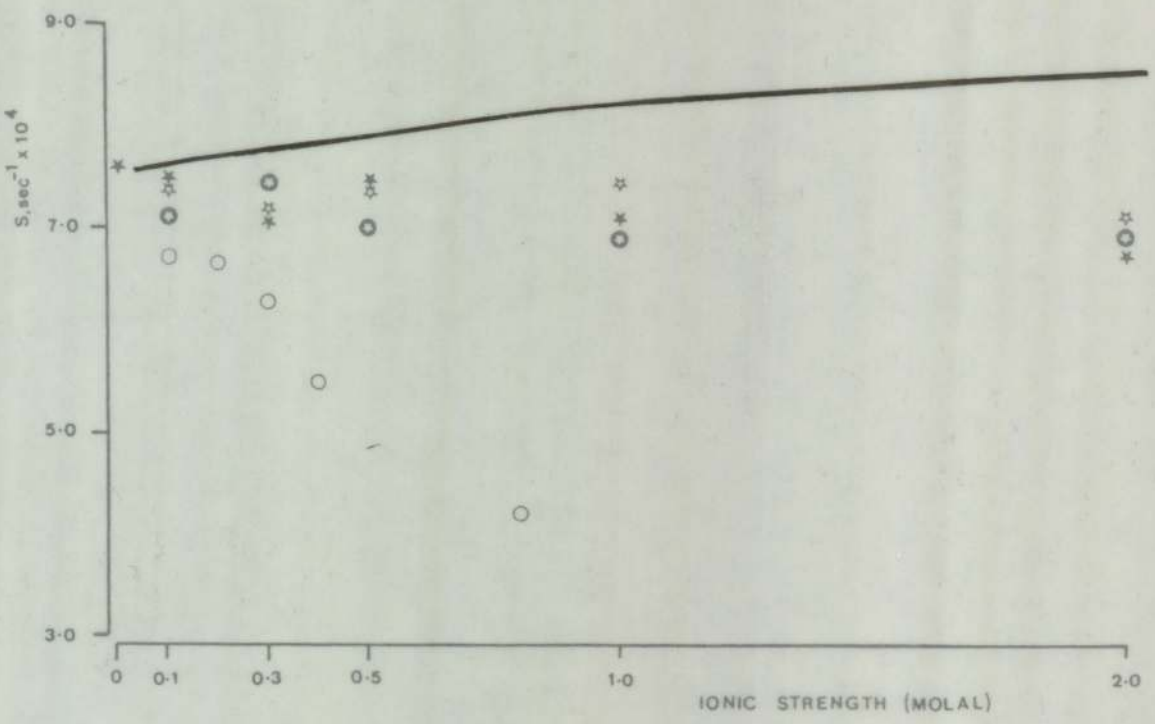

Figure 3.16 Experimental dependence of S for barbitone, essentially non-ionised in the aqueous phase, in the two-phase transfer cell (octanol : aqueous) 100 rpm, 37°C in which aqueous phase ionic strength and type are varied using (✱) NaCl, (✪) $CaCl_2$, (✡) KCl and (○) orthophosphate buffer solutions.

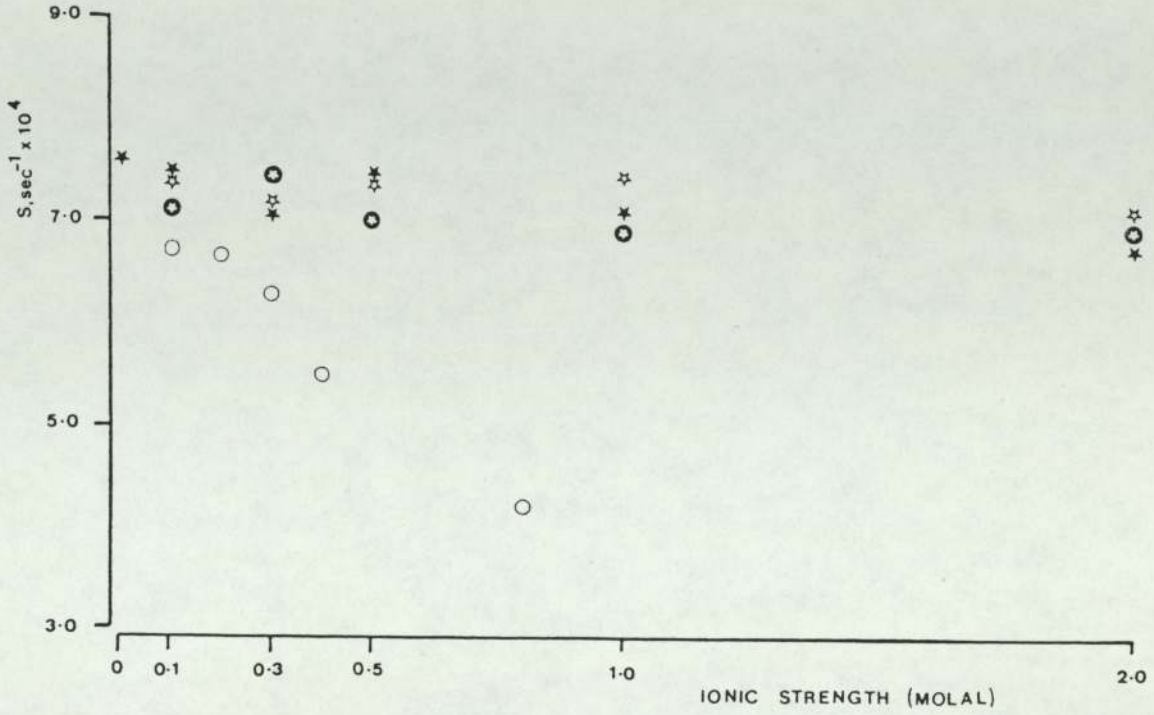

Figure 3.16 Experimental dependence of S for barbitone, essentially non-ionised in the aqueous phase, in the two-phase transfer cell (octanol : aqueous) 100 rpm, 37°C in which aqueous phase ionic strength and type are varied using (✶) NaCl, (✪) $CaCl_2$, (☆) KCl and (○) orthophosphate buffer solutions.

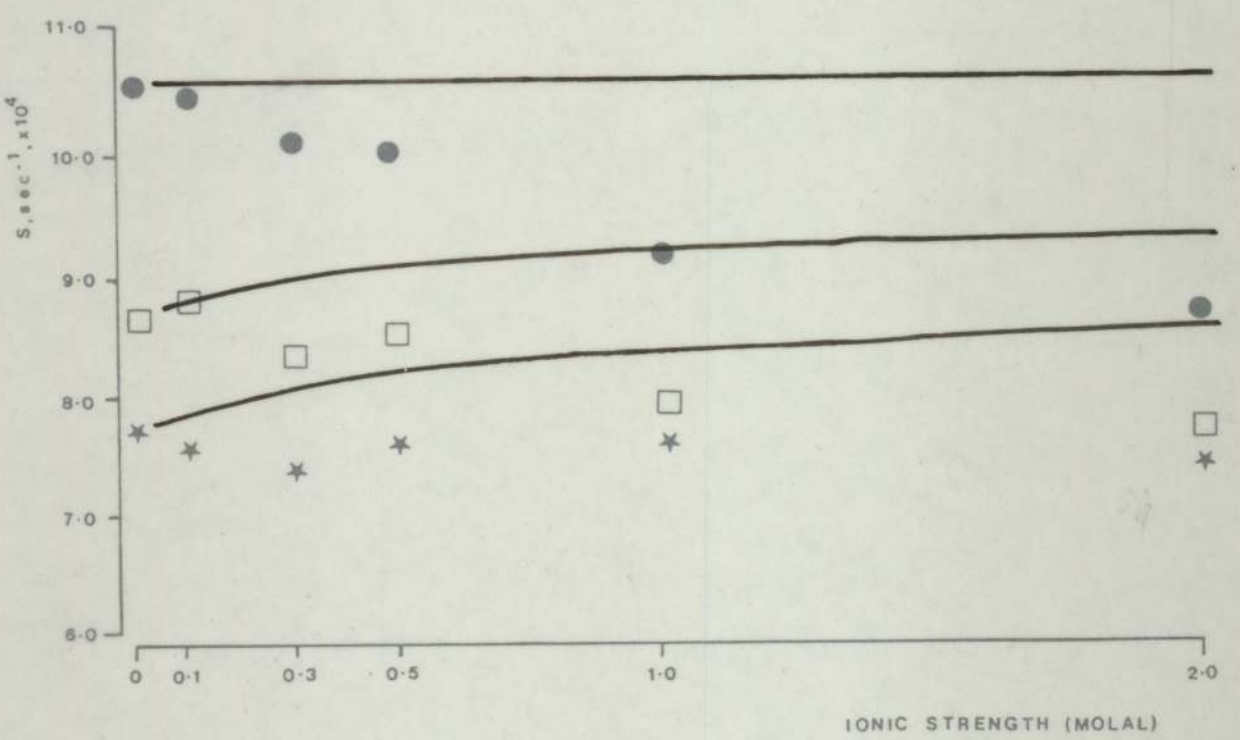

Figure 3.17 Experimental dependence of S on aqueous phase ionic strength for (✶) barbitone, (□) 5, 5'-diallybarbituric acid and (●) 5-allyl, 5'-isopentylbarbituric acid, each essentially non-ionised in the aqueous phase, in the two-phase transfer cell (octanol : aqueous) 100 rpm, 37°C in which aqueous phase ionic strength is varied using KCl.

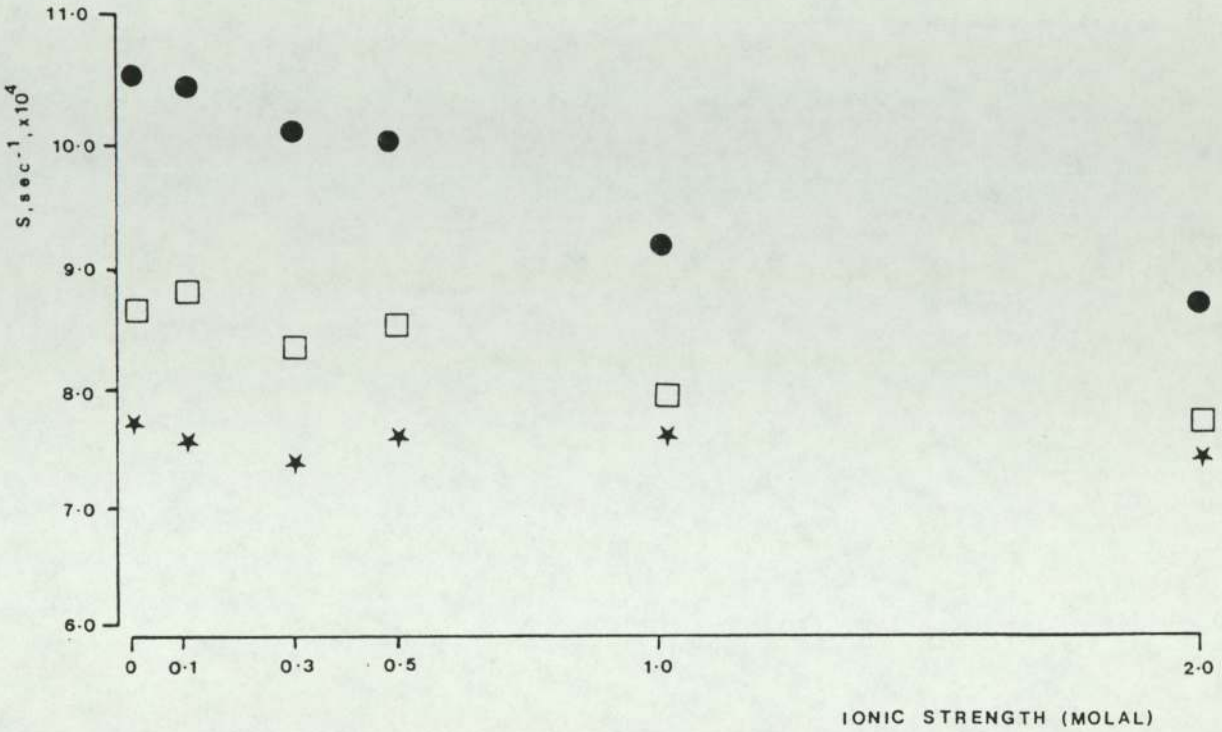

Figure 3.17 Experimental dependence of S on aqueous phase ionic strength for (✶) barbitone, (□) 5, 5'-diallybarbituric acid and (●) 5-allyl, 5'-isopentylbarbituric acid, each essentially non-ionised in the aqueous phase, in the two-phase transfer cell (octanol : aqueous) 100 rpm, 37^{o}C in which aqueous phase ionic strength is varied using KCl.

TABLE 3.14

Variation of the system-dependent parameter $[(R1)^{-2/3}\ (R2)^{1/6}\ (R3)^{1/3}]$ ($= K_D/\gamma$) with aqueous phase ionic strength (aqueous : octanol), 37°C.

Ionic strength[a]	R1	R2	R3	$[(R1)^{-2/3}\ (R2)^{1/6}\ (R3)^{1/3}]$
0	0.146	8.291	0.359	3.647
0.1	0.157	7.771	0.359	3.437
0.3	0.158	7.810	0.359	3.434
0.5	0.159	7.837	0.359	3.419
1.0	0.160	7.916	0.359	3.404
2.0	0.165	7.983	0.359	3.339

a. Ion type KCl; Molal.

independent of ion type, at a specified aqueous phase ionic strength, when either potassium chloride, sodium chloride or calcium chloride are used to adjust the ionic strength of the aqueous phase. However, when orthophosphate buffer solutions of varying aqueous phase ionic strength are employed as the aqueous phase, a marked deviation from theory is observed. Figure 3.17 shows how the effect of aqueous phase ionic strength (KCl) upon the transport kinetics of barbitone, 5, 5'-diallybarbituric acid and 5-allyl, 5'-isopentylbarbituric acid are poorly described by Eq. 1.9.

Deviation from theory could not be explained by ionic strength induced changes in pK_a (83). Less than 0.05 unit variation in pK_a could be detected following titration at 37°C in potassium chloride solutions with ionic strength values ranging 0 - 2.0 M (Table 3.15).

Values for viscosity, density and their ratio, kinematic viscosity, are shown in Table 3.16 for the mutually saturated octanol and aqueous phases, as functions of ion type and ionic strength variations in the aqueous phase. At a fixed stirring speed in the two-phase transfer cell, aqueous diffusive boundary layer thickness, h_1, should be given by the Levich equation (35, 36)

$$h_1 = 0.643 \, (\nu_1)^{1/6} \, (D_1)^{1/3} \, (\omega)^{-1/2} \qquad 3.35$$

Thus, if stirring speed and aqueous diffusivity remain constant, the term $h_1 \propto (\nu_1)^{1/6}$. The magnitude of change in $(\nu_1)^{1/6}$ due even to the extreme of ionic strength (Table 3.16) could thus induce a change in $h \simeq 0.5\%$. Changes in kinematic viscosity can thus be excluded as a means of inducing the variations in S (Figure 3.17).

Figure 3.18 shows how values for the organic/aqueous partition coefficient, K_D, of each solute studied varies with aqueous phase ionic strength. Marked variation in K_D values with differing buffer

TABLE 3.15

The effect of aqueous phase ionic strength and ion type on pK_a values for barbitone, 37°C.

Ionic strength[a]	Ion type	pK_a[b]
0	KCl	7.88
0.1	KCl	7.87
0.3	KCl	7.88
0.5	KCl	7.89
1.0	KCl	7.89
2.0	KCl	7.88
0.3	NaCl	7.85
0.3	$CaCl_2$	7.83

a. Aqueous phase; Molal.

b. Using 0.1 M NaOH as titrant; 37°C.

TABLE 3.16

Values for the viscosities, densities and kinematic viscosities of the mutually saturated aqueous and organic phases employed in the transfer studies at 37°C.

Ionic strength[a]	Physical constant	Aqueous phase[b] ion type			Organic phase[c]
		NaCl	$CaCl_2$	KCl	Octanol
0		0.693	0.693	0.693	4.734
0.1		0.685	0.686	0.696	4.434
0.3	viscosity[d]	0.701	0.701	0.697	4.423
0.5		0.719	0.721	0.699	4.407
1.0		0.748	0.751	0.705	4.395
2.0		0.826	0.816	0.722	4.367
0		0.994	0.994	0.994	0.819
0.1		0.998	0.997	0.999	0.819
0.3	density[e]	1.007	1.003	1.008	0.819
0.5		1.013	1.009	1.018	0.819
1.0		1.032	1.022	1.040	0.819
2.0		1.069	1.048	1.081	0.819
0		0.697	0.697	0.697	5.780
0.1		0.685	0.688	0.697	5.414
0.3	kinematic[f]	0.696	0.699	0.691	5.400
0.5	viscosity	0.709	0.715	0.687	5.380
1.0		0.725	0.735	0.678	5.366
2.0		0.772	0.779	0.668	5.332

a. Aqueous phase; Molal.

b. Saturated with octanol.

c. Saturated with aqueous phase; ion type KCl.

d. poise; x 10^{-2}.

e. gcm^{-3}.

f. viscosity/density; $cm^2\ sec^{-1}$ x 10^{-2}.

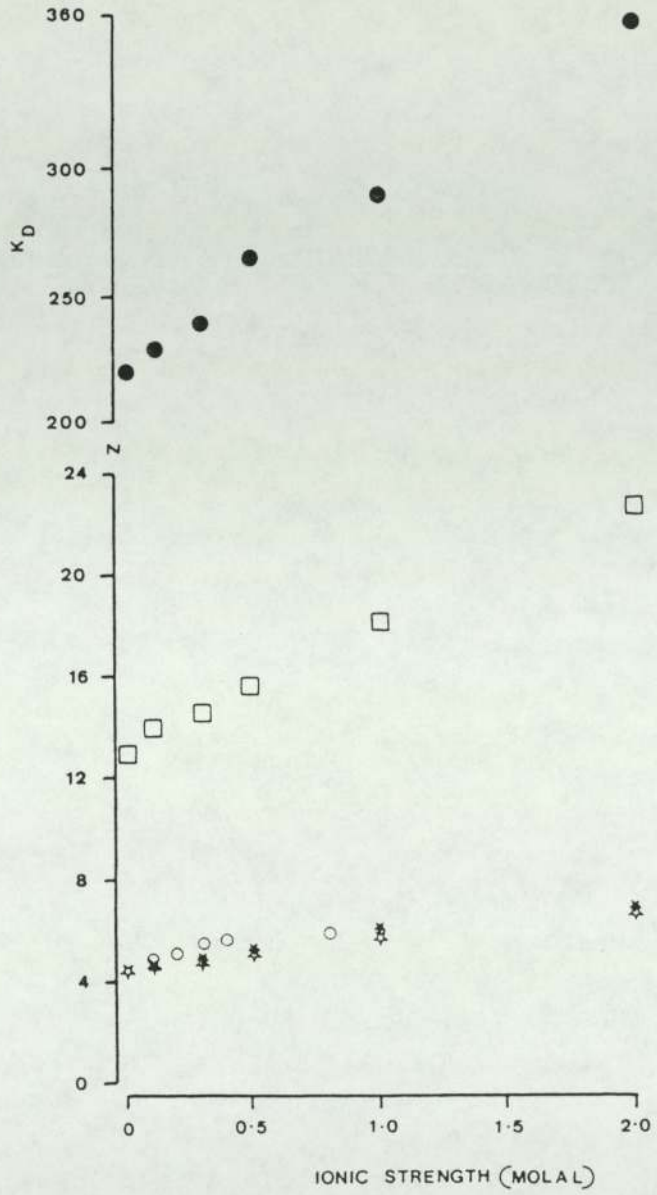

Figure 3.18 Experimental dependence of the organic/aqueous equilibrium partition coefficient, K_D, on aqueous phase ionic strength and type for (✱) barbitone, (□) 5, 5'-diallylbarbituric acid and (●) 5-allyl, 5'-isopentylbarbituric acid, 37°C, using (✱) KCl, (☆) $CaCl_2$ and (○) orthophosphate buffer solutions.

species and ionic strength have been observed in the literature (84, 85). It is apparent from Figure 3.18 that K_D remains effectively independent of ion type at a given ionic strength for barbitone when (✱) KCl, (✲) $CaCl_2$ and (○) orthophosphate buffer solutions are employed as the ion type. However, a marked increase in K_D is observed, for each solute investigated, with ionic strength. Partition coefficients play a significant role in the interfacial transport of solute in aqueous : organic phases (24 - 32). However at high values for K_D, transport rate constants in the two-phase transfer cell should remain independent of the organic/aqueous partition coefficient in accord with Eq. 3.36.

$$S_{(K_D \to \infty)} \to k_{12} \to \frac{D_1 A}{V_1 h_1} \qquad 3.36$$

In Chapter 2 it was shown that Eq. 3.36 was valid for solutes partitioning in the two-phase transfer cell when values for the resistance ratio, γ, indicate aqueous diffusional control ($\gamma \gtrsim 20$). Values for γ for each solute in the present study are documented in Table 3.13. Figure 3.17 shows, with reference to Table 3.13, that the most pronounced changes in S with aqueous phase ionic strength occur when values for γ indicate aqueous diffusional control (5-allyl, 5'-isopropylbarbituric acid). Under these circumstances partitioning kinetics should remain independent of K_D. Thus, the pronounced changes in K_D with aqueous phase ionic strength observed in Figure 3.18 cannot be used to account for the variation of S with aqueous phase ionic strength shown in Figure 3.17.

Equation 3.36 shows that as values for γ indicate aqueous diffusional control ($\gamma \gtrsim 20$) the apparent transport rate constants become controlled by the interfacial area, volume of the aqueous phase and boundary layer dimensions and diffusion coefficients of the

aqueous phase. In all studies performed in the two-phase transfer cell the area : volume ratio, A/V_1, was held constant. Thus when values for $\gamma \geq 20$, Eq. 3.36 shows that interfacial transport rate constants become controlled only by the boundary layer dimensions of the aqueous phase and aqueous phase diffusion coefficients. Thus, if the observed changes in S with aqueous phase ionic strength are due to changes in aqueous phase diffusion coefficients (85) and boundary layer thickness of the aqueous phase (35, 36) then as values of γ within a homologous series become smaller, (indicating a shift from aqueous diffusional control toward organic diffusional control), the effect of aqueous phase ionic strength should become less pronounced. The experimentally observed dependence of S upon aqueous phase ionic strength shown in Figure 3.17 are observed to be consistent with this hypothesis.

Thus, the absence of significant partitioning of the ionised species, changes in the kinematic viscosities of the phases and pk_a of the solute, appears to suggest that the most probable cause for the failure of Eqs. 3.19 and 3.33 to predict the dependence of S as a function of aqueous phase pH may be ascribed to either

(a) a resistance to solute transfer at the interface itself (73 - 80).

(b) changes in aqueous phase diffusion coefficients with ionic strength (86).

(c) some hydrodynamic phenomena (35, 36).

CHAPTER FOUR

SOLUTE IONISATION AND AQUEOUS PHASE IONIC STRENGTH EFFECTS IN THE ROTATING DIFFUSION CELL

4.1 INTRODUCTION

Octanol-aqueous interfacial transport kinetics of a variety of weakly acidic solutes were reported in the previous Chapter as functions of aqueous phase pH and ionic strength in the two-phase transfer cell. Transfer rate constants varied unpredictably with pH and fell significantly with increasing aqueous phase ionic strength. Results could not be explained by ionic strength induced variations in partition coefficient, pK_a, or kinematic viscosity of the phases. The deviation between theory and experiment was ascribed to either (a) some hydrodynamic phenomena (b) a resistance to solute transfer at the interface itself or (c) modification of aqueous phase diffusion coefficients in the presence of inorganic ions.

In the rotating diffusion cell (Figure 4.1) a stable aqueous : organic interface is established on either side of an organic phase impregnated porous membrane filter of fixed interfacial area. The hydrodynamic conditions that prevail on either side of the membrane are controlled by rotating disc hydrodynamics (87). Following experimentation in the rotating diffusion cell aqueous phase diffusion coefficients and interfacial resistances to mass transfer may be evaluated. This contrasts markedly to the two-phase transfer cell in which aqueous and organic diffusive boundary layers are formed on either side of an aqueous : organic interface, the absolute thickness of which are unknown.

In this Chapter, interfacial transfer kinetics of a variety of model solutes are estimated under conditions of varying aqueous phase pH and ionic strength in the rotating diffusion cell. S versus pH profiles determined in the rotating diffusion cell are compared to those estimated in the two-phase transfer cell (Chapter 3). Aqueous phase pH and ionic strength effects upon interfacial resistances and

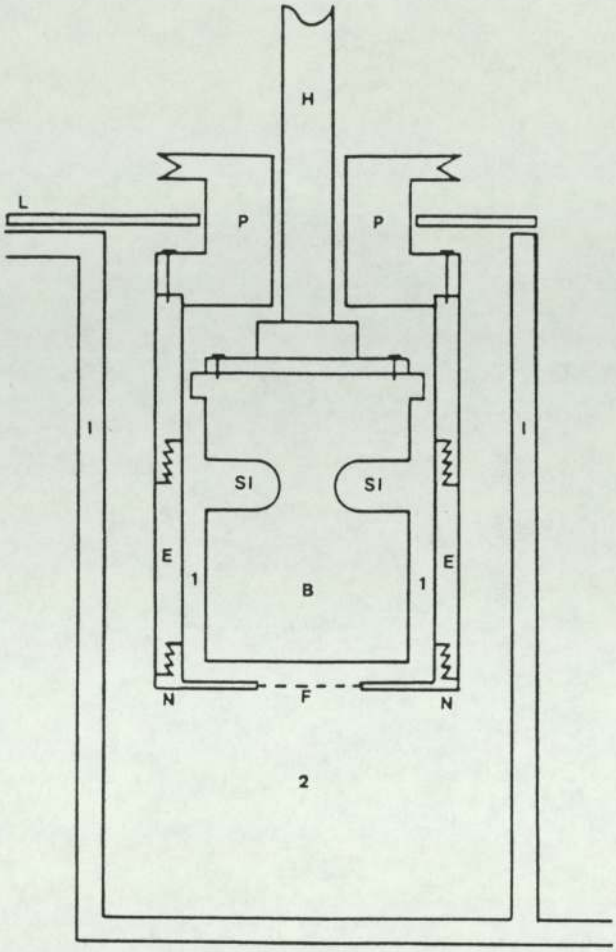

Figure 4.1 The rotating diffusion cell. A central stainless steel cylinder (E) of internal diameter = 3.9 cm rotates within a jacketed glass cell (I) of internal diameter = 6.0 cm and internal height = 12.0 cm. A pretreated millipore filter (F) divides the cell into two compartments, inner (1) and outer (2). A removable membrane holder (N) with bevelled annulus of angle = 10^{o} secures the filter exposing a membrane surface area of 3.142 cm^2. The inner compartment (1) with aqueous phase working volume V_1 = 35 ml incorporates a stationary PTFE baffle (B) of internal diameter = 2.6 cm, height = 4.3 cm and slots (S1) of width 1.0 cm positioned rigidly by means of a hollow stainless steel shaft (H). The stationary baffle (B) prevents the rotational motion of the cylinder being imparted to the central column of liquid above the exposed filter. A perspex lid (L) prevents excessive evaporation from the outer compartment (2) of organic phase working volume, V_2 = 160 ml. Rotation of the cell is achieved via the pulley (P).

aqueous phase diffusion coefficients in aqueous : octanol two-phase systems are examined. The absence of interfacial resistance, significant variation in aqueous phase diffusion coefficients, kinematic viscosity or pK_a and the adherence to theory in the rotating diffusion cell, suggest that interfacial instability appears to be variable and moderated by the ionic content of the aqueous phase in the octanol : aqueous two-phase transfer cell system.

4.1.1 THEORY

The rotating diffusion cell is shown in Figure 4.1. The general description of the rotating diffusion cell is given below where bracketed terms refer to Figure 4.1. A central stainless steel cylinder (E) of internal diameter = 3.9 cm rotates within a jacketed glass cell (I) of internal diameter = 6.0 cm and internal height = 12.0 cm. A pretreated millipore filter (F) divides the cell into two compartments, inner (1) and outer (2). A removable membrane holder (N) with bevelled annulus of angle = 10^{o} secures the filter exposing a membrane surface area of 3.142 cm^3. The inner compartment (1) with aqueous phase working volume, V_1 = 35 ml incorporates a stationary PTFE baffle (B) of internal diameter = 2.6 cm, height 4.3 cm and slots (S1) of width 1.0 cm positioned rigidly by means of a hollow stainless steel shaft (H). The stationary baffle (B) prevents the rotational motion of the cylinder being imparted to the central column of liquid directly above the exposed filter. A perspex lid (L) prevents excessive evaporation from the outer compartment (2) of organic phase working volume, V_2 = 160 ml. Rotation of the cell is achieved via the pulley (P). In all of the experiments documented in this Chapter, where interfacial transfer kinetics have been determined in the rotating diffusion cell (Figure 4.1) an interface is established between the aqueous phase (saturated with octanol), contained in the

inner compartment, and filter membrane, impregnated with the organic (aqueous saturated octanol) phase, held in the outer compartment. With mixing, the concentration of solute in the bulk phases of both the aqueous and organic phases are homogeneous, with rapidly changing solute concentration gradients being found in the organic phase impregnated filter membrane and in the areas directly adjacent to the filter membrane surface, where movement of the liquids is nil (45). These areas are the stagnant diffusive boundary layers of thickness, h, which are fixed by rotating disc hydrodynamics (87) and described through the Levich equation (35, 36)

$$h = 0.643\ \nu^{1/6}\ D^{1/3}\ \omega^{-1/2} \qquad 4.1$$

where ν refers to kinematic viscosity of the solvent (where $\nu = \eta/\rho$ and η is viscosity and ρ is density), D is the diffusion coefficient of the solute and ω is the frequency of rotation of the rotating diffusion cell.

Scheme 4.1 represents a concentration profile across the rotating filter membrane of length, l, and stagnant diffusive boundary layers of the aqueous, h_1, and organic, h_2, phases in the rotating diffusion cell.

Scheme 4.1

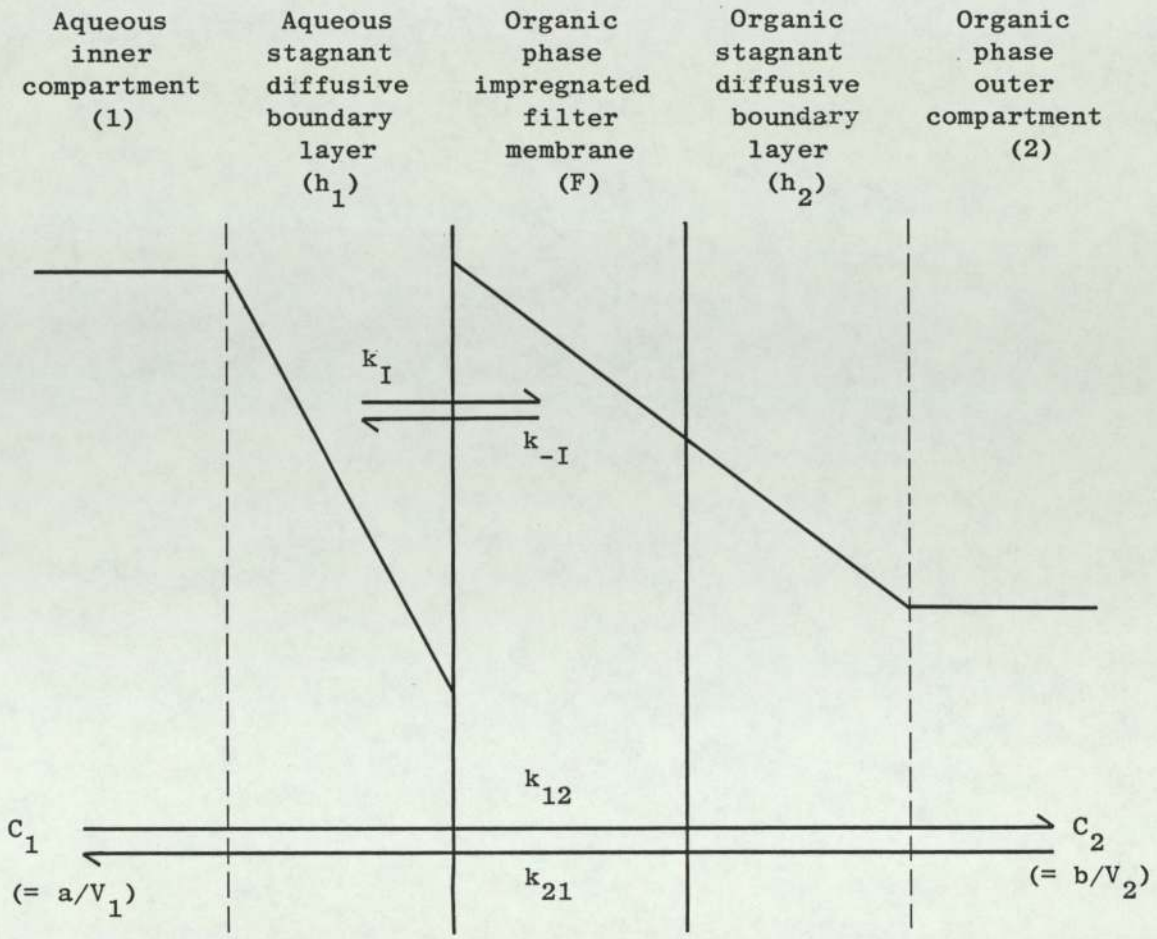

Where k_I and k_{-I} represent the forward and reverse rate constants for interfacial transfer, respectively, between the aqueous and organic phase impregnated membrane. Interfacial transfer kinetics for non-ionised solute transport from the bulk of the aqueous phase of the concentration C_1, to the bulk of the organic phase of concentration C_2, are also shown in Scheme 4.1 where k_{12} and k_{21} refer to the apparent first-order rate constants for partitioning in the forward and reverse direction, respectively. Scheme 4.1 shows four distinct resistances to solute transfer across the aqueous : organic interface. Individual resistances to solute transfer are additive (8, 88 - 91) and may be summated to define the total diffusional resistance to solute transfer. In accord with Scheme 4.1, the total diffusional

resistance to solute transfer may be defined as (45, 92 - 94).

$$R_T = \frac{1}{\vec{k}} = \frac{h_1}{D_1} + \frac{1}{\alpha k_I} + \frac{1}{\alpha D_2 K_D} + \frac{h_2}{D_2 K_D} \qquad 4.2$$

The four terms on the right hand side of Eq. 4.2 (with reference to Scheme 4.1) have the following significance (45, 92 - 94).

(a) h_1/D_1 describes the resistance to solute transfer through the aqueous stagnant diffusive boundary layer.

(b) $1/\alpha k_I$ represents the resistance to solute movement across the aqueous : organic interface where α is a fractional term defined as the area of the pores of the filter divided by its total area.

(c) $1/\alpha D_2 K_D$ describes the resistance to solute diffusion through the filter of length l.

(d) $h_2/D_2 K_D$ is the resistance to solute movement through the organic phase stagnant diffusive boundary layer.

Substitution of h form Eq. 4.1 into Eq. 4.2 gives

$$\frac{1}{\vec{k}} = \left[(0.643\ \nu_1^{1/6}\ D_1^{-2/3}) - \frac{(0.643\ \nu_2^{1/6}\ D_2^{-2/3})}{K_D}\right]\omega^{-\frac{1}{2}} + \frac{1}{\alpha k_I} - \frac{1}{\alpha D_2 K_D} \qquad 4.3$$

For the case where K_D is large (aqueous diffusional control, $\nu > 20$), the organic diffusive boundary layers and the organic phase impregnated filter play an insignificant role in the control of transfer kinetics and the terms $(0.643\ \nu_2^{1/6} D_2^{-2/3})/K_D$ and $1/\alpha D_2 K_D$ tend to a zero value. Under these conditions Eq. 4.3 reduces to

$$\frac{1}{\vec{k}} = (0.643\ \nu_1^{1/6}\ D_1^{-2/3})\omega^{-\frac{1}{2}} + \frac{1}{\alpha k_I} \qquad 4.4$$

and a plot of $1/\vec{k}$ versus $\omega^{-\frac{1}{2}}$, in accord with Eq. 4.4, should be linear with a slope equal to

$$\text{slope} = 0.643\ \nu_1^{1/6}\ D_1^{-2/3} \qquad 4.5$$

and intercept equal to the resistance offered to solute transfer by the interface itself

$$\text{intercept} = 1/\alpha k_I \qquad 4.6$$

Thus, plots of $1/\vec{k}$ versus $\omega^{-\frac{1}{2}}$ may be conceived as plots of total diffusional resistance to solute transfer ($R_T = 1/\vec{k}$) from one phase to the other at each stirring speed. For the case where K_D is high, a significant intercept may be ascribed to a large interfacial resistance, while a constant slope (with increasing ionic strength or variation in pH) is indicative of a constant value for the diffusion coefficient in the aqueous phase (Eqs. 4.5 and 4.6, respectively).

4.1.1.1 ESTIMATION OF THE PERMEABILITY COEFFICIENT, $\vec{k}$, IN THE ROTATING DIFFUSION CELL UNDER CONDITIONS OF CONSTANT AQUEOUS PHASE pH FOR NON-IONISED SOLUTE TRANSFER.

The amount of solute, a, diffusing across the filter with respect to time, is dependent on Fick's first law and may be written as (45)

$$J = -da/dt = V_1(-dC_1/dt) = A(\vec{k}\,C_1 - \overleftarrow{k}\,C_2) \qquad 4.7$$

where A is the interfacial area of the filter over which transfer takes place and $\vec{k}$ and $\overleftarrow{k}$ refer to the permeability coefficients of the forward and reverse transfer process, respectively. $\vec{k}$ and $\overleftarrow{k}$ may be defined through (45)

$$\vec{k} = \frac{D_1(D_2)^2(\alpha)^2 k_I K_D}{(D_2)^2 h_1(\alpha)^2 k_I K_D + D_1(D_2)^2 \alpha K_D + D_1 D_2 \alpha k_I l + D_1 D_2 h_2(\alpha)^2 k_I} \qquad 4.8$$

and

$$\overleftarrow{k} = \frac{D_1(D_2)^2(\alpha)^2 k_I}{(D_2)^2 h_1(\alpha)^2 k_I K_D + D_1(D_2)^2 \alpha K_D + D_1 D_2 \alpha k_I l + D_1 D_2 h_2(\alpha)^2 k_I} \qquad 4.9$$

where, by definition (45)

$$K_D = \overrightarrow{k}/\overleftarrow{k} \qquad 4.10$$

Substitution of $\overleftarrow{k}$ ($= \overrightarrow{k}/K_D$) from Eq. 4.10 into Eq. 4.7 gives

$$J = \frac{-da}{dt} = A\left[\overrightarrow{k}\,C_1 - \frac{\overrightarrow{k}\,C_2}{K_D}\right] \qquad 4.11$$

Substitution of $C_1 = a/V_1$ and $C_2 = b/V_2$ into Eq. 4.11 yields

$$J = \frac{-da}{dt} = A\left[\frac{\overrightarrow{k}a}{V_1} - \frac{\overrightarrow{k}\,b}{V_2 K_D}\right] \qquad 4.12$$

since the amount of solute in the organic phase, b, may be calculated from $b = a^o - a$, Eq. 4.12 may also be written as

$$J = \frac{-da}{dt} = A\left[\frac{\overrightarrow{k}a}{V_1} - \frac{\overrightarrow{k}(a^o - a)}{K_D V_2}\right] \qquad 4.13$$

Intergration of Eq. 4.13 from t = 0 to t followed by substitution of C_∞ for $A\,\overrightarrow{k}\,a_o V_1/(A\,\overrightarrow{k}\,V_2\,K_D + AV_1\overrightarrow{k})$ yields:-

$$\ln(C_1 - C_1^\infty) = \ln\,(C_1^o - C_1^\infty) - St \qquad 4.14$$

where C_1^o and C_1^∞ are the initial and final concentrations of solute in the aqueous phase at time t = 0 and t = ∞, respectively. Thus a plot of $\ln(C_1 - C_1^\infty)$ versus time is linear with a negative slope, S, which provides a value for the apparent first-order rate constant for partitioning, S

$$S = k_{12} + k_{21} \qquad 4.15$$

where S is given by

$$S = \frac{A\,\overrightarrow{k}}{V_1} + \frac{A\,\overrightarrow{k}}{K_D V_2} \qquad 4.16$$

rearranging for $\vec{k}$ in Eq. 4.16 gives

$$1/\vec{k} = \frac{A[V_1^{-1} + (V_2K_D)^{-1}]}{S} \qquad 4.17$$

Thus, a solute may be introduced as a bolus at time t = 0 into the aqueous phase of a rotating diffusion cell. Its interfacial transfer kinetics, S, may be estimated from C_1 versus time profiles studied under previously defined conditions of aqueous phase pH which ensure essentially only the presence of non-ionised solute in the aqueous phase. A knowledge of A, V_1, V_2, the organic : aqueous partition coefficient, K_D, and the first-order rate constant for non-ionised solute transfer, S, enables an estimation of $\vec{k}$ from Eq. 4.17. Plots of $1/\vec{k}$ versus $\omega^{-\frac{1}{2}}$ may then be constructed after direct measurement of ω.

4.1.1.2 ESTIMATION OF THE PERMEABILITY COEFFICIENT, $\vec{k}$, IN THE ROTATING DIFFUSION CELL IN WHICH AQUEOUS PHASE pH IS VARIED.

For the case where an ionising solute is allowed, by variation of the aqueous phase pH, to possess a degree of dissociation, assuming that only the non-ionised solute may partition, then its partitioning kinetics in the rotating diffusion cell should accord with Scheme 4.2.

Scheme 4.2

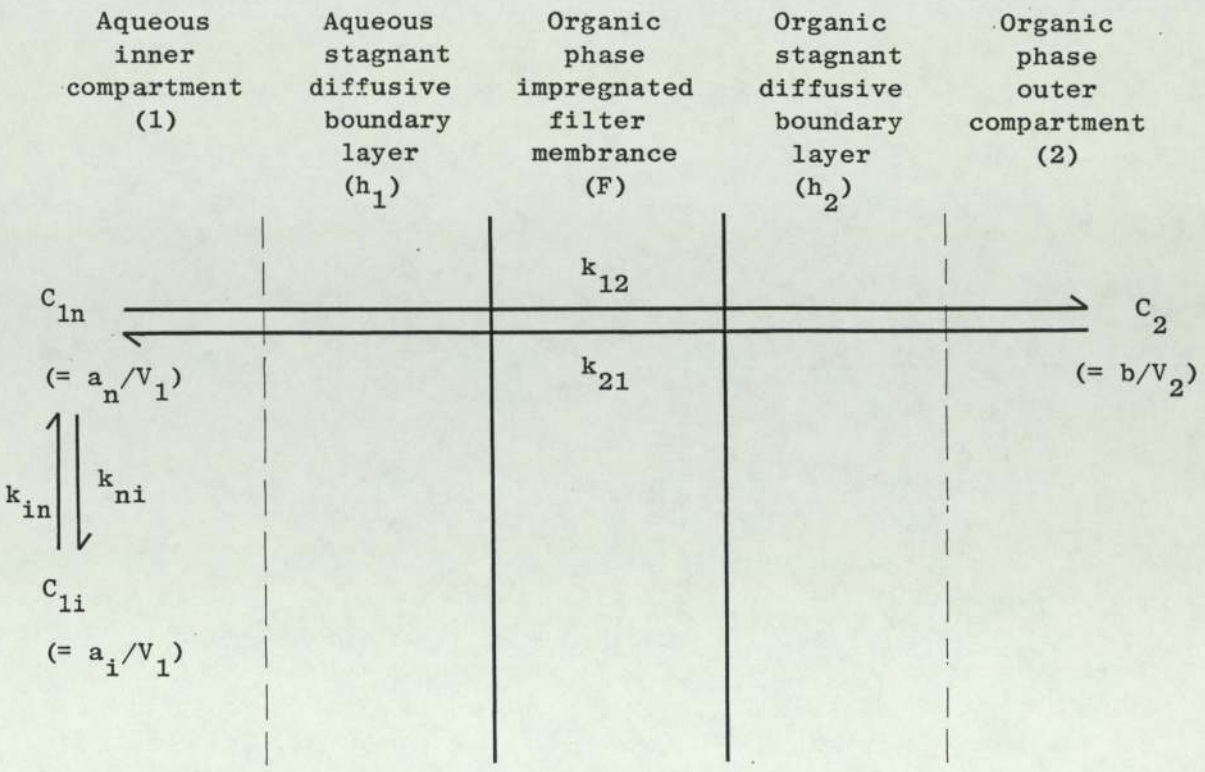

where symbols are defined in the glossary of terms. The flux, J, of solute from the bulk of the aqueous phase to the bulk of the organic phase may be given by

$$J = \frac{db}{dt} = \frac{-d(a_n + a_i)}{dt} = A(\vec{k}\, C_{1n} - \vec{k}\, C_2) \qquad 4.18$$

Substitution of $\vec{k}$ $(= k/K_D)$ from Eq. 4.10 into Eq. 4.18 gives

$$J = \frac{-d(a_n + a_i)}{dt} = A\left[\vec{k}\, C_{1n} - \frac{\vec{k}\, C_2}{K_D}\right] \qquad 4.19$$

Substitution of $C_{1n} = a_n/V_1$ and $C_2 = b/V_2$ into Eq. 4.19 yields

$$J = \frac{-d(a_n + a_i)}{dt} = A\left[\frac{\vec{k}\, a_n}{V_1} - \frac{\vec{k}\, b}{K_D V_2}\right] \qquad 4.20$$

since the amount of solute in the organic phase, b, may be calculated from $b = a_o - (a_n + a_i)$, Eq. 4.20 may also be written as

$$J = \frac{-d(a_n + a_i)}{dt} = \vec{Ak}\left[\frac{a_n}{V_1} - \frac{a_o}{K_D V_2} + \frac{a_n + a_i}{K_D V_2}\right] \qquad 4.21$$

Integration of Eq. 4.21 from t = 0 to t followed by substitution of C_∞ for $\vec{A}\vec{k}\, a_o V_1/(\vec{A}\vec{k}\, V_2 K_D\, fn + AV_1\vec{k})$ (where fn refers to the fraction of non-ionised solute in the aqueous phase) gives

$$\ln(C_1 - C_1^\infty) = \ln(C_1^o - C_1^\infty) - St \qquad 4.22$$

Thus, following experimentation in the rotating diffusion cell in which aqueous phase pH is varied, a plot of $\ln(C_1 - C_1^\infty)$ versus time, t, is linear with a negative slope, S,

$$S = k_{12}\, fn + k_{21} \qquad 4.23$$

where S is given by

$$S = \frac{fn\, A\vec{k}}{V_1} + \frac{A\vec{k}}{K_D V_2} \qquad 4.24$$

rearranging for $1/\vec{k}$ gives

$$1/\vec{k} = \frac{A\left[fn\, V_1^{-1} + (V_2 K_D)^{-1}\right]}{S} \qquad 4.25$$

Thus, in the rotating diffusion cell in which aqueous phase pH is varied, values of $1/\vec{k}$ for a chosen solute at a specified pH and rotation speed may be estimated using 4.25 from knowledge of V_1, V_2, A, the partitioning kinetics, partition coefficient, pK_a of the solute and pH of the aqueous phase (fn; Eq. 3.2). Thus plots of $1/\vec{k}$ versus $\omega^{-\frac{1}{2}}$ may be constructed after initial experimentation in the rotating diffusion cell in which aqueous phase pH is varied after direct measurement of ω.

A rotating diffusion cell is employed in the present study to

determine aqueous phase pH and ionic strength effects upon aqueous phase diffusion coefficients and interfacial resistance in aqueous : octanol two-phase systems. The information gained from partitioning studies performed using the rotating diffusion cell is employed to explain the experimentally observed dependence of S on aqueous phase ionic strength and pH in the two-phase transfer cell. Errors induced by variation in partition coefficient with the content of the aqueous phase in the rotating diffusion cell were avoided by investigating solutes whose interfacial transfer was subject to aqueous diffusional control and independent of K_D (Chapter 2), $\gamma \geq 20$ (5-allyl-5'-isopentyl-barbituric acid and butylparahydroxybenzoate).

4.2 EXPERIMENTAL

Interfacial transfer kinetics were studied for 5-allyl, 5'-isopentylbarbituric acid and butylparahydroxybenzoate in an aqueous : octanol two-phase system in which aqueous phase ionic strength was varied in the rotating diffusion cell (Figure 4.1). Transport kinetics were also investigated for 5-allyl, 5'-isopropyl barbituric acid, 5-allyl, 5'-isopentyl barbituric acid and ethylparahydroxy-benzoate in a aqueous : octanol two-phase system in which aqueous phase pH was varied in the rotating diffusion cell. Except where specified, the experimental procedure described below applies to experiments in which aqueous phase ionic strength and aqueous phase pH are varied. The general description of the rotating diffusion cell used in the present study is given in Figure 4.1. The inner compartment contained 35 ml of an aqueous phase saturated with octanol (Spectrograde, Fisons Ltd., Loughborough, England). The outer compartment contained 160 ml of organic phase comprising octanol saturated with aqueous phase. Mutual presaturation of the aqueous and organic phases was achieved by mixing for > 48 hours at 37 $\pm$ 0.1^{o}C (Model Grant Water Bath, Grant Instruments Ltd., Cambridge, England) prior to introduction into the respective compartments. Aqueous phases comprised either 0.3 M orthophosphate buffer (Table 3.2) systems or solutions adjusted to molal ionic strength, using potassium chloride (A.R. Grade, Fisons Ltd., Loughborough, England) to give aqueous phase ionic strength ranging 0 - 2.0 M. For the case of ionic strength experiments, the aqueous phase pH was adjusted to pH 4.0 using 1 M HCl or 1 M NaOH prior to the initiation of an experiment and ensured that essentially only the non-ionised species were present in the aqueous phase. The pH varied by no more than 0.3 pH units throughout a kinetic run, thereby precluding the need for buffers.

Aqueous and organic phases were separated by a porous polytetraflouroethane membrane [Millipore type FHUP 04700; 0.5μm pore size; 60μm thickness; porosity = 0.85 (Millipore S.A., 67120, Molsheim, France)] saturated with octanol (presaturated with aqueous phase). Saturation of the filter membrane was achieved by submerging in octanol for ~ 15 minutes and wiping away excess octanol with an absorbant tissue. A removable membrane holder secured the membrane in position, exposing a membrane surface area of 3.142 cm^2. Solutes were introduced into the aqueous donor phase as a 0.25 ml methanolic bolus in concentrations (~ 2×10^{-4} M; barbiturates, ~ 7.5×10^{-5} M; parahydroxybenzoates) to produce absorbances in the aqueous phase of ~ 0.9 absorbance units. The aqueous phase was pumped (Model RPD lab. pump, Fluid Metering Inc., Oyster Bay, N.Y., U.S.A.) through a flow cell in a spectrophotometer (Model CE 272, Cecil Instruments, Cambridge, England). The concentration of solute in the aqueous phase, C_1, was continually monitored by automatically recording (Model J.J. CR452 recorder, J.J. Lloyd Instruments Ltd., Warsash, Southampton, England) the absorbance as a function of time at wavelengths according to Table 2.2. The rotating diffusion cell was driven (Model RZR 50 stirrer, Heidolph, West Germany) via a set of pulleys. The rotation speed of the cell was monitored using an optical hand tachometer (Model TM2011, RS Components Ltd, England) and varied < 1% at each preselected rotation speed. Excessive evaporation losses were prevented by the addition of a perspex lid to the outer compartment, thus phase volumes were kept constant throughout a kinetic determination. All transfer studies were performed at $37 \pm 0.1^{\circ}C$.

Values for $1/\vec{k}$ were estimated for 5-allyl 5-isopentyl barbituric acid and butylparahydroxybenzoate under conditions of varying aqueous phase ionic strength (pH = constant and adjusted to allow the presence only of the non-ionized species) using Eq. 4.17 after experimental

determination of S (= $k_{12} + k_{21}$) at each rotation speed and ionic strength employed in the study. Values for $\vec{1/k}$ for 5-allyl, 5'-isopropylbarbituric acid, 5-ally, 5'-isopentylbarbituric acid and ethylparahydroxybenzoate were estimated under conditions of varying aqueous phase pH using Eq. 4.25 after experimental determination of S (= $k_{12}fn + k_{21}$) for each solute at each rotation speed and aqueous phase pH employed in the study.

Values for the forward, k_{12}, and reverse, k_{21}, first- order rate constant for partitioning were estimated for 5-allyl, 5'-isopropyl-barbituric and, 5-allyl, 5'-isopentylbarbituric acid and ethyl-parahydroxybenzoate at each pH value where essentially only the non-ionised form predominated (fn = 1; S = $k_{12} + k_{21}$) using Eqs. 2.7 and 2.8, respectively. k_{12} and k_{21} were estimated from knowledge of the apparent first-order rate constant for partitioning, S (= $k_{12} + k_{21}$) at these pH values and their (true) organic : aqueous equilibrium partition coefficient, K_D. Values for fn were estimated using Eq. 3.8 and used in Eq. 4.23 to generate theoretical values for S at each rotation speed, as a function of aqueous phase pH.

The surface tension of pure octanol and aqueous phases comprising various ionic strengths (molal; KCl) alongside aqueous phase saturated octanol and octanol saturated aqueous phase comprising various ionic strengths were determined using a modified Wilhelmy plate method (95 - 97) 20°C. A clean flat glass plate (10 mm x 5 mm x 0.15 mm) was attached to the beam of a sensitive micro-force balance (Model MK2B, CI Electronics Ltd., Salisbury, Wiltshire, England) and counter-balanced in air using small weights to attain a zero reading on the electrical control cabinet. 50 ml of liquid to be measured was placed in a jacketed glass beaker that rested upon a table of adjustable

height and allowed to attain a temperature of 20 $\pm$ 0.1°C. Prior to measurement, the thermostat was switched off to avoid excessive vibration in the liquid surface, which interfered with accuracy. The table was elevated until the flat glass plate made contact with the liquid surface and then slowly lowered until the plate detached itself from the liquid surface. The upward force applied by the torque on the wire to just exceed the downward pull on the flat glass plate by the liquid surface was measured by the micro-force balance and recorded (Model J.J. CRC52 recorder, J.J. Lloyd Instruments Ltd., Southampton, England). A standard curve was calibrated from knowledge of previously published surface tension values and experimentally determined pen deflection measurements. Solvents, source, grade and published surface tension values of the solvents employed to construct the calibration curve are documented in Table 4.21. Surface tension values of the solutions under investigation were estimated using pen deflection measurements by direct extrapolation of the standard curve.

The interfacial tension of aqueous : octanol systems in which aqueous phase ionic strength was varied (molal; KCl) were determined using a modified Wilhelmy plate method (95 - 97) at 20°C. A clean flat glass plate (10 mm x 5 mm x 0.15 mm) was attached to the beam of a sensitive micro-force balance (Model MK2B, C.I. Electronics Ltd., Salisbury, Wiltshire, England). The flat glass plate was completely immersed in the aqueous saturated organic phase at 20°C and counter-balanced using small weights, until a zero reading was attained on the connecting electrical control balance. The plate was then removed, cleaned and replaced on the beam of the balance. 50 ml of organic phase saturated aqueous phase was then added to a jacketed glass beaker. The glass beaker was raised until the flat glass plate became submerged in the aqueous phase. 50 ml of aqueous saturated organic

phase was slowly added on top of the aqueous phase and the system allowed to attain the working temperature (20 $\pm$ 0.1^{o}C) at which point the thermostat was switched off to avoid excessive surface movement. The adjustable table was then slowly lowered until the plate detached itself from the aqueous : organic interface and recorded (Model J.J. CR652, J.J. Lloyd Instruments Ltd., Southampton, England). A standard curve was calibrated from empirically determined pen deflection measurements using aqueous : organic two-phase systems of known interfacial tension. Solvents, source, grade and published interfacial tension values of the solvent systems employed to construct the calibration curve are determined in Table 4.22. The interfacial tension of the unknown systems were then determined from knowledge of their pen deflection measurements and direct extrapolation of the calibration curve.

4.3 RESULTS AND DISCUSSION

Table 4.1 documents experimental replicates for interfacial transport of 5-allyl, 5'-isopentyl barbituric acid, essentially non-ionised in the aqueous phase of the rotating diffusion cell [aqueous (0.3 M KCl; pH 4.0) : octanol impregnated filter : octanol] at different rotation speeds expressed in $\omega^{-\frac{1}{2}}$ where

$$\omega^{-\frac{1}{2}} = 1 / \sqrt{(rpm/60)} \qquad 4.26$$

rpm refers to revolutions of cell per minute. Errors in the determination of S under constant conditions in the rotating diffusion cell were always < 5%. The standard deviations of the rate constants compare favourably with those obtained by other workers using similar rotating diffusion cells (66, 98, 99). Experimentally determined transport rate constants, S, are shown to increase as a function of decreasing $\omega^{-\frac{1}{2}}$ (rpm increasing) (Table 4.1). Substitution for $1/\vec{k}$ ($\nu \geq 20$) from Eq. 4.2 into Eq. 4.17 and rearranging for S gives

$$S = \frac{A \left[V_1^{-1} + (V_2 K_D)^{-1} \right]}{(h_1/D_1) + (1/\alpha k_I)} \qquad 4.27$$

Substitution for h (= $0.643\, \nu^{1/6}\, D^{1/3}\, \omega^{-\frac{1}{2}}$) from Eq. 4.1 into Eq. 4.27 gives

$$S = \frac{A \left[V_1^{-1} + (V_2 K_D)^{-1} \right]}{0.643\, \nu_1^{1/6}\, D_1^{-2/3}\, \omega^{-\frac{1}{2}} + (1/\alpha k_I)} \qquad 4.28$$

At different values for $\omega^{-\frac{1}{2}}$ in the rotating diffusion cell (constant temperature) the terms D_1, A, α, V, k_I, K_D and ν should remain constant for a specified solute. Under these conditions Eq. 4.28 predicts a reciprocal dependence of S upon $\omega^{-\frac{1}{2}}$. The observed increase in S with decrease in $\omega^{-\frac{1}{2}}$ shown in Table 4.1 is consistent with Eq. 4.28.

TABLE 4.1

Reproducibility of S^a values for 5-allyl, 5'-isopentylbarbituric acid in the rotating diffusion cell using an aqueous (0.3 M KCl; pH 4.0) : octanol impregnated filter : octanol system at 37°C.

$\omega^{-\frac{1}{2}}$ [b]	Experiment number										Mean	n [d]
	1	2	3	4	5	6	7	8	9	10	(± SD) [c]	
1.0				7.98	7.85			8.37		8.03	8.07 (± 0.2)	4
0.9	8.15	8.68	8.13			8.50					8.37 (± 0.3)	4
0.8				10.1	9.55		9.58		10.7	9.87	9.97 (± 0.5)	5
0.7	10.6	11.1	10.6			10.4					10.7 (± 0.2)	4
0.65	12.2	12.7	12.7			12.2	11.6			12.9	12.4 (± 0.5)	6
0.6				13.2	13.5		14.1	14.5	13.6		13.8 (± 0.6)	5
0.5				17.5				16.7	15.5	15.9	16.4 (± 0.9)	4
0.4	18.0	20.8	21.2		17.5				18.7	17.7	18.9 (± 0.2)	6

a. Kinetic analysis based on Eq. 4.14; $sec^{-1} \times 10^5$.

b. Equation 4.26.

c. Standard deviation; $\times 10^5$ (49)

d. Number of estimates.

Experimental replicates for $1/\vec{k}$ (= R_T) for 5-allyl, 5'-isopentyl-barbituric acid at various rotation speeds ($\omega^{-\frac{1}{2}}$) in the rotating diffusion cell [aqueous (0.3 M KCl; pH 4.0) : octanol impregnated filter : octanol] are documented in Table 4.2. Values for the total diffusional resistance to solute transfer (= $1/\vec{k}$) were estimated using Eq. 4.17 with values for V_1, V_2, A and K_D held constant at their experimentally determined values of 35, 160, 2.67 and 249, respectively. S values were taken from Table 4.1. The small standard deviations (SD) associated with the mean $1/\vec{k}$ values compare favourably with those obtained by other workers using similar rotating diffusion cells (72). Figure 4.2 shows the relationship found between $1/\vec{k}$ and $\omega^{-\frac{1}{2}}$ in the rotating diffusion cell. The increase in $1/\vec{k}$ with increasing $\omega^{-\frac{1}{2}}$ and linearity of data (correlation coefficient >0.99, $n = 8$) was consistent with earlier observations based on Eq. 4.4. The absence of a significant intercept in the plots of $1/\vec{k}$ versus $\omega^{-\frac{1}{2}}$ (Figure 4.2) for 5-allyl, 5'-isopentylbarbituric acid showed that interfacial resistance was negligible in this case (Eq. 4.4).

4.3.1 EFFECT OF SOLUTE IONISATION IN THE AQUEOUS PHASE ON SOLUTE TRANSFER KINETICS IN THE ROTATING DIFFUSION CELL (AQUEOUS : OCTANOL IMPREGNATED FILTER : OCTANOL) 37°C

The effect of solute ionisation in the aqueous phase of a rotating diffusion cell (aqueous : octanol impregnated filter : octanol), 37°C, upon the transport kinetics of 5-allyl, 5'-isopropyl-barbituric acid, 5-allyl, 5'-isopentylbarbituric acid and ethyl-parahydroxybenzoate at various rotation speeds are documented as S_{obs} in Tables 4.3 through 4.5. Values for S_{obs} were used to test the validity of a theoretical equation (Eq. 4.23) derived in Section 4.1.1.2 In order to test Eq. 4.23, mean values for S and their corresponding k_{12} and k_{21} values were estimated from values of S determined at each

TABLE 4.2

Reproducibility of $1/\vec{k}^{a}$ values for 5-allyl, 5'-isopentylbarbituric acid in the rotating diffusion cell using an aqueous (0.3 M KCl; pH 4.0) : octanol impregnated filter : octanol system at 37°C.

$-\frac{1}{2}$ [b]	Experiment number										Mean	n [d]
	1	2	3	4	5	6	7	8	9	10	(± SD) [c]	
1				954	972			912		984	947 (± 25)	4
0.9	936	876	936			894					912 (± 31)	4
0.8				756	798		798		714	774	768 (± 35)	5
0.7	714	690	720			732					714 (± 17)	4
0.65	630	600	600			630	654			592	618 (± 24)	6
0.6				581	565		542	524	563		555 (± 22)	5
0.5				436				458	491	479	466 (± 24)	4
0.4	434	367	361		436				409	432	405 (± 33)	6

a. Equation 4.17; cm sec^{-1}.

b. Equation 4.26.

c. Standard deviation (49).

d. Number of estimates.

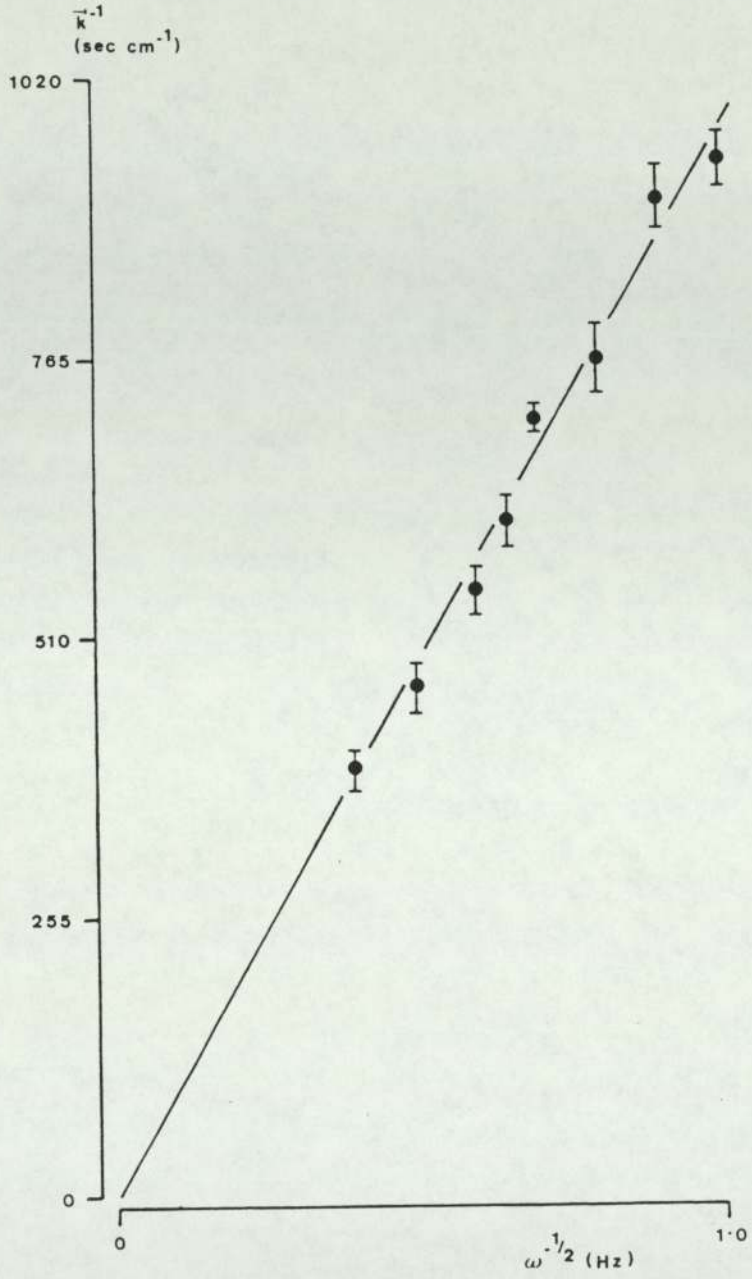

Figure 4.2 Plot of $1/\vec{k}$ versus $\omega^{-\frac{1}{2}}$ for 5-allyl, 5-isopentylbarbituric acid in an octanol : aqueous (0.3 M KCl; pH 4.0) two-phase mode at various rotation speeds in the rotating diffusion cell, 37°C.

TABLE 4.3

Theoretical (S_{th}; Eq. 4.23) and experimental (S_{obs}) estimates of S (= k_{12} fn + k_{21}) for 5-allyl, 5'-isopropylbarbituric acid (pk_a = 7.81) at various aqueous phase pH and rotation speeds in the rotating diffusion cell, 37°C.

rpm	pH[a]	fn[b]	S_{obs}[c]	S_{th}[d]	% error[e]
	4.34	1	6.12	6.22	+ 1.6
	4.86	1	6.31	6.22	- 1.4
60	5.85	1	5.88	6.22	+ 4.8
	6.92	0.88	5.74	5.39	- 6.1
	7.31	0.76	4.42	4.68	+ 5.8
	7.98	0.40	2.70	2.56	- 5.2
	4.34	1	7.42	7.35	- 0.9
	4.86	1	7.64	7.35	- 3.8
	5.85	1	6.99	7.35	+ 5.2
94	6.92	0.88	6.90	6.50	- 5.8
	7.31	0.76	5.11	5.64	+ 10.3
	7.98	0.40	3.20	3.09	- 3.4
	4.34	1	9.86	9.66	- 2.0
	4.86	1	10.00	9.66	- 3.4
	5.85	1	9.13	9.66	+ 5.8
167	6.92	0.88	9.11	8.54	- 6.3
	7.31	0.76	6.64	7.42	+ 10.7
	7.98	0.40	4.22	4.05	- 4.0
	4.34	1	12.9	12.9	0
	4.86	1	13.9	12.9	- 7.2
	5.85	1	12.1	12.9	+ 6.6
375	6.92	0.88	12.0	11.6	- 5.0
	7.31	0.76	7.79	9.91	+ 27.2
	7.98	0.40	5.59	5.41	- 3.2

a. Aqueous phase; 37°C.

b. Eq. 3.2.

c. Based on kinetic analysis; Eq. 4.22; $sec^{-1} \times 10^5$.

d. Eq. 4.23: $sec^{-1} \times 10^5$.

e. $100\ (S_{th} - S_{obs})/S_{obs}$.

TABLE 4.4

Theoretical (S_{th}; Eq. 4.23) and experimental (S_{obs}) estimates of S (= k_{12} fn + k_{21}) for 5-allyl, 5'-isopentylbarbituric acid (pK_a = 7.90) at various aqueous phase pH and rotation speeds in the rotating diffusion cell, 37°C.

rpm	pH[a]	fn[b]	S_{obs}[c]	S_{th}[d]	% error[e]
	4.34	1	7.94	7.94	0
	4.86	1	8.24	7.94	- 3.6
	5.85	1	7.65	7.94	+ 3.8
60	6.92	0.91	7.67	7.23	- 5.7
	7.31	0.79	7.45	6.28	- 15.7
	7.98	0.45	5.81	3.59	- 38.2
	4.34	1	10.0	10.2	+ 2.0
	4.86	1	10.4	10.2	- 1.9
	5.85	1	10.2	10.2	0
94	6.92	0.91	9.78	9.23	- 5.6
	7.31	0.79	9.25	8.02	- 13.2
	7.98	0.45	7.04	4.59	- 34.8
	4.34	1	14.0	14.4	+ 2.9
	4.86	1	14.8	14.4	- 2.7
	5.85	1	14.5	14.4	- 0.7
167	6.92	0.91	14.1	13.1	- 7.1
	7.31	0.79	12.8	11.4	- 10.9
	7.98	0.45	9.35	6.49	- 30.5
	4.34	1	20.7	21.9	+ 5.8
	4.86	1	23.0	21.9	- 4.8
	5.85	1	21.9	21.9	0
375	6.92	0.91	26.2	19.9	- 6.1
	7.31	0.79	17.7	17.3	- 2.3
	7.98	0.45	11.8	9.89	- 16.2

a. Aqueous phase; 37°C.

b. Eq. 3.2.

c. Based on kinetic analysis; Eq. 4.22; $sec^{-1} \times 10^5$.

d. Eq. 4.23; $sec^{-1} \times 10^5$.

e. $100 (S_{th} - S_{obs})/S_{obs}$.

TABLE 4.5

Theoretical (S_{th}: Eq. 4.23) and experimental (S_{obs}) estimates for S (= k_{12} fn + k_{21}) for ethylparahydroxybenzoate (pK_a = 8.28) at various aqueous phase pH and rotation speeds in the rotating diffusion cell, 37°C.

rpm	pH[a]	fn[b]	S_{obs}[c]	S_{th}[d]	% error[e]
	4.34	1	8.97	8.97	0
	4.86	1	8.97	8.97	0
	5.85	1	8.98	8.97	- 0.1
60	6.92	0.98	8.75	8.76	+ 0.1
	7.31	0.90	8.49	8.08	- 5.0
	7.98	0.67	5.59	6.01	+ 7.5
	4.34	1	10.9	11.1	+ 1.8
	4.86	1	11.2	11.1	- 0.9
	5.85	1	11.3	11.1	- 1.8
94	6.92	0.98	11.1	10.8	- 2.7
	7.31	0.90	10.4	9.94	- 4.4
	7.98	0.67	6.85	7.41	+ 8.1
	4.34	1	14.9	15.2	+ 2.0
	4.86	1	15.2	15.2	0
	5.85	1	15.6	15.2	- 2.6
167	6.92	0.98	14.6	14.8	+ 1.4
	7.31	0.90	13.2	13.6	+ 3.0
	7.98	0.67	9.56	10.1	+ 5.6
	4.34	1	20.3	21.3	+ 4.9
	4.86	1	21.8	21.3	- 2.3
	5.85	1	21.7	21.3	- 1.8
375	6.92	0.98	20.6	20.8	+ 0.9
	7.31	0.90	18.4	19.1	+ 3.8
	7.98	0.67	12.8	14.3	+ 11.7

a. Aqueous phase; 37°C.

b. Eq. 3.2.

c. Based on kinetic analysis; Eq. 4.22; $sec^{-1} \times 10^5$.

d. Eq. 4.23; $sec^{-1} \times 10^5$.

e. $100 (S_{th} - S_{obs})/S_{obs}$.

pH value investigated in the rotating diffusion cell that dictated essentially only the presence of non-ionised solute in the aqueous phase (fn = 1; Tables 4.3 - 4.5). Values for k_{12} and k_{21} were estimated using Eqs. 2.7 and 2.8, respectively, from knowledge of the partitioning kinetics and partition coefficient of the solute. Mean values for S_{obs} and their corresponding k_{12} and k_{21} values are documented in Tables 4.6 - 4.8 for each solute and rotation speed employed in the study. The standard deviations (SD) associated with the mean values of S in Tables 4.6 - 4.8 are consistent with those observed in Table 4.1 and show that, in accord with Eq. 4.15, transport kinetics in the rotating diffusion cell should remain independent of pH at each value for pH that allows only the presence of non-ionised solute in the aqueous phase (fn = 1). Theoretical values for S (S_{th}) were generated using Eq. 4.23, at each rotation speed, from knowledge of k_{12} and k_{21} for the solute under study and fn from the pK_a of the solute and pH of the aqueous phase using Eq. 3.2. Theoretical values for S are documented as S_{th} in Table 4.3 - 4.5 for 5-allyl, 5' isopropylbarbituric acid, 5-allyl, 5'-isopentyl-barbituric acid and ethylparahydroxybenzoate, respectively, together with % errors involved in estimating values for S, using Eq. 4.23 (S_{th}) as opposed to experimentally (S_{obs}) in the rotating diffusion cell. The good agreement between theory and experiment (theoretical prediction of S frequently varies $<10\%$ from experimental determinations; Tables 4.3 - 4.5) attest to the validity of Eq. 4.23 in describing the transport kinetics of solutes subject to differing degrees of ionisation in the aqueous phase of a rotating diffusion cell. Moreover, Figures 4.3 - 4.5 show clearly how the characteristic sigmoidal dependence of S versus pH profiles, may be predicted in the rotating diffusion cell, given values for k_{12}, k_{21} and fn using Eq. 4.23.

TABLE 4.6

Mean experimental estimates of $S(S_{obs})$ for 5-allyl, 5'-isopropyl-barbituric acid (pK_a = 7.81) for non-ionised solute transfer in the rotating diffusion cell and corresponding values for k_{12} and k_{21}.

rpm	pH[a]	fn[b]	S_{obs}[c]	S_{obs}[c] (mean ± SD)	k_{12}[d]	k_{21}[e]
	4.34	1	6.12			
				6.10		
60	4.86	1	6.31		5.91	1.95
				± 0.22		
	5.85	1	5.88			
	4.34	1	7.42			
				7.35		
94	4.86	1	7.64		7.11	2.45
				± 0.33		
	5.85	1	6.99			
	4.34	1	9.86			
				9.66		
167	4.86	1	10.0		9.35	3.09
				± 0.47		
	4.85	1	9.13			
	4.34	1	12.9			
375	4.86	1	13.9	12.9	12.5	4.12
	4.85	1	12.1	± 0.90		

a. Aqueous phase; 37°C.

b. Eq. 3.8.

c. Based on kinetic analysis; Eq. 4.22; $sec^{-1} \times 10^5$.

d. Eq. 2.7; $sec^{-1} \times 10^5$.

e. Eq. 2.8; $sec^{-1} \times 10^7$.

TABLE 4.7

Mean experimental estimates of $S(S_{obs})$ for 5,allyl, 5'-isopentyl-barbituric acid (pK_a = 7.90) for non-ionised solute transfer in the rotating diffusion cell and corresponding values for k_{12} and k_{21}.

rpm	pH[a]	fn[b]	S_{obs}[c]	S_{obs}[c] (mean ± SD)	k_{12}[d]	k_{21}[e]
	4.34	1	7.94			
60	4.86	1	8.24	7.94 ± 0.29	7.91	3.20
	5.85	1	7.65			
	4.34	1	10.0			
94	4.86	1	10.4	10.2	10.1	4.10
	5.85	1	10.2	± 0.20		
	4.34	1	14.0			
167	4.86	1	14.8	14.4	14.3	5.80
	5.85	1	14.5	± 0.40		
	4.34	1	20.7			
375	4.86	1	23.0	21.9	21.8	8.70
	5.85	1	21.9	± 1.15		

a. Aqueous phase; 37°C.

b. Eq. 3.8.

c. Based on kinetic analysis; Eq. 4.22; $sec^{-1} \times 10^5$.

d. Eq. 2.7; $sec^{-1} \times 10^5$.

e. Eq. 2.8; $sec^{-1} \times 10^7$.

TABLE 4.8

Mean experimental estimates of S (S_{obs}) for ethylparahydroxybenzoate (pK_a = 8.28) for non-ionised solute transfer in the rotating diffusion cell and corresponding values for k_{12} and k_{21}.

rpm	pH[a]	fn[b]	S_{obs}[c]	S_{obs}[c] (mean ± SD)	k_{12}[d]	k_{21}[e]
	4.34	1	8.97			
				8.97		
60	4.86	1	8.47	± 0.06	8.94	2.99
	5.85	1	8.98			
	4.34	1	10.9			
				11.1		
94	4.86	1	11.2	± 0.2	11.0	3.71
	5.85	1	11.3			
	4.34	1	14.9			
167	4.86	1	15.2	15.3	15.1	5.07
	5.85	1	15.6	± 0.35		
	4.34	1	20.3			
375	4.86	1	21.8	21.3	21.2	7.70
	5.85	1	21.7	± 0.84		

a. Aqueous phase; 37°C.

b. Eq. 3.8.

c. Based on kinetic analysis; Eq. 4.22; $sec^{-1} \times 10^5$.

d. Eq. 2.7; $sec^{-1} \times 10^5$.

e. Eq. 2.8; $sec^{-1} \times 10^7$.

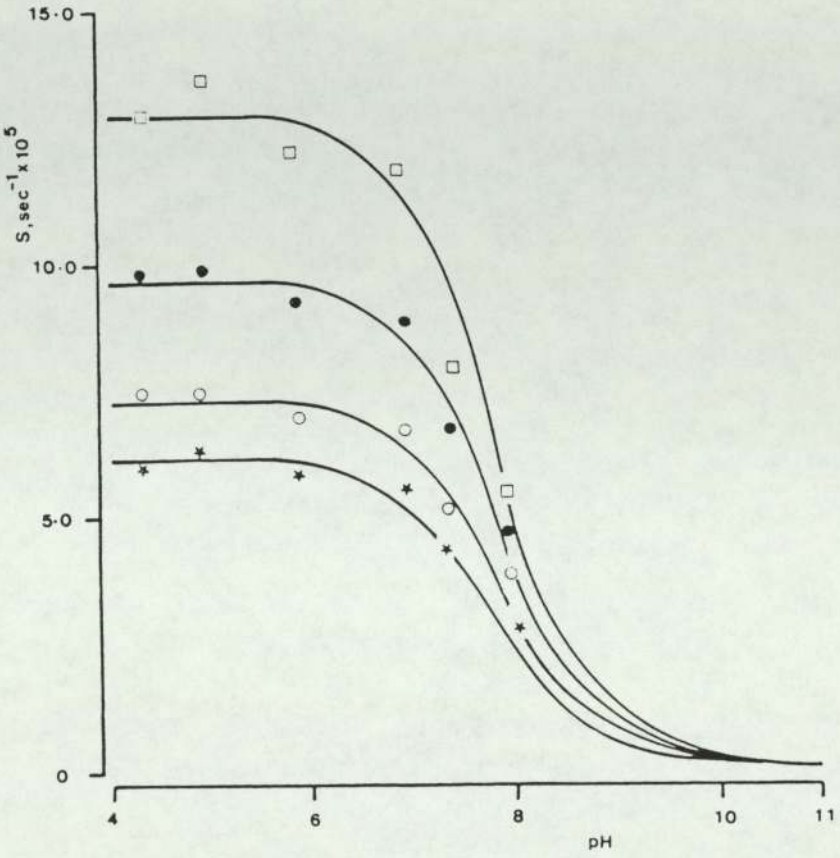

Figure 4.3 Theoretical (solid profiles; Eq. 4.23) and experimental (symbols) dependence of S(= k_{12} fn + k_{21}; Scheme 4.2) for 5-allyl, 5'-isopropylbarbituric acid (pK_a = 7.81) at various aqueous phase pH in the rotating diffusion cell at (✱) 60, (○) 94, (●) 167 and (□) 375 rpm, 37°C.

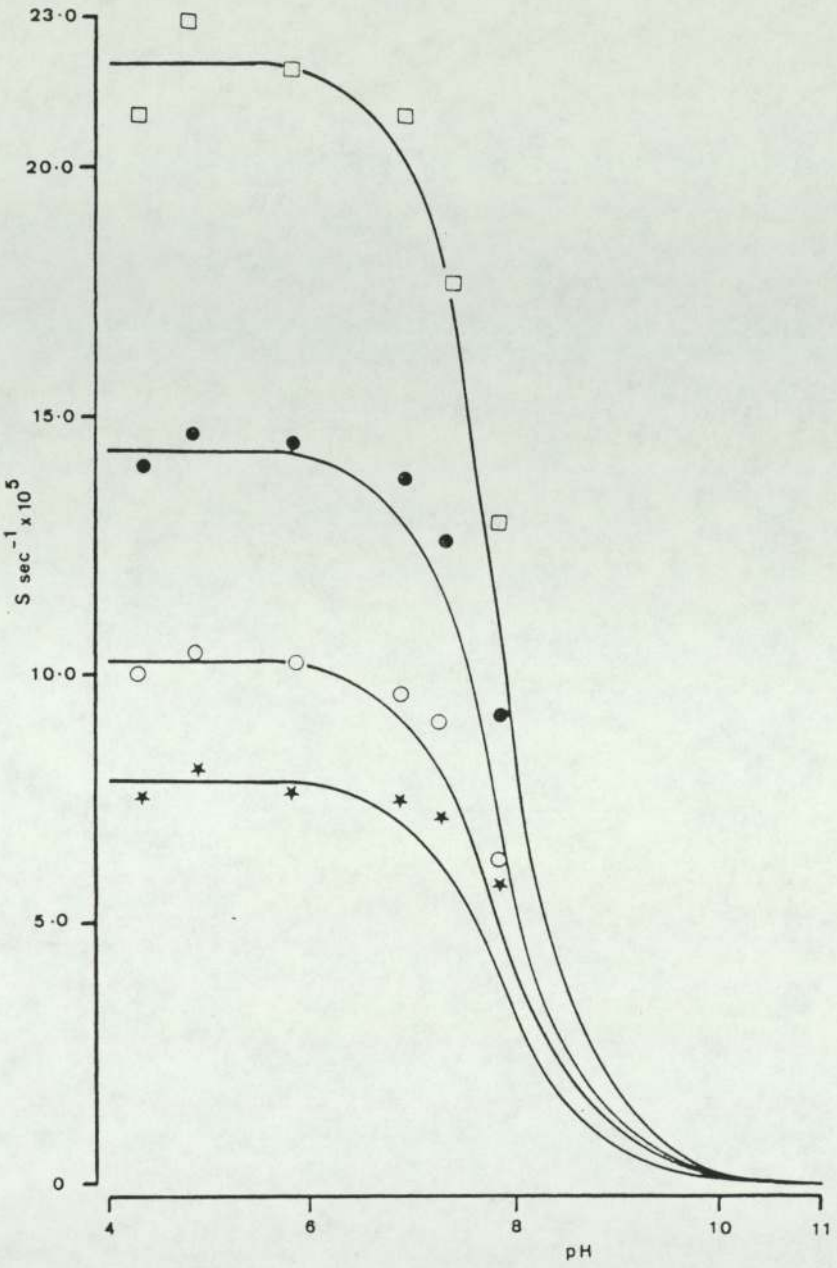

Figure 4.4 Theoretical (solid profiles; Eq. 4.23) and experimental (symbols) dependence of S (= k_{12} fn + k_{21}; Scheme 4.2) for 5-allyl, 5'-isopentylbarbituric acid (pK_a = 7.90) at various aqueous phase pH in the rotating diffusion cell at (✶) 60, (○) 94, (●) 167 and (□) 375 rpm, 37°C.

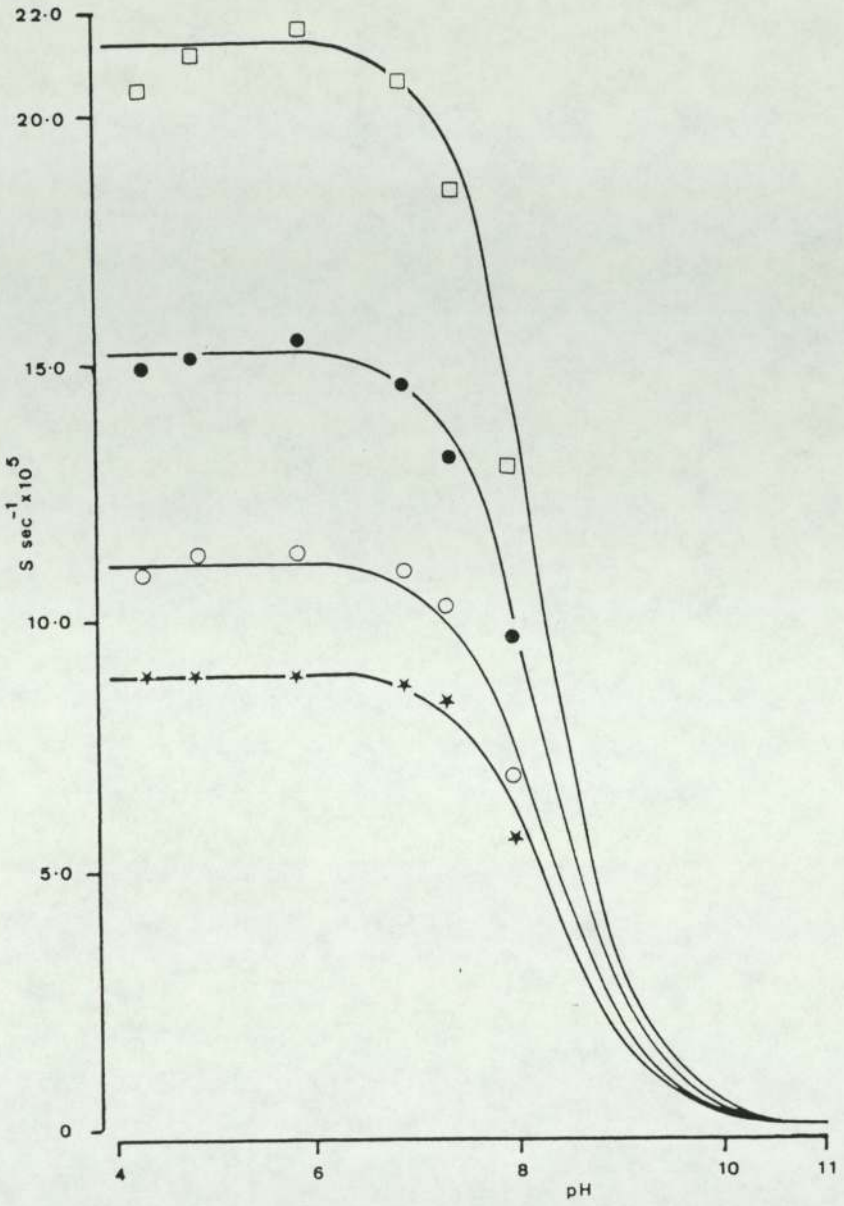

Figure 4.5 Theoretical (solid profiles; Eq. 4.23) and experimental (symbols) dependence of S (= k_{12} fn + k_{21}; Scheme 4.2) for ethyl-parahydroxybenzoate (pK_a = 8.28) at various aqueous phase pH in the rotating diffusion cell at (✱) 60, (○) 94, (●) 167 and (□) 375 rpm, 37^{o}C.

4.3.2 EFFECT OF AQUEOUS PHASE IONIC STRENGTH UPON THE TRANSFER KINETICS OF NON-IONISED SOLUTES IN THE ROTATING DIFFUSION CELL (AQUEOUS (KCl) : OCTANOL IMPREGNATED FILTER : OCTANOL) 37°C

The effect of ionic strength in the aqueous phase of a rotating diffusion cell[(aqueous (KCl): pH 4.0) : octanol impregnated filter : octanol)]37°C, upon the transport kinetics of 5-allyl, 5'-isopentyl-barbituric acid and butylparahydroxybenzoate essentially non-ionised in the aqueous phase, at various rotation speeds, are documented as S_{obs} in Tables 4.9 and 4.10, respectively. The agreement between values of S at various aqueous phase ionic strengths as high as 2.0 molal (constant rotation speed), shows that the presence of KCl is not altering the transport properties of these solutes across the interface at a level that is detectable using the rotating diffusion cell (Tables 4.9 and 4.10). The relationships found between the apparent rate constant and aqueous phase ionic strength for 5-allyl, 5'-isopentylbarbituric acid and butylparahydroxybenzoate at differing rotation speeds in the rotating diffusion cell are shown in Figures 4.6 and 4.7. Inspection of these Figures shows that transfer kinetics of non-ionised solutes remain independent of aqueous phase ionic strength in the rotating diffusion cell (aqueous : octanol system, 37°C). The solid profiles in Figures 4.6 and 4.7 represent mean values for the rate constants determined at each aqueous phase ionic strength and rotation speed. Negligible ionic strength-induced variations in S are consistent with the observations of Guy and Honda (73). Guy and Honda (73) employed a rotating diffusion cell (aqueous : isopropylmyristate impregnated filter : aqueous) at 25°C to investigate the transfer of methylnicotinate from the inner to the outer compartment. Plots of $1/\vec{k}$ versus $\omega^{-\frac{1}{2}}$ for methynicotinate transport when the aqueous phases comprised either water or 1 M KCl were

TABLE 4.9

Experimental estimates of S^a (= $k_{12} + k_{21}$) for 5-allyl, 5'-isopentyl-barbituric acid at different aqueous phase ionic strengths and rotation speeds in the rotating diffusion cell, 37°C.

Rotation speed ($\omega^{-\frac{1}{2}}$)	Ionic strength[b] (molal)				
	0	0.1	0.3	1.0	2.0
1	7.88	7,88	8.07	8.02	7,73
0.8	10.2	9.93	9.97	10.5	10.0
0.6	14.3	13.7	13.8	14.9	14.3
0.5	16.8	15.3	16.4	18.2	16.6

a. Kinetic analysis; Eq. 4.14; $sec^{-1} \times 10^5$.

b. Aqueous phase; ion type KCl; pH 4.0.

TABLE 4.10

Experimental estimates of S^a ($= k_{12} + k_{21}$) for butylparahydroxybenzoate at different aqueous phase ionic strengths and rotation speeds in the rotating diffusion cell, 37°C.

Rotation speed ($\omega^{-\frac{1}{2}}$)	Ionic strength[b] (molal)					
	0	0.1	0.3	0.5	1.0	2.0
1	8.88	9.00	9.32	8.98	9.28	8.99
0.8	11.2	11.1	11.7	11.3	11.0	10.9
0.6	15.9	15.7	15.8	16.4	14.2	15.3
0.4	23.3	22.3	-	23.3	22.0	22.9

a. Kinetic analysis; Eq. 4.14; $sec^{-1} \times 10^5$.

b. Aqueous phase; ion type KCl; pH 4.0.

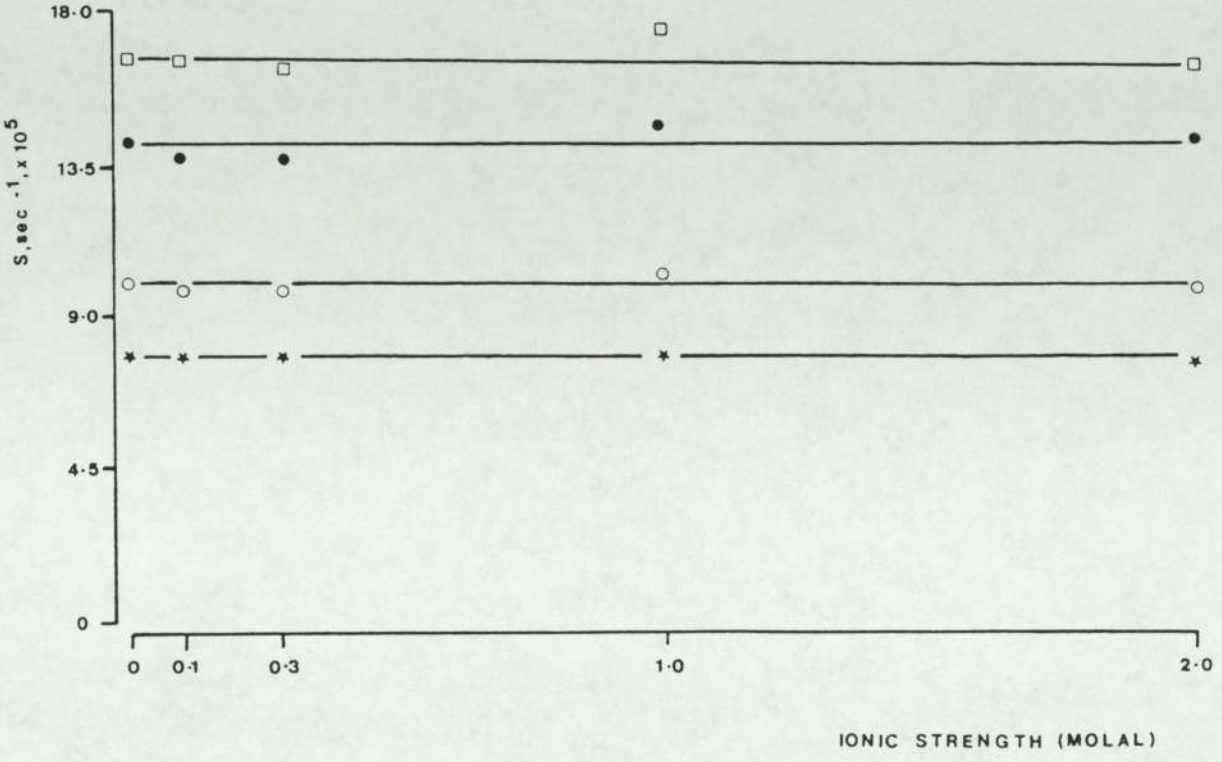

Figure 4.6 Experimental estimates of S(=k_{12} + k_{21}; Scheme 4.1) for non-ionised solute partitioning of 5-allyl,5'-isopentylbarbituric acid (pK_a = 7.90) in the rotating diffusion cell octanol : aqueous (KCl; pH 4.0) at various aqueous phase ionic strength at (✱) 60, (○) 94, (●) 167 and (□) 240 rpm, 37°C. Solid profiles represent the average value for the rate constant at each stirring speed.

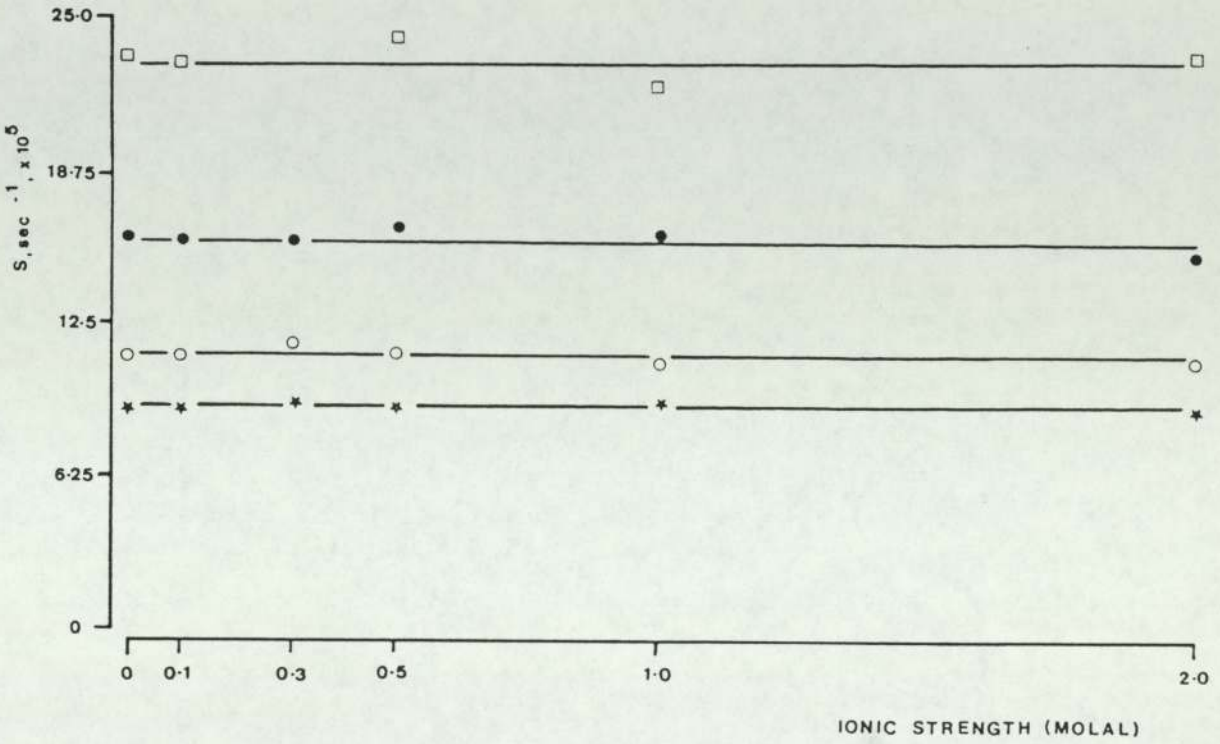

Figure 4.7 Experimental estimates of S(= $k_{12} + k_{21}$; Scheme 4.1) for non-ionised solute partitioning of butylparahydroxybenzoate (pK_a = 8.22) in the rotating diffusion cell octanol : aqueous (KCl; pH 4.0) at (✱) 60, (○) 94, (●) 167 and (□) 375 rpm, 37°C. Solid profiles represent the average value for the rate constant at each stirring speed.

indistinguishable. Agreement between the two studies showed that the presence of KCl in the aqueous phases did not alter the transport kinetics of the solute across the aqueous : organic interface.

4.3.3 IONIC STRENGTH AND SOLUTE IONISATION EFFECTS UPON INTERFACIAL RESISTANCES AND AQUEOUS PHASE DIFFUSION COEFFICIENTS IN AQUEOUS : OCTANOL TWO PHASE SYSTEMS

Estimates of $1/\vec{k}$ (= R_T) at various aqueous phase pH and rotation speeds in the rotating diffusion cell (aqueous : octanol impregnated filter : octanol), 37°C, for 5-allyl, 5'-isopropylbarbituric acid, 5-allyl, 5'-isopentylbarbituric acid and ethylparahydroxybenzoate are documented in Tables 4.11 through 4.13, respectively. Values for $1/\vec{k}$ were estimated using Eq. 4.25 assigning values for V_1, V_2 and A as 35, 160 and 2.67, respectively. Values for S were taken from Tables 4.3 - 4.5, organic/aqueous partition coefficients from Table 3.8 and values of fn from knowledge of the pK_a of the solute and pH of the aqueous phase using Eq. 3.2. Within the sensitivity of the technique, Tables 4.11 - 4.13 show that, for each solute under study, values for the total diffusional resistance to mass transfer, $1/\vec{k}$, remain indistinguishable at each aqueous phase pH and rotation speed employed in the study. This observation may be explained by assuming that only the non-ionised species partition, (assumption; Scheme 4.2) and that the permeability of the ionised and non-ionised solute are practically the same in the aqueous diffusive boundary layer. Under these circumstances the aqueous diffusive boundary layer, the interface, the organic phase impregnated filter and organic diffusive boundary layer offer resistance only to the transfer of non-ionised solute, irrespective of the presence, or absence, of ionised solute in the aqueous phase. Guy et al (99) studied the transport of salicylic acid (pK_a = 2.97) in the rotating diffusion cell (aqueous : isopropyl-

TABLE 4.11

Experimental estimates of $1/\vec{k}$ [a] for 5-allyl, 5'-isopropylbarbituric acid (pK_a = 7.81) at various aqueous phase pH (0.3 M orthophosphate buffer system) and rotation speeds in the rotating diffusion cell, 37°C.

Rotation speed ($\omega^{-\frac{1}{2}}$)	pH[b]					
	4.34	4.86	5.85	6.92	7.31	7.98
1	1256	1218	1207	1179	1324	1151
0.8	1036	1006	1099	1325	1146	971
0.6	779	768	842	743	882	736
0.4	596	553	635	564	751	556

a. Eq. 4.25; sec cm^{-1}.

b. Aqueous phase; 37°C.

TABLE 4.12

Experimental estimates of $1/\vec{k}^{a}$ for 5-allyl, 5'-isopentylbarbituric acid (pK_a = 7.90) at various aqueous phase pH (0.3 M orthophosphate buffer system) and rotation speeds in the rotating diffusion cell, 37°C.

Rotation speed ($\omega^{-\frac{1}{2}}$)	pH[b]					
	4.34	4.86	5.85	6.92	7.31	7.98
1	961	926	998	906	809	592
0.8	763	733	748	711	652	489
0.6	545	516	526	493	471	368
0.4	369	332	349	328	341	292

a. Eq. 4.25; sec cm^{-1}.

b. Aqueous phase; 37°C.

TABLE 4.13

Experimental estimates of $1/\vec{k}$ [a] ethylparahydroxybenzoate (pK_a = 8.28) at various aqueous phase pH (0.3 M orthophosphate buffer system) and rotation speeds in the rotating diffusion cell.

Rotation speed ($\omega^{-\frac{1}{2}}$)	pH[b]					
	4.34	4.86	5.85	6.92	7.31	7.98
1	851	851	850	855	809	915
0.8	700	682	676	674	661	747
0.6	512	502	489	512	521	535
0.4	376	350	352	363	373	399

a. Eq. 4.25; sec cm^{-1}.

b. Aqueous phase; 37°C.

myristate impregnated filter : aqueous), 20°C, in which aqueous phase of the inner compartment varied from pH 1.4 to 3.2. These authors observed no statistical difference between values for $1/\vec{k}$ across the range of pH values investigated. The observations made on Tables 4.11 - 4.13 support those described by Guy et al (99). Tables 4.14 - 4.16 give the regression equations and correlation coefficients describing these various $1/\vec{k}$ versus $\omega^{-\frac{1}{2}}$ relationships for 5-allyl, 5'-isopropyl-barbituric acid, 5-allyl, 5'-isopentylbarbituric acid and ethylpara-hydroxybenzoate, respectively. Regression equations were based on Eq. 4.4. Tables 4.14 - 4.16 show that for each solute studied the value for the slope remains independent of aqueous phase pH. Thus, with reference to Eq. 4.4, aqueous phase diffusion coefficients appear to be constant and independent of aqueous phase pH. The absence of a significant intercept in the plots of $1/\vec{k}$ versus $\omega^{-\frac{1}{2}}$ for 5-allyl, 5'-isopentylbarbituric acid and ethylparahydroxybenzoate (Tables 4.15 and 4.16), show that interfacial resistance was negligible in these cases. For the case of 5-allyl, 5'-isopropylbarbituric acid a significant, yet constant intercept is observed in Table 4.14. In contrast to the other solutes studied in this investigation, 5-allyl, 5'-isopropylbarbituric acid displays a resistance ratio value of $\gamma = 8.4$ and implies the solute is subject to both aqueous and organic diffusional control. For the case of solutes where $\gamma > 20$ transfer is controlled by the resistance of the aqueous phase. For the case where $0.05 < \gamma > 20$, Eq. 4.3 is more appropriate than Eq. 4.4. Examination of Eq. 4.3 suggests that a likely explanation for the observed intercept, is diffusion of the solute through the organic phase impregnated filter.

Experimental estimates of $1/\vec{k}$ ($= R_T$) at various aqueous phase ionic strengths and rotation speeds in the rotating diffusion cell [aqueous (KCl; pH 4.0) : octanol impregnated

TABLE 4.14

Linear regression analysis according to Eq. 4.4 for the data given in Table 4.11 for 5-allyl, 5'-isopropylbarbituric acid (pK_a = 7.81) at various aqueous phase pH, 37°C.

pH[a]	regression equation[b] $\vec{1/k} = (0.643 \nu_1^{1/6} D_1^{-2/3}) \omega^{-\frac{1}{2}} + \vec{1/k}_I$	correlation coefficient	n[c]
4.34	$\vec{1/k} = 1119\ \omega^{-\frac{1}{2}} + 134$	0.998	4
4.86	$\vec{1/k} = 1117\ \omega^{-\frac{1}{2}} + 105$	0.999	4
5.85	$\vec{1/k} = 1137\ \omega^{-\frac{1}{2}} + 175$	0.999	4
6.92	$\vec{1/k} = 1214\ \omega^{-\frac{1}{2}} + 103$	0.998	4
7.31	$\vec{1/k} = 992\ \omega^{-\frac{1}{2}} + 132$	0.994	4
7.78	$\vec{1/k} = 1010\ \omega^{-\frac{1}{2}} + 146$	0.989	4

a. Aqueous phase: 37°C.

b. Eq. 4.4.

c. Number of points.

TABLE 4.15

Linear regression analysis according to Eq. 4.4 for the data given in Table 4.12 for 5-allyl, 5'-isopentylbarbituric acid (pK_a = 7.90) at various aqueous phase pH, 37°C.

pH[a]	regression equation[b] $1/\vec{k} = (0.643\nu_1^{1/6} D_1^{-2/3})\omega^{-\frac{1}{2}} + 1/\vec{k}_I$	correlation coefficient	n[c]
4.34	$1/\vec{k} = 997\ \omega^{-\frac{1}{2}} - 38$	0.999	4
4.86	$1/\vec{k} = 996\ \omega^{-\frac{1}{2}} - 69$	0.999	4
5.85	$1/\vec{k} = 1076\ \omega^{-\frac{1}{2}} - 10.3$	0.997	4
6.92	$1/\vec{k} = 976\ \omega^{-\frac{1}{2}} - 74$	0.998	4
7.31	$1/\vec{k} = 793\ \omega^{-\frac{1}{2}} + 13.5$	0.998	4
7.98	$1/\vec{k} = 511\ \omega^{-\frac{1}{2}} + 77$	0.996	4

a. Aqueous phase; 37°C.

b. Eq. 4.4.

c. Number of points.

TABLE 4.16

Linear regression analysis according to Eq. 4.4 for the data given in Table 4.13 for ethylparahydroxybenzoate (pK_a = 8.28) at various aqueous phase pH, 37°C.

pH[a]	regression equation[b] $1/\vec{k} = (0.643\nu_1^{1/6} D_1^{-2/3})\omega^{-\frac{1}{2}} + 1/\vec{k}_I$	correlation coefficient	n[c]
4.34	$1/\vec{k} = 807\ \omega^{-\frac{1}{2}} + 45$	0.998	4
4.86	$1/\vec{k} = 841\ \omega^{-\frac{1}{2}} + 7.3$	0.999	4
5.85	$1/\vec{k} = 841\ \omega^{-\frac{1}{2}} + 3.4$	0.998	4
6.92	$1/\vec{k} = 818\ \omega^{-\frac{1}{2}} + 28$	0.999	4
7.31	$1/\vec{k} = 724\ \omega^{-\frac{1}{2}} + 8.4$	0.999	4
7.98	$1/\vec{k} = 880\ \omega^{-\frac{1}{2}} + 33$	0.996	4

a. Aqueous phase; 37°C.

b. Eq. 4.4.

c. Number of points.

filter : octanol], 37°C, for 5-allyl, 5'-isopentylbarbituric acid and butylparahydroxybenzoate are documented in Table 4.17 and 4.18, respectively. Values for $1/\vec{k}$ remain independent of aqueous phase ionic strength in the range 0 - 2.0 M at constant rotation speed for each solute under study (Tables4.17 and 4.18) in the rotating diffusion cell. Regression equations, based on Eq. 4.4, describing the various $1/\vec{k}$ versus $\omega^{-\frac{1}{2}}$ relationships are documented in Tables 4.19 and 4.20 for 5-allyl, 5'-isopentylbarbituric acid and butylparahydroxybenzoate, respectively. With reference to Eq. 4.4, the absence of a significant intercept and constant slope with increasing aqueous phase ionic strength, indicates that interfacial resistance was negligible and aqueous phase diffusion coefficients are constant and independent of aqueous phase ionic strength for these solutes in the rotating diffusion cell.

4.3.4 PARTITIONING KINETICS IN TWO-PHASE AQUEOUS : OCTANOL SYSTEMS IN WHICH AQUEOUS PHASE IONIC STRENGTH AND pH ARE VARIED

In Chapter 3 it was shown that in the two-phase transfer cell (octanol : aqueous) transport rate constants varied unpredictably with pH and fell significantly with increasing aqueous phase ionic strength. In this Chapter the rotating diffusion cell was used in a two-phase mode (aqueous : octanol) with A, V_1 and V_2 held constant. Plots of S versus pH for the same solutes used in Chapter 3 conformed to theory (Eq. 4.23) when the rotating diffusion cell was employed. Rate constants remained independent of aqueous phase ionic strength, in the range 0 - 2.0 M KCl, for solutes subject to aqueous diffusional control ($\gamma > 20$) in the rotating diffusion cell. Experiments performed in the rotating diffusion cell have shown that aqueous phase diffusion coefficients remained unaffected by pH or ionic strength. Interfacial resistance to transfer at the aqueous : octanol interface, was

TABLE 4.17

Experimental estimates of $1/\vec{k}$ [a] for 5-allyl, 5'-isopentylbarbituric acid (essentially non-ionised) at various aqueous phase ionic strength and rotation speeds in the rotating diffusion cell, 37°C.

Rotation speed ($\omega^{-\frac{1}{2}}$)	Ionic strength [b] (molal)				
	0	0.1	0.3	1.0	2.0
1	969	969	946	952	987
0.8	749	769	766	727	763
0.6	534	557	553	512	534
0.5	455	499	466	419	459

a. Eq. 4.17; sec cm^{-1}.

b. Aqueous phase; ion type KCl; pH 4.0.

TABLE 4.18

Experimental estimates of $1/\vec{k}$ [a] for butylparahydroxybenzoate (essentially non-ionised) at various aqueous phase ionic strength and rotation speeds in the rotating diffusion cell, 37°C.

Rotation speed ($\omega^{-\frac{1}{2}}$)	Ionic strength (molal)					
	0	0.1	0.3	0.5	1.0	2.0
1	859	848	819	849	822	848
0.8	681	687	675	675	693	699
0.6	479	486	483	465	487	489
0.4	327	342	-	327	347	343

a. Eq. 4.17; sec cm^{-1}.

b. Aqueous phase; ion type KCl; pH 4.0.

TABLE 4.19

Linear regression analysis according to Eq. 4.4 for the data given in Table 4.17 for 5-allyl, 5'-isopentylbarbituric acid at various aqueous phase ionic strength, 37°C.

Ionic Strength[a] (molal)	regression equation[b] $1/\vec{k} = (0.643 \nu_1^{1/6} D_1^{-2/3}) \omega^{-\frac{1}{2}} + 1/\vec{k}_I$	correlation coefficient	n[c]
0	$1/\vec{k} = 1040\ \omega^{-\frac{1}{2}} - 78$	0.998	4
0.1	$1/\vec{k} = 965\ \omega^{-\frac{1}{2}} - 0.7$	0.997	4
0.3	$1/\vec{k} = 974\ \omega^{-\frac{1}{2}} - 23$	0.999	4
1.0	$1/\vec{k} = 1071\ \omega^{-\frac{1}{2}} - 24$	0.999	4
2.0	$1/\vec{k} = 1075\ \omega^{-\frac{1}{2}} - 93$	0.998	4

a. Aqueous phase; ionic type KCl; 37°C.

b. Eq. 4.4.

c. Number of points.

TABLE 4.20

Linear regression analysis according to Eq. 4.4 for the data given in Table 4.18 for butylparahydroxybenzoate at various aqueous phase ionic strength, 37°C.

Ionic strength [a] (molal)	Regression equation [b] $1/\vec{k} = (0.643\nu_1^{-\frac{1}{2}} D_1^{-2/3})\omega^{-\frac{1}{2}} + 1/\vec{k}_I$	correlation coefficient	n [c]
0	$1/\vec{k} = 899\ \omega^{-\frac{1}{2}} - 43$	0.998	4
0.1	$1/\vec{k} = 860\ \omega^{-\frac{1}{2}} - 11$	0.998	4
0.3	$1/\vec{k} = 840\ \omega^{-\frac{1}{2}} - 20$	0.999	4
0.5	$1/\vec{k} = 888\ \omega^{-\frac{1}{2}} - 43$	0.997	4
1.0	$1/\vec{k} = 815\ \omega^{-\frac{1}{2}} + 16$	0.996	4
2.0	$1/\vec{k} = 862\ \omega^{-\frac{1}{2}} - 9$	0.998	4

a. Aqueous phase; ion type KCl; 37°C.

b. Eq. 4.4.

c. Number of points.

negligible for each solute studied.

In the rotating diffusion cell a mechanically stabilised interface is established between the aqueous phase and organic phase impregnated filter. This is in marked contrast to the two- phase transfer cell in which aqueous and organic diffusive boundary layers are formed on either side of the aqueous : organic interface.

The existence of an unstable aqueous : organic interface in the two-phase transfer cell has been observed by many authors (100 - 112). Davies et al (100) noted that when a solute partitioned across an aqueous : organic interface two complicating factors occurred which may affect the rate of interfacial transport. These factors were (a) spontaneous emulsification and (b) interfacial turbulence. The subject of spontaneous emulsification in two-phase systems was studied by Davies and Haydon (101). They advanced three theories to account for the phenomena; (i) interfacial instability due to non-uniform diffusion across the interface causing "kicking" violent enough to dislodge droplets of the adjacent bulk phase, (ii) simultaneous diffusion of (say) organic phase and solute into the aqueous phase; the solute is diluted by the aqueous phase and the organic phase is left stranded, forming emulsion droplets, and (iii) interfacial tension becomes temporarily negative, resulting in an increase in the effective area of the interface. Lewis (102, 103) noted that in two-phase systems spontaneous emulsification occurred even in the absence of agitation of the two-phases. Other authors observed that the interfacial transport of acetone across a number of aqueous : organic interfaces was associated with a high degree of spontaneous emulsification (104 - 107).

Lewis and Pratt (108) noted ripples, erratic pulsations and surface activity of drops in the course of interfacial tension

measurements using the pendent-drop method (109). Where marked interfacial turbulence occurred they also noted an increase in the rate of solute transport (102). Photographs of drops formed within a second immiscible liquid and horizontal views of liquid/liquid interfaces often showed regions of violent activity (110). It appeared that interfacial turbulence at the points of contact of two liquids was always associated with simultaneous mass transfer and that the effect was more pronounced when mass transfer was rapid (100). In some cases the surface activity was strong with mass transfer in one direction, but completely absent when the solute partitioned in the opposite direction (100).

These phenomena were believed to stem from random variations of interfacial tension (111 - 113) which resulted from local concentration variations when mass transfer occurred. This resulted in ripples at the interface and was known as the Marargoni effect (113, 114). The significant feature of the phenomena was that the hydrodynamic instability of the interface only persisted as long as mass transfer continued (115, 116) and resulted in unpredictable rates of solute transport.

The absence of interfacial resistance to solute transfer at the aqueous : octanol interface, lack of significant variation of aqueous phase diffusion coefficients with either aqueous phase ionic strength or pH, insignificant variation in kinematic viscosity or solute pK_a with ionic strength and finally the adherence to theory in the rotating diffusion cell, all point to variations in interfacial instability induced at the aqueous : organic interface by different ionic contents in the aqueous phase as the most likely cause for the non-agreement between theory and experiment in the two-phase transfer cell.

It is probable that the octanol : aqueous interface is more susceptible to instability problems than other two-phase systems. Most liquid : liquid interfacial tension values fall between the air : liquid surface tensions of the separate components (117) a fact which indicates their absence of interaction (118, 119). Values for the surface and interfacial tensions for the octanol : aqueous system under conditions of varying aqueous phase ionic strength are shown in Tables 4.23 and 4.24. These Tables show that this is not true of the aqueous : octanol system. With these, the low values for interfacial tension compared to the air : liquid surface tensions of the separate components indicate that the octanol : aqueous interface has little tendency to contract or resist deformation (101, 105 - 107, 112, 113, 118) during mixing and solute transfer. The ionic strength induced variations in surface and interfacial tension were consistent with observations made by other authors (73, 120, 121).

Interfacial instability in the two-phase transfer cell appears to be variable and moderated by the ionic content of the aqueous phase in octanol : aqueous systems. The validity of Byron et al's (24) theory for prediction of non-ionised solute transfer kinetics in the two-phase transfer cell (constant ionic strength) indicated that if interfacial instability existed, it remained constant and apparently unaffected when the transfer of different solutes were studied. Although the two-phase transfer cell appeared adequate for transfer studies with a variety of non-ionised solutes, experiments involving variation in the ionic content of the aqueous phase should employ a diffusion cell which possesses a stabilized interface.

TABLE 4.21

Experimental pen deflection measurements for solvents with known surface tension values at 20°C.

Organic phase	Surface tension [a]	pen deflection [b] mean (± SD [c])
acetone [d]	23.70	31.5 ± 0.09
benzene [e]	28.85	36.4 ± 0.08
benzylalcohol [e]	39.0	51.5 ± 0.10
nitrobenzene [e]	43.9	57.5 ± 0.11
glycol [d]	47.7	61.7 ± 0.08
glycerol [d]	63.4	81.7 ± 0.13

a. Ref (122); mNm^{-1}.

b. mm; direct measurement.

c. Ref (49).

d. A.R. Grade, Fisons Ltd., Loughborough, England.

e. Analar Grade, BDH Ltd., England.

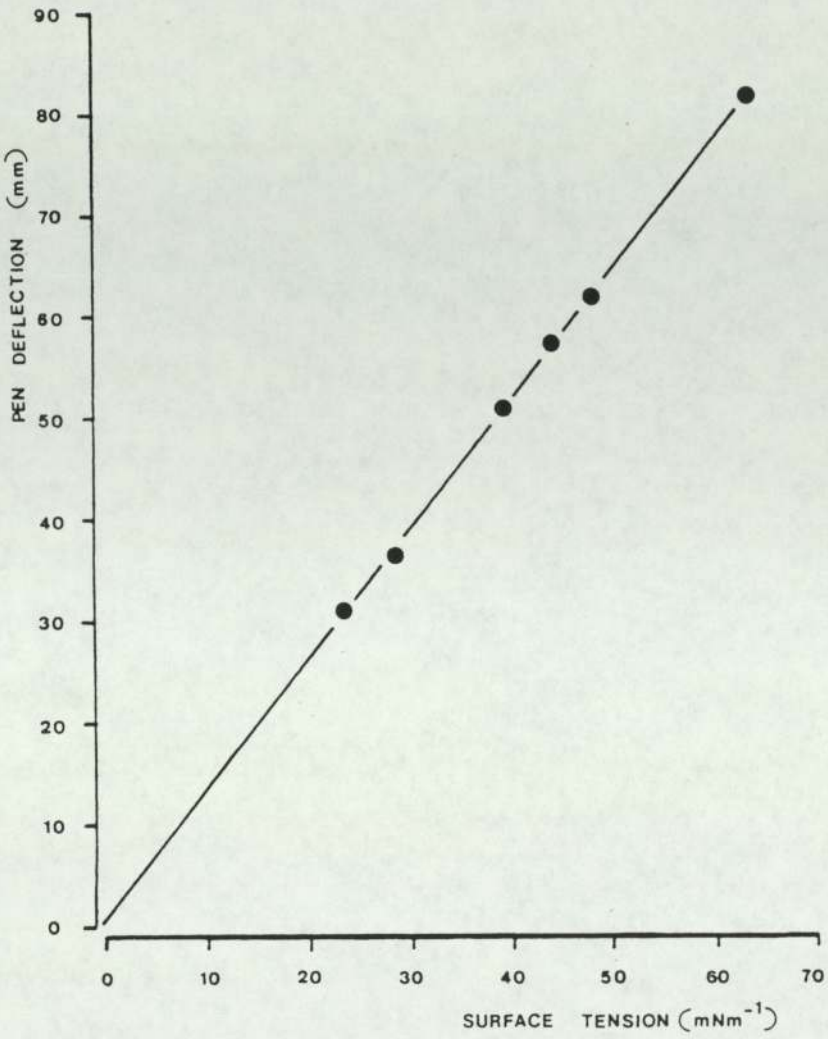

Figure 4.8 Surface tension calibration curve constructed using experimentally observed pen deflection measurements and documented surface tension values, 20°C.

TABLE 4.22

Experimental pen deflection measurements for solvents with known interfacial tension values at 20°C.

organic [a] phase	interfacial tension	pen deflection [b] mean (± SD [c])
Butanol	1.6 [d]	2.0 ± 0.08
diethylether	20.7 [e]	26.4 ± 0.12
Benzene	25.0 [e]	69.2 ± 0.6
hexane	51.1 [e]	114.3 ± 0.34

a. Saturated with aqueous phase; 20°C.

b. mm; direct measurement.

c. Ref (49).

d. Ref (100).

e. Ref (122).

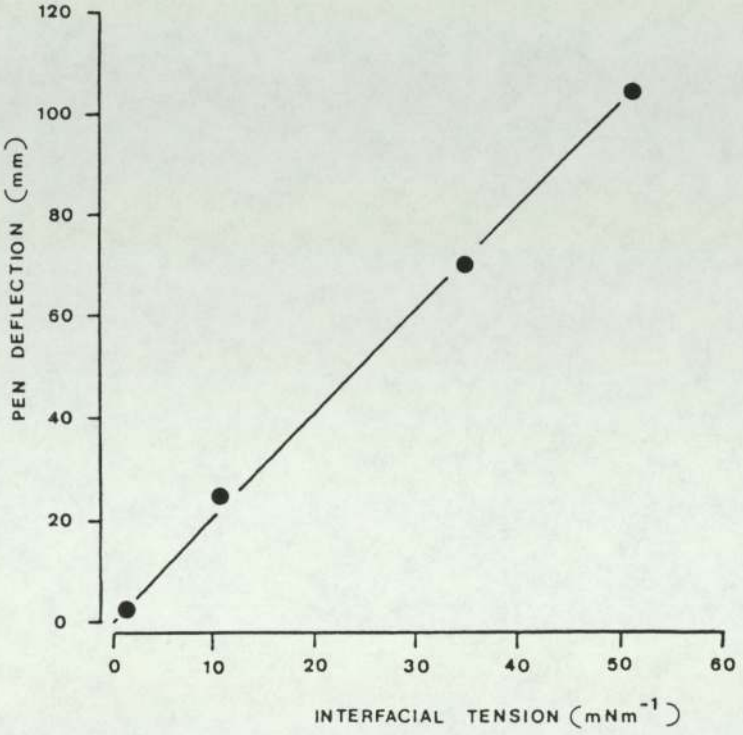

Figure 4.9 Interfacial tension calibration curve constructed using experimentally observed pen deflection measurements and documented interfacial tension values, 20°C.

TABLE 4.23

Experimental estimates of surface tension values for water and octanol at various aqueous phase ionic strengths, 20°C.

solvent	ionic strength [a]	Pen deflection [b]	Surface tension [c]
Water	0	93.8	72.54
Octanol	0	36.3	27.79
	0	35.9	27.49
	0.1	35.4	27.09
Octanol [d]	0.3	35.9	27.49
	0.5	35.4	27.09
	1.0	35.4	27.09
	2.0	35.2	26.94
	0	41.8	32.08
	0.1	41.7	32.00
	0.3	42.1	32.31
Water [e]	0.5	41.3	31.69
	1.0	43.3	33.25
	2.0	45.7	35.11

a. Molal; KCl.

b. mm; direct measurement.

c. Extrapolated from Fig. 4.21; mNm^{-1}.

d. Saturated with aqueous phase; 20°C.

e. Saturated with octanol; 20°C.

TABLE 4.24

Experimental estimatesof interfacial tension values for water : octanol systemsat various aqueous phase ionic strengths, 20°C.

organic phase	aqueous phase [a] ionic strength	pen [b] deflection	interfacial [c] tension
octanol [d]	0	17.3	8.36
	0.1	17.7	8.54
	0.3	18.0	8.68
	0.5	18.1	8.73
	1.0	19.1	9.18
	2.0	19.5	9.36

a. molal; KCl.

b. mm; direct measurement.

c. extrapolated from Fig. 4.22; mNm^{-1}.

d. saturated with aqueous phase, 20°C.

CHAPTER FIVE

GENERAL CONCLUSION

5.1 GENERAL CONCLUSION

Interfacial transfer kinetics in the two-phase transfer cell were examined. A predictive theory developed by Byron et al (24) was tested and factors controlling interfacial transport in the two-phase transfer cell were critically analysed. The importance of aqueous and organic diffusional resistance to solute transfer in the two-phase transfer cell was investigated. A method was described to calculate a theoretical solute and solvent system-dependent ratio, γ (= R_{aq}/R_{org}). This ratio enabled estimation of the dominant diffusional resistance for a particular solute in a given solvent system.

Three homologous series (Table 2.1) were employed as model solutes. Their kinetics of interfacial transport across a variety of aqueous : organic (octanol, chloroform and cyclohexane) interfaces were determined in a standardised two-phase transfer cell of known dimensions. There was good agreement between experimentally determined solute transport kinetics and theoretical estimates generated according to the predictive equation derived by Byron et al (24). Variation of solute and solvent systems allowed the predictive theory to be tested under conditions where aqueous, organic and mixed diffusional control predominated. Successful prediction of the transfer kinetics of any homologue in a series was possible in all cases from a knowledge of the partition coefficient and transfer kinetics of the parent compound, the partition coefficient of the homologue and some easily determined system-dependent variables.

Theoretical considerations on the symmetrically stirred two-phase transfer cell for non-ionised solute transport enabled inter-relationships between kinetic rate constants and mass transfer descriptors to be established. Equations were developed to show that the individual transport rate constants of the forward, k_{12}, and

reverse, k_{21}, partitioning process always rise and fall respectively, with increasing K_D as a homologous series is ascended, independently of the solvent system employed in the study. Equations were also developed to show the dependence of the overall transfer rate constant, S (= $k_{12} + k_{21}$; Scheme 2.1), upon mass transfer descriptors. In this case S was shown to rise, fall or remain constant as the value for K_D increases when a homologous series is ascended dependent upon the physical properties of the solvent system. The theoretical dependence of S, k_{12} and k_{21} upon K_D were shown to hold true after experimentation in the two-phase transfer cell. In the aqueous : octanol system transport rate constants rose as the solute series was ascended. Rate constants remained effectively constant when cyclohexane was used as the organic phase, while the employment of chloroform as the organic phase clearly demonstrated a fall in apparent rate constants as a homologous series was ascended. However, in each case the forward and reverse rate constants for partitioning always rose and fell, respectively, independently of organic phase composition.

The theory of Byron et al (24) was extended to account for differing degrees of solute dissociation in the aqueous phase of the two-phase transfer cell. A theory was developed to allow prediction of solute transport kinetics for any solute in a homologous series at any given pH of the aqueous phase without exhaustive experimentation from some simply determined solute and solvent-dependent variables. The theory, as it pertained to a variety of weakly acidic monoprotic acids, was tested in an aqueous : octanol two-phase transfer cell in which aqueous phase pH was varied. The experimentally determined rate constants for partitioning did not accord with theoretical predictions. Results could not be explained by changes in kinematic viscosity of the phases, pK_a of the solute, partitioning of the ionised species, chemical stability or association or dissociation of the solute in

the organic phase . Marked changes in apparent transport kinetics were observed for solutes, essentially non-ionised in the aqueous phase, as a function of aqueous phase ionic strength ranging 0 - 0.2 M in the two-phase transfer cell (aqueous : octanol) 100 rpm, 37°C. These changes could not be explained by ionic strength induced variations in solute pK_a or partition coefficient or changes in kinematic viscosity of the phases.

In Chapter 4 the same solutes were studied in the rotating diffusion cell (aqueous : octanol impregnated filter : octanol). Transfer rate constants remained constant and independent of aqueous phase ionic strength. There was excellent agreement between experimental values and theoretical estimates for interfacial transfer kinetics for solutessubject to differing degrees of ionisation in the aqueous phase. In the rotating diffusion cell, which has a mechanically stabilized interface, aqueous phase diffusion coefficients were shown to be unaffected by pH or ionic strength variations. Interfacial resistance to solute transfer was negligible at each pH and aqueous phase ionic strength employed in the study.

The absence of interfacial resistance to solute transfer, lack of significant variation of aqueous phase diffusion coefficients, pK_a, kinematic viscosities of the phases and the adherence to theory in the rotating diffusion cell suggested that variations in interfacial instability were induced at the aqueous : organic interface by different ionic contents of the aqueous phase in the two-phase transfer cell. These variations in interfacial instability were the most likely cause for the poor agreement between theory and experiment in the two-phase transfer cell when aqueous phase pH and ionic strength are varied. The aqueous : octanol interface was also shown to be more susceptible to instability problems than other two-phase

systems.

Interfacial instability in the two-phase transfer cell appeared to be variable and moderated by the ionic content of the aqueous phase in octanol : aqueous systems. The validity of Byron et al (24) theory for non-ionised solute transfer in the two-phase transfer cell (constant ionic strength) indicated that if interfacial instability existed, it remained constant and apparently unaffected when the transfer of different solutes were studied. Although the two-phase transfer cell appeared adequate for transfer studies with a variety of non-ionised solutes, experiments involving variation in the ionic content of the aqueous phase should employ a diffusion cell with a stabilized interface.

GLOSSARY OF TERMS

GLOSSARY OF TERMS

A	interfacial area; cm^2.
AQ	aqueous phase (Figure 1.1).
a	amount of solute in aqueous phase; g^{-1}.
B	baffle (Figure 4.1).
b	amount of solute in organic phase.
C	concentration of solute; molal.
^oC	degrees centigrade.
$CaCl_2$	calcium chloride.
cm	centimeter.
D	diffusion coefficient; $cm^2 sec^{-1}$.
E	central stainless steel cylinder (Figure 4.1).
Eq.	equation.
Eqs.	equations.
F	filter membrane (Figure 4.1).
Fig.	figure.
Figs.	figures.
fn	fraction of non-ionised solute in the aqueous phase.
g	gram.
H	hollow stainless steel shaft (Figure 4.1).
HCl	hydrochloric acid.
Hz	hertz.
h	stagnant diffusive boundary layer; cm.
I	jacketed glass beaker (Figure 4.1).
J	flux; mol. sec^{-1} cm^{-2}.
KCl	potassium chloride.
KH_2PO_4	potassium dihydrogen orthophosphate.
K_D	organic : aqueous partition coefficient.
$(K_D)_{app}$	apparent organic : aqueous partition coefficient.

$K_{D(max)}$ maximum organic : aqueous partition coefficient (Figure 2.1).

k_{aq} aqueous diffusion rate constant Waterbeemd (28) .

k_{org} organic diffusion rate constant Waterbeemd (28) .

k_{obs} experimentally observed apparent first-order forward or reverse rate constant for partitioning Waterbeemd (28) ; sec^{-1}.

k_{I} aqueous : organic rate constant for interfacial transfer; sec^{-1}.

k_{-I} organic : aqueous rate constant for interfacial transfer; sec^{-1}.

k_{ni} forward rate constant for dissociation; sec^{-1}.

k_{in} reverse rate constant for dissociation; sec^{-1}.

k_{12} forward apparent first-order rate constant for partitioning; sec^{-1}.

k_{21} reverse apparent first-order rate constant for partitioning; sec^{-1}.

$\vec{k}$ forward permeability coefficient; cm sec^{-1}.

$\overleftarrow{k}$ reverse permeability coefficient; cm sec^{-1}.

L lid (Figure 4.1).

Ltd. Limited.

l length; cm.

M molecular weight.

$\underline{M}$ molal.

ml millimeter.

N removable membrane holder (Figure 4.1).

NaCl sodium chloride.

NaOH sodium hydroxide.

$Na_2HPO_4.12\ H_2O$ di-sodium hydrogen orthophosphate (dodecahydrate).

$Na_3PO_4.\ H_2O$ tri-sodium orthophosphate (monohydrate).

n	number.
ORG	organic phase (Figure 1.1).
P	pulley (Figure 4.1).
pH	- log hydrogen ion concentration.
pK_a	- log acid dissociation constant.
R_{aq}	resistance of aqueous diffusive boundary layer; sec cm^{-1}.
R_{org}	resistance of organic diffusive boundary layer; sec cm^{-1}.
R_T	total diffusional resistance; sec cm^{-1}.
R1	$= \eta_1/\eta_2$.
R2	$= \nu_2/\nu_1$.
R3	$= (\phi_1 M_1)/(\phi_2 M_2)$.
r	aqueous : organic phase ratio (V_1/V_2).
rpm	revolutions per minute.
S	apparent first-order rate constant for partitioning; sec^{-1}.
Sl	slots (Figure 4.1).
sec	seconds.
T	temperature; ^{o} Kelvin (Equation 2.25).
t	time; sec^{-1}.
V	volume; cm^3.
$\overline{V}_A$	molal volume (Equation 2.25).

Greek Symbols

α	porosity.
β	ratio of limit value for k_{12} at high values for K_D to the limit value for k_{21} at low values for K_D ($= k_{org}/k_{aq}$) Waterbeemd (28) .
ρ	viscosity; poise.
ω	speed of rotation; Hertz.
ν	kinematic viscosity ($= \eta/\rho$); $cm^2 sec^{-1}$.

$\emptyset$	physical parameter.
ρ	density; g cm^{-3}.
Δ	defined time interval; sec^{-1}.
ψ	association parameter Wilke-Chang (33).
γ	resistance ratio (= R_{aq}/R_{org}).

Superscripts

o	initial.
∞	final or equilibrium.
/	value at t.

Subscripts

AB	solute A in solvent B (Equation 2.25).
app	apparent.
aq	aqueous.
i	ionised.
in	ionised to non-ionised.
max	maximum.
n	non-ionised.
ni	non-ionised to ionised.
obs	observed.
org	organic.
T	Total.
th	theoretical.
0	initial.
1	aqueous.
2	organic.
12	aqueous to organic.
21	organic to aqueous.

APPENDIX

APPENDIX A

Derivation of an equation describing the concentration of a solute in a donor aqueous phase of the two-phase transfer cell.

The kinetic Scheme for non-ionised solute transfer in the two-phase transfer cell is shown as Scheme A.1.

Scheme A.1.

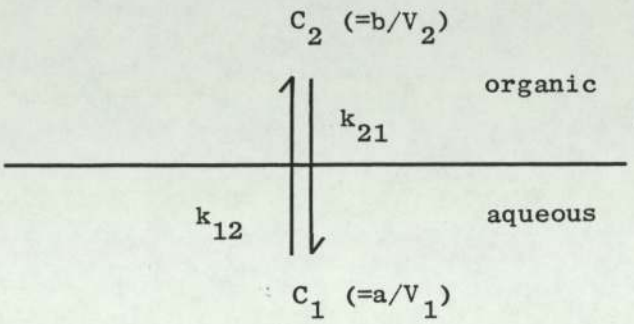

where C_1 and C_2 are the concentrations of solute in the aqueous and organic phase respectively of corresponding amounts a and b, and k_{12} and k_{21} are the apparent first-order rate constants of the forward and reverse partitioning processes. Initial conditions at time t = 0 are such that $C_1 = C_1^o$ and $C_2 = 0$ where according to Scheme A.1. the amounts of solute are $a = a^o$, b = 0. Thus the rates of change of solute amount in each of the phases is given by (rate in - rate out) as

$$\frac{da}{dt} = - k_{12}a + k_{21}b \qquad \text{A.1.}$$

and

$$\frac{db}{dt} = k_{12}a - k_{21}b \qquad \text{A.2.}$$

Integration of Eqs. A.1. and A.2. with respect to time between t = 0 and t = t by the method of Laplace (55) and solving for a yields:

$$(a - a^{\infty}) = (a^{o} - a^{\infty})\, e^{-(k_{12} + k_{21})t} \qquad \text{A.3.}$$

where a is the amount of solute in the donor phase at equilibrium. Since concentration = amount/volume, Eq. A.3. may be written in terms of concentration by dividing by V_1 giving

$$(C_1 - C_1^{\infty}) = (C_1^{o} - C_1^{\infty})\, e^{-(k_{12} + k_{21})t} \qquad \text{A.4.}$$

where C_1^{∞} is the concentration of solute remaining in the donor phase at time $t = \infty$ (i.e. at equilibrium). Thus a first-order plot of ln $(C_1 - C_1^{\infty})$ versus time is linear with a negative slope S, where

$$S = (k_{12} + k_{21}) \qquad \text{A.5.}$$

and S refers to the overall or observed apparent first-order rate constant for partitioning.

Equation A.5. also represents the apparent first-order rate constant for partitioning in the rotating diffusion cell when employed in a two-phase mode (aqueous : organic phase impregnated filter : organic phase).

APPENDIX B

Derivation of an equation describing the total concentration of a solute in the donor phase of the two-phase transfer cell in which aqueous phase pH is varied.

The kinetic Scheme for simultaneous first-order partitioning of non-ionised solute with reversible aqueous phase ionisation to a non-partitioning species in the two-phase transfer cell (Figure 1.1a) is shown in Scheme B.1.

Scheme B.1.

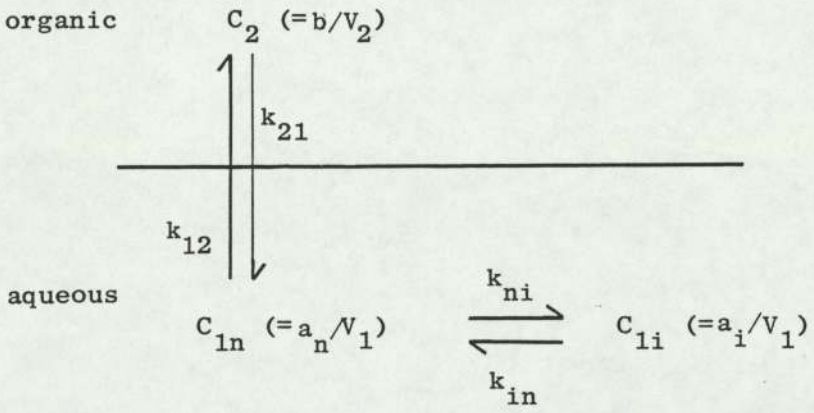

where symbols are defined in the glossary of terms. Initial conditions at time t = 0 are such that C_1 $(= C_{1n}^o + C_{1i}^o) = C_1^o$ and $C_2 = 0$ where, in accord with Scheme B.1. the amounts of solute correspond to a $(= a_n^o + a_i^o) = a^o$, b = 0. Thus the rate of change of solute amount in the aqueous phase may be given by (rate in - rate out) as

$$-d(a_n + a_i)/dt = -da/dt = -fn\ k_{12}a + k_{21}b \qquad \text{B.1.}$$

which is true because the ionisation equilibrium is so rapidly

achieved in the aqueous phase. Since by definition $b = a^o-(a_n + a_i) = a^o - a$, substituting for b into Eq. B.1. gives

$$-da/dt = -fn\ k_{12}\ a + k_{21}\ (a^o - a) \qquad B.2.$$

which expands to

$$-da/dt = -fn\ k_{12}\ a + k_{21}\ a^o - k_{21}\ a \qquad B.3.$$

Integration of Eq. B.3. with respect to time between time t = 0 and t = t using the method of Laplace (55) and solving for a yields

$$(a - a^\infty) = (a^o - a^\infty)\ e^{-(k_{12}\ fn + k_{21})t} \qquad B.4.$$

Division of both sides of Eq. B.4. by V_1 and taking natural logarithms provides the first-order rate equation in terms of concentration

$$\ln\ (C_1 - C_1^\infty) = \ln\ (C_1^o - C_1^\infty) - (k_{12}\ fn + k_{21})t \qquad B.5.$$

Thus a first-order plot of $\ln\ (C_1 - C_1^\infty)$ versus time is linear with a negative slope, S, where

$$S = k_{12}\ fn + k_{21} \qquad B.6.$$

and S represents the observed apparent first-order rate constant for partitioning for solutes subject to differing degrees of dissociation in the aqueous phase of the two-phase transfer cell.

Equation B.6. also represents the observed first-order rate constant for partitioning in the rotating diffusion cell when employed in a two-phase mode (aqueous : organic phase impregnated filter : organic phase) under conditions of varying aqueous phase pH.

APPENDIX C

Methods for estimating the apparent first-order kinetic rate constant for partitioning in the two-phase transfer cell from concentration versus time profiles with and without knowledge of the initial and final concentration of partitioning species.

When a partitioning process is well behaved the integrated form of the kinetic equation provides an accurate method for estimating the partitioning rate constant. In the two-phase transfer cell in which solute is allowed to partition across the interface in both directions, the apparent rate constant, S, may be estimated from plots of ln (transferable concentration) versus time in accord with Eq. C.1.

$$\ln (C_1 - C_1^{\infty}) = \ln (C_1^{o} - C_1^{\infty}) - St \qquad \text{C.1.}$$

Equation C.1. is identical to Equation 2.1. Thus, given a reliable estimate for the equilibrium concentration of the solute in the aqueous phase, C_1^{∞}, a first-order plot of ln $(C_1 - C_1^{\infty})$ versus time should be linear with a negative slope S equal to the apparent first-order rate constant for partitioning.

A major problem associated with estimating transport rate constants from plots of ln $(C_1 - C_1^{\infty})$ versus time in the two-phase transfer cell is the accurate experimental determination of C_1^{∞} at time $t = \infty$. This is because the equilibrium concentration of the solute at time $t = \infty$, C_1^{∞}, is often below the minimum concentration detectable by the analytical technique. However, several authors have reported methods for estimating the rate constant of a first-order reversible process that do not require a knowledge of the initial or final concentration of the reacting species (61 - 64). These methods are applicable to partitioning processes of the type experienced in the two-phase transfer cell. (65).

Guggenheim (61) described a method for estimating the apparent first-order rate constant of a reversible process. The course of a first-order reversible process may be followed by measurement of some physical property of the system $\emptyset$ (e.g. concentration) which varies with time, t according to

$$(\emptyset_t - \emptyset_\infty) = (\emptyset_o - \emptyset_\infty)\, e^{-St} \qquad C.2.$$

The initial and final values of the physical property are $\emptyset_o$ and $\emptyset_\infty$, respectively, and S refers to the rate constant for an apparent first-order process. If readings $\emptyset_1, \emptyset_2, \ldots\ldots \emptyset_n$ are made at times $t_1, t_2, \ldots\ldots t_n$, and a second series $\emptyset_1', \emptyset_2', \ldots\ldots \emptyset_n'$ are made at the corresponding times $t_1 + \Delta t, t_2 + \Delta t, \ldots\ldots t_n + \Delta t$ (where Δt is constant) then,

$$(\emptyset_n - \emptyset_\infty) \quad (\emptyset_o - \emptyset_\infty)\, e^{-S\,(St_n)} \qquad C.3.$$

and

$$(\emptyset_n' - \emptyset_\infty) = (\emptyset_o - \emptyset_\infty)\, e^{-S\,(t_n + \Delta t)} \qquad C.4.$$

Subtraction of Eq. C.4. from Eq. C.3 yields

$$(\emptyset_n - \emptyset_n') = (\emptyset_o - \emptyset_\infty)\left[1 - e^{-S\Delta t}\right]\left[e^{-St_n}\right] \qquad C.5.$$

Taking natural logarithms of Eq. C.5. gives

$$\ln (\emptyset_n - \emptyset_n') = \ln (\emptyset_o - \emptyset_\infty) + \ln\left[1 - e^{-S\Delta t}\right] - St_n \qquad C.6.$$

For a given kinetic run, $\emptyset_\infty$, $\emptyset_o$ and Δt are constant, and therefore

$$\log (\emptyset_n - \emptyset_n') = \text{constant} - St_n/2.303 \qquad C.7.$$

A plot of $\log (\emptyset_n - \emptyset')$ versus time, t, will be linear with slope equal to $-S/2.303$. The most appropriate value to be chosen for the time interval, Δt, depends upon the accuracy of the recorded values of

$\emptyset$, but for most data Δt should be of the order of one half life. Therefore for application of the Guggenheim method the partitioning process should be well behaved over at least two half-life periods (61).

Related to the Guggenheim plot is a plot independently proposed by Kezdy (62) and Swinbourne (63). This plot is based on Eq. C.8. which is derived from the division of Eq. C.3. by C.4. and subsequent rearrangement.

$$\emptyset_n = \emptyset_\infty \left[1 - e^{s\Delta t} \right] + \emptyset_n' \, e^{s\Delta t} \qquad \text{C.8.}$$

The last equation demonstrates that a straight line is obtained when the valuesof $\emptyset_n$ are plotted directly against the corresponding values of $\emptyset_n'$; an estimate of the rate coefficient may be evaluated from the logarithm of the slope of this line.

Hartley has outlined a method for obtaining, directly from tabulated data for associated variables x and y, a least-squares fit for a straight line relationship between the differential coefficient dx/dy, and x (64). The procedure, known as the "method of internal least squares", is based upon finite differential calculus and is applicable to concentration versus time data for partitioning processes obeying a first-order kinetic law (65). Hartley's method does not require assumptions concerning the initial and final concentrations of solute, but it involves more laborious computations than either the Guggenheim (61) or Kezdy-Swinbourne methods (62, 63). The following is an illustration of the application of the method of internal least squares to the data given in Table C.1 with reference to Tables C.2 and C.3. The calculations have been made on 15 data points, and the instructions given are for an odd number of data; slightly modified instructions are required for an even number of data.

TABLE C.1

Experimental absorption data for barbitone partitioning between an aqueous (pH 4.85; 0.3 M orthophosphate buffer) : octanol system in the two-phase transfer cell 100 rpm, 37° and corresponding kinetic, Guggenheim and Kezdy-Swinbourne parameters.

time, t (mins)	ϕ_n (t)	$\phi_n - \phi_\infty$	ln $(\phi_n - \phi_\infty)$	ϕ' (t + 40)	$\phi_n - \phi'_n$	log $(\phi_n - \phi'_n)$
5	0.511	0.386	-0.95	0.179	0.332	-0.479
10	0.430	0.305	-1.19	0.166	0.264	-0.578
15	0.365	0.240	-1.43	0.156	0.209	-0.679
20	0.314	0.189	-1.67	0.149	0.165	-0.783
25	0.273	0.148	-1.91	0.144	0.129	-0.889
30	0.243	0.118	-2.14	0.138	0.105	-0.979
35	0.215	0.090	-2.41	0.134	0.081	-1.092
40	0.195	0.070	-2.66			
45	0.179	0.054	-2.92			
50	0.166	0.041	-3.19			
55	0.156	0.031	-3.47			
60	0.149	0.024	-3.73			
65	0.146	0.019	-3.96			
70	0.138	0.013	-4.34			
75	0.134	0.009	-4.71			
∞	0.125					

TABLE C.2

Summation table for the method of internal least-squares (Hartley analysis)(64).

Column 1	Column 2	Column 3	Column 4	Column 5
0.511	-0.511	0.511	-4.386	19.237
1.452	-0.941	0.430	-3.445	11.868
2.758	-1.306	0.365	-2.650	7.023
4.378	-1.620	0.314	-1.971	3.885
6.271	-1.893	0.273	-1.384	1.915
8.407	-2.136	0.243	-0.868	0.753
10.758 (iv)	-2.351 (ii)	0.215	-0.410	0.168
0	0	0.195 (i)	0	0
4.061 (v)	1.066 (iii)	0.179	0.374	0.139
2.995	0.887	0.166	0.719	0.517
2.108	0.721	0.156	1.041	1.084
1.387	0.565	0.149	1.346	1.812
0.822	0.416	0.144	1.639	2.686
0.406	0.272	0.138	1.921	3.690
0.134	0.134	0.134	2.193	4.809
46.45	-6.697	3.612	-5.881	59.59

n = number of Ø values = 15.

Δt = 40.

TABLE C.3

Instructions for the method of internal least-squares (Hartley analysis) (64)).

Symbol	Instruction	Value
A	Σ column 3	3.612
B	A/n	0.241
C	Σ column 4/2	-2.941
D	C^2/n	0.576
E	Σ column 5/4	14.89
F	Σ column 2	-6.697
G	$2\,\Sigma$ column 1 - (iv) - (v)	78.08
H	G - MA/n	10.656
L	E - D + B (G - 2MA/n)	0.633
M	$n\,(n^2 - 1)/12$	280
P	$ML - H^2/4$	53.33
Q	- 2L/H	-0.119
R	- FH/2P	0.232
Ø	Q + B	0.119
K	log (2 + R) - log (2 - R)	0.101
S	$(2.303/\Delta t)/S$	7.78×10^{4} sec^{-1}

The first step is the construction of Table C.2 in which the recorded absorption readings, $\emptyset_n$ (Table C.1), are listed in column 3. Zeros are placed at the central positions of columns 1, 2, 4 and 5. The remainder of column 2 consists of the cumulative sums of the absorption values, summation proceeding toward the centre from both ends of column 3. Second cumulative sums are made in column 1 from the values in column 2. Column 4 consists of special cumulative sums proceeding in both directions from the centre of the table and obtained in the following way: the value 0.410 is obtained by adding the zero in column 4 to the values 0.195 and 0.215 in column 3; the value 0.868 is obtained by adding the 0.410 from column 4 to the value 0.215 and 0.243 in column 3; and so on. Column 5 consists of the squares of the values in column 4. The values in the top halves of columns 2 and 4 are made negative, and the columns are summed. Values in the table are referenced (i), (ii), (iii), (iv) and the remaining calculations follow the instructions listed in Table C.3, rounding off S and $\emptyset_\infty$ at the end of the computations. The validity of these methods [Guggenheim (Eq. C.7), Kezdy-Swinbourne (Eq. C.8) and Hartley] for estimating apparent first-order rate constants for partitioning in the two-phase transfer cell was established by analysing experimentally determined spectrophotometric absorbtion data for a barbitone / aqueous (pH 5.0) : octanol system at 100 rpm, 37°C. The experimentally observed absorbtion data for barbitone at time, t, is documented in Table C.1 alongside estimates for the kinetic ($\ln[\emptyset_n - \emptyset_\infty]$), Guggenheim ($\log[\emptyset_n - \emptyset_n']$) and Kezdy-Swinbourne ($\emptyset_n'$) parameters, while Tables C.2 and C.3 document the method of Hartley for the barbitone data (Table C.1). Figures C.1 - C.3 document plots in accord with the methods of kinetic analysis (Eq. C.1.), Guggenheim (Eq. C.7.) and Kezdy-Swinbourne (Eq. C.8.), respectively. Figures C.1 - C.3 and Table C.3 document the values for S

as 7.90, 7.87, 7.82 and 7.78 $sec^{-1} \times 10^4$ estimated using kinetic, Guggenheim, Kezdy-Swinbourne and Hartley methods, respectively. The excellent agreement for S between these methods attests to their validity for estimations of first-order rate constants for partitioning in the two-phase transfer cell.

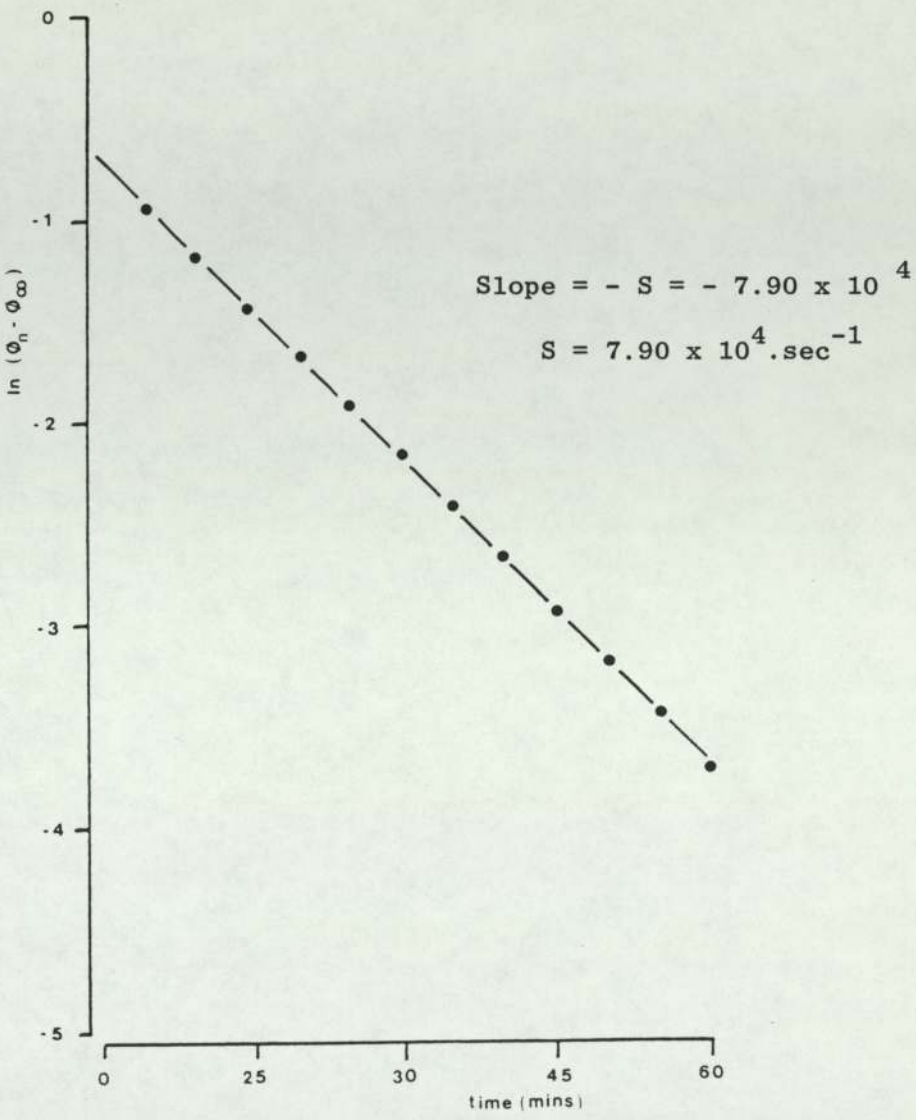

Figure C.1 First-order plot of ln (transferable concentration) versus time.

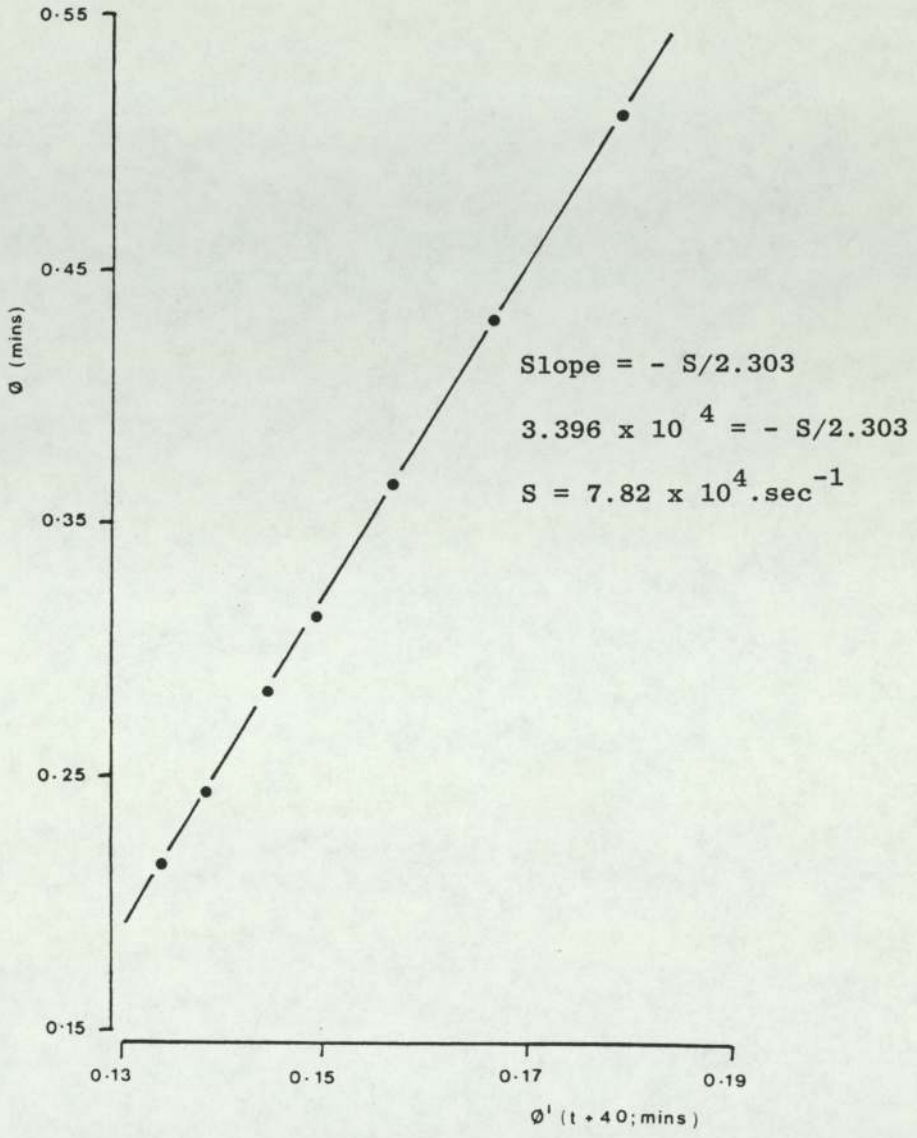

Figure C.2 Kezdy-Swinbourne plot for estimating apparent first-order partitioning rate constants in the two-phase transfer cell.

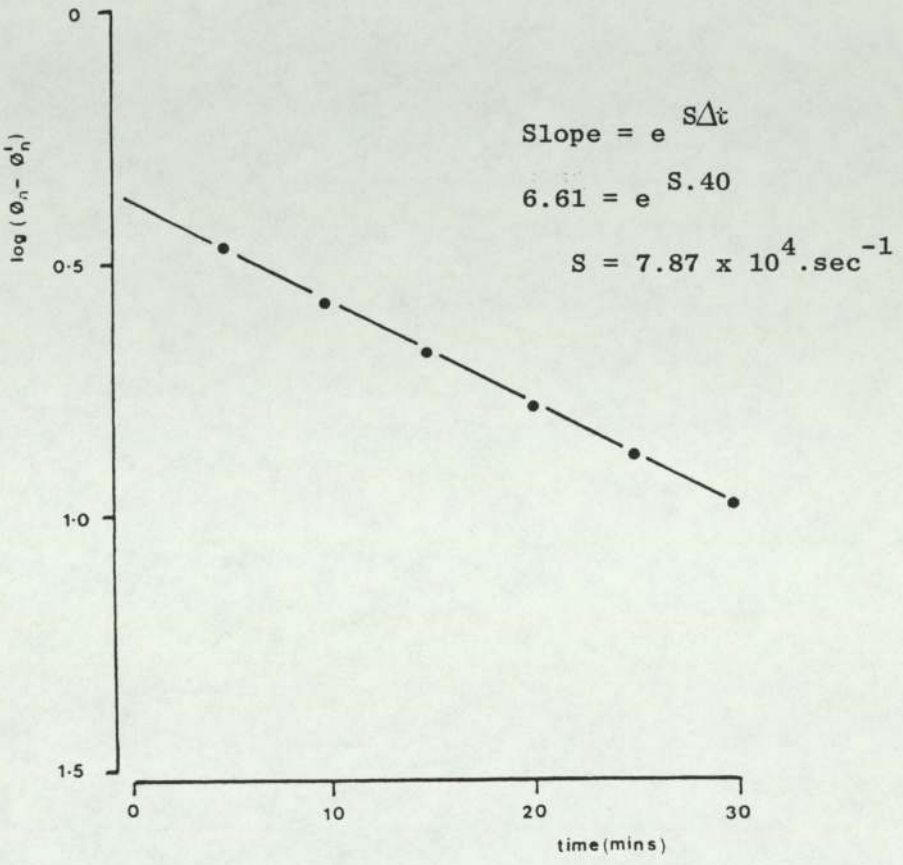

Figure C.3 Guggenheim plot for estimating apparent first-order partitioning rate constants in the two-phase transfer cell.

LIST OF REFERENCES

1. Doluisio , J.T. and Swintosky, J.V. (1964). Drug Partitioning II : In vitro model for drug absorption. *J. Pharm. Sci.*, 53, 597-601.

2. Perrin, J. (1967). An in vitro model for soluble drug absorption. *J. Pharm. Pharmac .*, 19, 25-31.

3. Robertson, J.S. and Bode, O. (1970). An in vitro model for drug absorption studies. *J. Pharm. Pharmac .*, 22, 423-426.

4. Khalil, S.A. and Martin, A.M. (1967). Drug transport through model membranes and its correlation with solubility parameters. *J. Pharm. Sci.*, 56, 1225-1233.

5. Sjölin, S. (1942). The oil/water interface, with and without monomolecular film, as a model of the living cell membrane. *Acta Physiol. Scand.*, 4, 365-372.

6. Gordon, K.F. and Sherwood, T.K. (1954). Mass transfer between two liquid phases. *Chem. Eng. Prog. Symp. Ser.*, 50, 15-23.

7. Lewis, W.K. and Whitman, W.G. (1924). Principles of gas absorption. *Ind. Eng. Chem.*, 16, 1215-1220.

8. Byron, P.R., Notari, R.E. and Tomlinson, E. (1980). Calculation of partition coefficient of an unstable compound using kinetic methods. *J. Pharm. Sci.*, 69, 527-531.

9. Ting, H.P., Bertrand, G.L. and Sears, D.F. (1966). Diffusion of salts across a butanol-water interface. *Biophys. J.*, 6, 813-823.

10. Schumacher, G.E. and Nagwekar, J.B. (1974). Kinetic and thermodynamic aspects of in vitro interphase transfer of sulphonamides I : Influence of methyl group substitution on transfer of unionised sulphonamides. *J. Pharm. Sci.*, 63, 240-244.

11. Schumacher, G.E. and Nagwekar, J.B. (1974). Kinetic and thermodynamic aspects of in vitro interphase transfer of sulphonamides II : Influence of interface composition on transfer of unionised sulphonamides. *J. Pharm. Sci.*, 63, 245-249.

12. Zecchi, V., Rodriguez, L. and Cini, M. (1978). Partizione di farmaci in sistemi bifasici. *Farmaco. Ed. Prat.*, 34, 176-185.

13. Koprivc, L., Polla, E. and Hranilovic, J. (1976). Kinetic and thermodynamic aspects of in vitro interphase transfer of some barbituric acid derivatives. *Acta Pharm. Jugoslav.*, 26, 29-36.

14. Augustine, M.A. and Swarbrick, J. (1970). Effect of lipid polarity and cell design on the in vitro transport of salicylic acid. *J. Pharm. Sci.*, 59, 314-317.

15. Shore, P.A., Brodie, B.B. and Hogben, C.A.M. (1957). The gastric secretion of drugs : A pH partition hypothesis. *J. Pharmac. Exp. Ther.*, 119, 361-369.

16. Schanker, L.S., Shore, P.A., Brodie, B.B. and Hogben, C.A.M. (1957). Absorption of drugs from the stomach I. The rat. *J. Pharmac. Exp. Ther.*, 120, 528-539.

17. Hogben, C.A.M., Schanker, L.S., Tocco, D.J. and Brodie, B .B. (1957). Absorption of drugs from the stomach II. The human. *J. Pharmac. Exp. Ther.*, 120, 540-545.

18. Hogben, C.A.M., Tocco, D.J., Brodie, B.B. and Schanker, L.S. (1959). On the mechanism of intestinal absorption of drugs. *J. Pharmac. Exp. Ther.*, 125, 275-282.

19. Kubinyi, H. (1979). Lipophilicity and biological activity. *Arzneim-Forsch.*, 29, 1067-1080.

20. Hansch, C. and Dunn, W.J. (1972). Linear relationships between lipophilic character and biological activity of drugs. *J. Pharm. Sci.*, 61, 1-19.

21. Hansch, C. and Clayton, J.M. (1973). Lipophilic character and biological activity of drugs II : The parabolic case. *J. Pharm. Sci.*, 62, 1-21.

22. Kubinyi, H. (1979). Lipophilicity and drug activity in "Progress in Drug Research". Ed. Jucker, E. Pub. Birkhauser Verlag, Stuttgart. pp. 97-198.

23. Guest, R.T. (1980). Kinetic rational of two- and three-phase transfer cells as drug absorption models. PhD Thesis, University of Aston, Birmingham, England.

24. Byron, P.R., Guest, R.T. and Notari, R.E. (1981). Thermodynamic dependence of interfacial transfer kinetics of nonionized barbituric acid derivatives in two-phase transfer cell. *J. Pharm. Sci.*, 70, 1265-1269.

25. Van de Waterbeemd, H., Van Boeckel, S., Jansen, A. and Gerritsma, K. (1980). Transport in QSAR II. Rate-equilibrium relationships and the interfacial transfer of drugs. *Eur. J. Med. Chem.*, 15, 279-282.

26. Van de Waterbeemd, J.Th.M., Van Boekel, C.C.A.A., de Sévaux, R.L.F.M., Jansen, A.C.A. and Gerritsma, K.W. (1981). Transport in QSAR IV. The interfacial drug transfer model. Relationships between partition coefficients and rate constants of drug partitioning. *Pharmaceut. Weekbl. Sci. Ed.*, 3, 12-25.

27. Van de Waterbeemd. H., Van Bakel, P. and Jansen, A. (1981). Transport in QSAR VI. Relationship between transport rate constants and partition coefficients. *J. Pharm. Sci.*, 70, 1081-1082.

28. Van de Waterbeemd, J.T.M. (1980). The relationship between partition coefficients and rate constants of drug partitioning and the application in QSAR. Thesis, Leiden, The Netherlands.

29. Van de Waterbeemd, H. (1983). The theoretical basis for relationships between drug transport and partition coefficients. in "Fourth European Activity : Quantitative Approaches". Ed. J.C. Dearden. Pub. Elsevier, Amsterdam. pp. 183-192.

30. De Haan, F.H.N., De Vringer, T., Van de Waterbeemd, J.T.M. and Jansen, A.C.A. (1983). Transport rate constants and transport rate parameters in various organic solvent - water systems. *Int. J. Pharm.*, 13, 75-87.

31. De Haan, F.H.N. and Jansen, A.C.A. (1984). The hydrodynamics in a simple transport vessel in two-phase systems of organic solvent - water. *Int. J. Pharm.*, 18, 311-324.

32. De Haan, F.H.N. and Jansen, A.C.A. (1983). Transport in QSAR VIII. The influence of viscosity on transport rate constants in two-phase systems organic solvent - water. *Pharmaceut. Weekbl. Sci. Ed.*, 5, 222-227.

33. Wilke, C.R. and Chang , P. (1955). Correlation of diffusion coefficients in dilute solutions. *Am. Inst. Chem. Engrs. J.*, 1, 264-270.

34. Bretszajder, S. (1971) in "Prediction of Transport and Other Physical Properties of Fluids". Pub. Pergamon Press. Chapter 8.

35. Levich, B. (1947). The theory of concentration polarisation. *Disc Farad. Soc.*, 1, 37-43.

36. Levich, B. (1982) in "Physicochemical Hydrodynamics". Pub. Prentice Hall, Englewood Cliffs, N.J. pp. 69.

37. Merck Index. 7th Edn. Pub. Merck and Co. Inc., N.J., U.S.A.

38. Leo, A., Hansch, C. and Elkins, D. (1971). Partition coefficients and their uses. *Chem. Rev.*, 71, 525-616.

39. Rekker, R.F. (1977) in "The Hydrophobic Fragmental Constant". Pub. Elsevier, Amsterdam.

40. Notari, R.E. (1975) in "Biopharmaceutics and Pharmacokinetics". Pub. Marcel Dekker Inc., N.Y., U.S.A.

41. Sten-knudsen, O. (1978) in "Membrane Transport in Biology I. Concepts and Models". Ed. Giebisch, G., Tosteson, D.C. and Ussing, H.H. Pub. Springer-Verlag, Berlin, Germany. pp. 53.

42. Chang, P. and Wilke, C.R. (1955). Some measurements of diffusion in liquids. *J. Phys. Chem.*, 59, 592-596.

43. Reid, R.C. and Sherwood, T.K. (1966) in "The Properties of Gasses and Liquids. Their Estimation and Correlation". 2nd Edn. Pub. McGraw-Hill Book Company, N.Y. Chapter 11.

44. Reid, R.C., Prausnitz, J.M. and Sherwood, T.K. (1977) in "The Properties of Gasses and Liquids". 3rd Edn. Pub. McGraw-Hill Book Company, N.Y. Chapter 11.

45. Albery, W.J., Burke, J.F., Leffler, E.B. and Hadgraft, J. (1976). Interfacial transfer studied with a rotating diffusion cell. *J. Chem. Soc. Farad. Trans.*, 72, 1618-1626.

46. Smith, R.N., Hansch, C. and Ames, M.M. (1975). Selection of a reference partitioning system for drug design work. *J. Pharm. Sci.*, 64, 599-606.

47. Hayslett, H.T. and Murphy, P. (1981) in "Statistics Made Simple". Pub. William Heinemann Ltd., England. pp. 140-143.

48. Albert, A. and Sergeant, E.P. (1962) in "Ionisation Constants of Acids and Bases". Pub. John Wiley and Sons, Inc., New York.

49. Hayslett, H.T. and Murphy, P. (1981) in "Statistics Made Simple". Pub. William Heinemann Ltd., England. pp. 30-35.

50. Forgō, I., Büchi, J. and Perlia, X. (1970). Synthese, physikalisch-chemische, eigenschaften und antioxydative wirkung einiger gallussäure ester 3. *J. Pharm. Acta Helv.*, 45, 237-247.

51. Doluisio, J.T. and Swintosky, J.V. (1965). Drug Partitioning III : Kinetics of drug transfer in an in vitro model for drug absorption. *J. Pharm. Sci.*, 54, 1594-1599.

52. Lamy, P.P. (1969). The effect of macromolecules on drug transfer in vitro. *Pharm. Acta Helv.*, 44, 79-84.

53. Martin, A.N., Swarbrick, J. and Cammarata, A. (1969) in "Physical Pharmacy". Lea and Febiger, Philadelphia. 2nd Edn. Chapter 10.

54. Riggs, D.S. (1975) in "The Mathematical Approach to Physiological Problems". Pub. The MIT Press, Cambridge, Mass., U.S.A. pp. 202-203.

55. Gibaldi, M. and Perrier, D. (1975) in "Pharmacokinetics". Pub. Marcel Dekker Inc., N.Y. Appendix I, pp. 267-272.

56. Perrin, D.D., Dempsey, B. and Sergeant, E.P. (1981) in "pK_a Prediction for Organic Acids and Bases". Pub. Chapman and Hall, London, England.

57. Florence, A.T. and Attwood, D. (1981) in "Physicochemical Principles of Pharmacy". Pub. Macmillan Press Ltd., London, England. pp. 163.

58. Rosano, H.L., Duby, P. and Schulman, J.H. Mechanism of the selective flux of salts and water migration through non-aqueous liquid membranes. *J. Phys. Chem.* 65, 1704-1708.

59. Rosano, H.L. (1967). Mechanisms of water transport through nonaqueous liquid membranes. *J. Coll. Int. Sci.*, 23, 73-79.

60. Christian, G.D. and Purdy, W.C. (1962). The residual current in orthophosphate medium. *J. Electroanal. Chem.*, 3, 363-367.

61. Guggenheim, E.A. (1926). On the determination of the velocity constant of a unimolecular reaction. *Phil. Mag.*, 2, 583-543.

62. Kezdy, F.J., Jaz, J. and Bruylants, A. (1958). Cinétique de L'action de L'acide nitreux sur les amides. 1. Méthode générale. *Bull. Soc. Chim. Belg.*, 67, 687-706.

63. Swinbourne, E.S. (1960). Method for obtaining the rate coefficient and final concentration of a first-order reaction. *J. Chem. Soc.*, 2371-2372.

64. Hartley, H.O. (1948). The estimation of non-linear parameters by "internal least squares". *Biometrika*, 35, 32-45.

65. Swinborne, E.S. (1971) in "Analysis of Kinetic Data". Pub. Nelson and Sons, England. pp. 78-84.

66. Blaug, S.M. and Grant, D.E. (1974). Kinetics of degradation of the parabens. *J. Soc. Cosmet. Chem.*, 25, 495-506.

67. Sunderland, V.B. and Watts, D.W. (1984). Kinetics of the degradation of methyl, ethyl and n-propyl 4-hydroxybenzoate esters in aqueous solutions. *Int. J. Pharm.*, 19, 1-15.

68. Newling, W.B.S. and Hinshelwood, C.M. (1936). The kinetics of the acid and the alkaline hydrolysis of esters. *J. Chem. Soc.*, 1357-1361.

69. Garrett, E.R., Bojarski, J.T. and Yakatan, G.J. (1971). Kinetics of hydrolysis of barbituric acid derivatives. *J. Pharm. Sci.*, 60, 1145-1154.

70. Hermann, T. (1976). Kinetics and mechanism of degradation of some 5-allylbarbituric acid derivatives. *Pharmazie*, 31, 618-623.

71. Eriksson, S.O. and Holmgren, A. (1965). Hydrolysis of barbituric acids. *Acta Pharm. Suecica*, 2, 293-304.

72. De Meere, A.L.J. and Tomlinson, E. (1983). Theoretical and experimental studies on the origin of pH-absorption shifts. *Int. J. Pharm.*, 17, 331-346.

73. Guy, R.H. and Honda, D.H. (1984). Solute transport resistance at the octanol-water interface. *Int. J. Pharm.*, 19, 129-137.

74. Guy, R.H., Aquino, T.R. and Honda, D.H. (1982). Kinetics of solute transfer across aqueous phase - liquid hydrocarbon interfaces. *J. Phys. Chem.*, 86, 280-283.

75. Albery, W.J. and Hadgraft, J. (1979). Percutaneous absorption : interfacial transfer kinetics. *J.Pharm.Pharmac.*, 31, 65-68.

76. Sagert, N.H., Quinn, M.J. and Dixon, R.S. (1981). The transfer of alkanoic acids from dodecane to water. *Can. J. Chem.*, 59, 1096-1100.

77. Brown, A.H. (1965). Interfacial resistance to mass transfer in liquid-liquid systems. *Brit. Chem. Eng.*, 10, 622-626.

78. Davies, J.T. and Wiggill, J.B. (1960). Diffusion across the oil/water interface. *Proc. Roy. Soc.*, 255A, 277-291.

79. Tung, L.H. and Drickamer, H.G. (1952). Diffusion through an interface-Ternary systems. *J. Chem. Phys.*, 20, 10-12.

80. Sinfelt, J.H. and Drickamer, H.G. (1955). Resistance in a liquid-liquid interface. III. The effect of molecular properties. *J. Chem. Phys.*, 23, 1095-1099.

81. Documenta Geigy Scientific Tables (1975). 7th Edn. Ed. Diem, K. and Lentner, C., Geigy Pharmaceuticals, Macclesfield, England. pp. 280 *et seq.*

82. Byron, P.R. Personal communication.

83. Newton, D.W. and Kluza, R.B. (1978). pK_a values of medicinal compounds in pharmacy practice. *Drug Int. Clin. Pharm.*, 12, 546-554.

84. Cools, A.A. and Janssen, L.H.M. (1983). Influence of sodium ion-pair formation on transport kinetics of warfarin through octanol-impregnated membranes. *J. Pharm. Pharmac.*, 35, 689-691.

85. Wang, P.H. and Lien, E.J. (1980). Effects of different buffer species on partition coefficients of drugs and in Quantitative Structure-Activity Relationships. *J. Pharm. Sci.*, 69, 662-668.

86. Tyrrell, H.J.V. (1961) in "Diffusion and Heat Flow in Liquids". Pub. Butterworths, London, England. pp. 165 *et seq.*

87. Riddiford, A.C. (1966). The rotating disc system. *Adv. in Elec. and Electrochem. Eng.*, 4, 47-116.

88. Flynn, G.L., Yalkowsky, S.H. and Roseman, T.J. (1974). Mass transport phenomena and models : Theoretical concepts. *J. Pharm. Sci.*, 63, 479-509.

89. Zwolinski, B.J., Eyring, H. and Reese, C.E. (1949). Diffusion and membrane permeability. *J. Phys. Chem.*, 53, 1426-1453.

90. Scholtens, B.J.R. and Bijsterbosch, B.H. (1976). Rate-determining step in the diffusion of solutes across a liquid/liquid interface. *Febs Letters*, 62, 233-235.

91. Friedman, M. and Donbrow, M. (1980). Diffusion of drugs through multibarrier. *Pharm. Weekbl. Sci. Ed.*, 2, 1417-1420.

92. Guy, R.H. and Fleming, R. (1979). The estimation of diffusion coefficients using the rotating diffusion cell. *Int. J. Pharm.*, 3, 143-149.

93. Guy, R.H.,Honda, D.H. and Aquino, T,R. (1982). The influence of urea on the kinetics of interfacial transfer. *J. Coll. Int. Sci.*, 87, 107-114.

94. Fleming, R., Guy, R.H. and Hadgraft, J. (1983). Kinetics and thermodynamics of interfacial transfer. *J. Pharm. Sci.*, 72, 412-145.

95. Prince, L.M. and Sears, D.F. (1973) in "Biological Horizons in Surface Science". Pub. Academic Press, New York.

96. Smith, A. (1975). The influence of the chemical nature of dispersed phase on stability in oil-in-water emulsions. PhD thesis, University of Aston, Birmingham, England.

97. Sherman, P. (1968) in "Emulsion Science". Pub. Academic Press, New York. Chapter 3.

98. Amidon, G.E., Higuchi, W.I. and Ho, N.F.H. (1982). Theoretical and experimental studies of transport of micelle-solubilized solute. *J. Pharm. Sci.*, 71, 77-84.

99. Guy, R.H. and Hadgraft, J. (1981). Interfacial transport of salicylic acid. *J. Coll. Int. Sci.*, 81, 69-74.

100. Davies, J.T. and Rideal, E.K. (1963) in "Interfacial Phenomena". Pub. Academic Press, New York, 2nd Edn. Chapter 7.

101. Davies, J.T. and Haydon, D.A. (1957) in "Spontaneous Emulsification. Second International Congress of Surface Activity. I. Gas-Liquid and Liquid-Liquid Surfaces". 2nd Edn. Butterworths Scientific Publications, London, England. 417-425.

102. Lewis, J.B. (1953). Discussion in Murdoch, R. and Pratt, H.R.C. Liquid-liquid extraction : Part VIII. The extraction of uranyl nitrate in a wetted wall column. *Trans. Inst. Chem. Eng.*, 31, 323-325.

103. Lewis, J.B. (1953). Written contribution in Murdoch, R. and Pratt, H.R.C. Liquid-liquid extraction : Part VIII. The extraction of uranyl nitrate in a wetted wall column. *Trans. Inst. Chem. Eng.*, 31, 325-326.

104. Blokker, P.C. (1957). On mass transfer across liquid/liquid interfaces in systems with and without surface active agents. In Gas/Liquid and Liquid/Liquid Interface. Proceedings of the Second International Congress of Surface Activity. Vol. 1. Pub. Butterworths, London, England.

105. Lewis, J.B. (1954). The mechanism of mass transfer of solutes across liquid-liquid interfaces. Part II. The transfer of organic solutes between solvent and aqueous phases. *Chem. Eng. Sci.*, 3, 260-278.

106. Lewis, J.B. (1958). The mechanism of mass transfer of solutes across liquid-liquid interfaces. Part III. The transfer of uranyl nitrate between solvent and aqueous phases. *Chem. Eng. Sci.*, 8, 295-308.

107. Sherwood, T.K. and Wei, J.C. (1957). Interfacial phenomena in liquid extraction. *Ind. Eng. Chem.*, 49, 1030-1034.

108. Lewis, J.B. and Pratt, H.C.R. (1953). Oscillating droplets. *Nature*, 171, 1155-1156.

109. Andreas, J.M., Hauser, E.A. and Tucker, W.B. (1938). Boundary tension by pendent drops. *J. Phys. Chem.*, 42, 1001-1019.

110. Thomas, W.J. and Nicholl, E. MCK. (1967). An optical study of interfacial turbulence occurring during the absorption of CO_2 into monoethanolamine. *Chem. Eng. Sci.*, 22, 1877-1878.

111. Ellis, S.R.M. and Biddulph, M. (1966). Interfacial turbulence measurements. *Chem. Eng. Sci.*, 21, 1107-1109.

112. Davies, J.T. (1966). The effects of surface films in damping eddies at a free surface of a turbulent liquid. *Proc. Roy. Soc.*, 290A, 515-526.

113. Sternling, C.V. and Scriven, L.E. (1958). Interfacial turbulence : Hydrodynamic instability and the Marangoni effect. *A.I. Ch. E.J.*, 5, 514-523.

114. Jaycock, M.J. and Parfitt, G.D. (1981) in "Chemistry of Interfaces". Pub. John Wiley and Sons, New York. 1st Edn.

115. Haydon, D.A. (1955). Oscillating droplets and spontaneous emulsification. *Nature*, 176, 839-840.

116. Haydon, D.A. (1958). An investigation of droplet oscillation during mass transfer I. The conditions necessary and the source of energy for the oscillations. *Proc. Roy. Soc.*, 243A, 483-491.

117. Glasstone, S. and Lewis, D. (1981) in "Elements of Physical Chemistry". Pub. Macmillan Press Ltd., London, England.

118. Davies, J.T. and Rideal, E.K. (1963) in "Interfacial Phenomena". Pub. Academic Press, New York, 2nd Edn. Chapter 1.

119. Florence, A.T. and Attwood, D. (1981) in "Physicochemical Principles of Pharmacy". Pub. Macmillan Press Ltd., London, England. Chapter 3.

120. Moore, W.J. (1972) in "Physical Chemistry". Pub. Longman Ltd., London, England. 5th Edn. Chapter 11.

121. Maron, S.H. and Prutton, C.F. (1965) in "Principles of Physical Chemistry". Pub. Macmillan Press Ltd., London, England. 4th Edn. Chapter 20.

122. Weast, R.C. (1979) in "CRC Handbook of Chemistry and Physics". Pub. CRC Press Inc., Florida, 59th Edn.